

Aus dem Zentrum für Kinder- und Jugendmedizin der Universität zu Köln
Klinik und Poliklinik für Kinder- und Jugendmedizin
Direktor: Universitätsprofessor Dr. med. J. Dötsch

Quantification of echo intensity in fascicle-aligned ultrasound: ex-vivo validation of spatial gain sonography

Inaugural-Dissertation zur Erlangung der Doktorwürde
der Medizinischen Fakultät
der Universität zu Köln

vorgelegt von
Clara Sophie Rosahl
aus Hannover

promoviert am 17. März 2025

Gedruckt mit Genehmigung der Medizinischen Fakultät der Universität zu Köln
2025

Dekan: Universitätsprofessor Dr. med. G. R. Fink

1. Gutachter: Universitätsprofessor Dr. med. J. Rittweger

2. Gutachterin: Professorin Dr. Sportwiss. A. Niehoff

Erklärung

Ich erkläre hiermit, dass ich die vorliegende Dissertationsschrift ohne unzulässige Hilfe Dritter und ohne Benutzung anderer als der angegebenen Hilfsmittel angefertigt habe; die aus fremden Quellen direkt oder indirekt übernommenen Gedanken sind als solche kenntlich gemacht.

Bei der Auswahl und Auswertung des Materials sowie bei der Herstellung des Manuskriptes habe ich Unterstützungsleistungen von folgenden Personen erhalten:

Prof. Dr. Jörn Rittweger, Dr. rer. nat. Uwe Mittag, Prof. Dr. Thomas Voigtmann, Philipp Rauschendorfer

Weitere Personen waren an der Erstellung der vorliegenden Arbeit nicht beteiligt. Insbesondere habe ich nicht die Hilfe einer Promotionsberaterin/eines Promotionsberaters in Anspruch genommen. Dritte haben von mir weder unmittelbar noch mittelbar geldwerte Leistungen für Arbeiten erhalten, die im Zusammenhang mit dem Inhalt der vorgelegten Dissertationsschrift stehen.

Die Dissertationsschrift wurde von mir bisher weder im Inland noch im Ausland in gleicher oder ähnlicher Form einer anderen Prüfungsbehörde vorgelegt.

Im Rahmen erster Versuche zu Spatial Gain Sonography wurde das Ethikvotum für die Verwendung von Rindermuskeln bereits durch Philipp Rauschendorfer und Prof. Dr. Jörn Rittweger eingeholt. Nach Konzeption der Studie durch mich mit Unterstützung von Prof. Jörn Rittweger erfolgte die Aufnahme der Ultraschallsequenzen durch mich. Das Programm zur Bestimmung der relevanten Parameter in den Ultraschallbildern entwickelte Dr. rer. nat. Uwe Mittag mit der Software „Python“. Die Analyse der Bilder mithilfe dieser nahm ich vor. Die daraus extrahierten Daten wurden statistisch von Prof. Jörn Rittweger mit der Software „R“ ausgewertet. Die mathematisch-physikalische Einordnung der Ergebnisse erfolgte mit Unterstützung durch Prof. Thomas Voigtmann.

Erklärung zur guten wissenschaftlichen Praxis:

Ich erkläre hiermit, dass ich die Ordnung zur Sicherung guter wissenschaftlicher Praxis und zum Umgang mit wissenschaftlichem Fehlverhalten (Amtliche Mitteilung der Universität zu Köln AM 132/2020) der Universität zu Köln gelesen habe und verpflichte mich hiermit, die dort genannten Vorgaben bei allen wissenschaftlichen Tätigkeiten zu beachten und umzusetzen.

Köln, den 24.06.2024

Unterschrift:

¹Bei kumulativen Promotionen stellt nur die eigenständig verfasste Einleitung und Diskussion die Dissertationsschrift im Sinne der Erklärung gemäß dieser Erklärung dar.

Danksagung

Für die geduldige und vielschichtige Unterstützung durch alle Phasen der wissenschaftlichen Arbeit und deren Ermöglichung möchte ich mich vor allem bei meinem Doktorvater Prof. Dr. Jörn Rittweger herzlich bedanken.

Dr. rer. nat. Uwe Mittag danke ich vielmals für die umfangreiche programmiertechnische Unterstützung. Philipp Rauschendorfer hat seine ultraschalltechnische Expertise in außerordentlicher Weise eingebracht und Prof. Dr. Thomas Voigtmann hat dankenswerterweise geholfen, die mathematischen Feinheiten zu justieren.

Mein herzlicher Dank geht an alle Kolleg:innen am Institut für Luft- und Raumfahrtmedizin des Deutschen Zentrums für Luft- und Raumfahrt in Köln, nicht nur für die freundliche Aufnahme und angenehme Zusammenarbeit, sondern auch für die uneingeschränkte Bestärkung meines raumfahrtmedizinischen Interesses.

Bei den Mitarbeitenden der Arbeitsgruppe „Experimentelle Neonatologie“ von Prof. Dr. Bent Brachvogel des Universitätsklinikums Köln bedanke ich mich herzlich für die exzellente Beratung, insbesondere bei Christian Frie für das Einlernen in spezielle Labormethoden. Auch wenn die vorliegende Arbeit sich letztendlich auf makroskopische Methoden fokussiert, habe ich hier wertvolle Erfahrungen sammeln dürfen.

Meiner Familie, insbesondere meinen Eltern, kann ich nicht genug danken für die bedingungslose Unterstützung auch im Rahmen dieser Promotion. Danke für die Weitergabe wissenschaftlicher Neugier!

In Memoriam

Am 21.04.2025 verstarb Prof. Dr. med. Jörn Rittweger unerwartet. Während unserer Zusammenarbeit durfte ich durch seine geduldige Zielstrebigkeit und wissenschaftliche Präzision lernen, was es bedeutet, Forschung an der Schnittstelle von Muskelphysiologie und Raumfahrtmedizin voranzutreiben. Ich bin ihm sehr dankbar für die Begleitung auf dem Weg zur Promotion.

Mit der Veröffentlichung dieser Dissertation hoffe ich, einen Beitrag zur Verwirklichung seiner wissenschaftlichen Vision und zur Anwendung der Erkenntnisse in der Muskelanatomie und Bildgebung leisten zu können.

Table of Contents

LIST OF ABBREVIATIONS	6
1. SUMMARY	7
2. ZUSAMMENFASSUNG	9
3. INTRODUCTION	11
3.1. Outline of the dissertation	11
3.2. Anatomy of intramuscular connective tissue	11
3.2.1. Gross anatomic organization of muscle	11
3.2.2. Microscopic structure	14
3.2.3. Molecular composition of intramuscular connective tissue	15
3.3. Physiological function of intramuscular connective tissue	16
3.3.1. Organization of intramuscular structures	16
3.3.2. Force transmission	16
3.3.3. Elastic energy storage capacity of intramuscular connective tissue	17
3.4. Methods to quantify intramuscular connective tissue	17
3.5. Principles of muscle ultrasound analysis	18
3.5.1. Advantages of ultrasound compared to other modalities	18
3.5.2. Ultrasound wave generation	19
3.5.3. Ultrasound image generation	20
3.5.4. Current methods to quantify echo intensity in ultrasound	24
3.5.5. Influence of pennation angle on echo intensity in muscle	25
3.6. Physiological changes affecting echo intensity and intramuscular connective tissue	27
3.6.1. Echo intensity with age	27
3.6.2. Echo intensity with immobilization	28
3.6.3. Echo intensity with exercise	29
3.7. Measurement variables affecting echo intensity	31
3.7.1. Device settings and processing	31
3.7.2. Insonation angle	32
3.7.3. Pressure	34
3.7.4. Size of region of interest	34
3.7.5. Subcutaneous adipose tissue	34

3.7.6.	Scanning depth	34
3.7.7.	Scanning site in the muscle	35
3.8.	Hypotheses and objective of this study	36
4.	PUBLICATION	38
5.	DISCUSSION	58
5.1.	Summary of results	58
5.2.	Relevance of mean gray value and tilt echo gain	58
5.3.	Factors affecting mean gray value and tilt echo gain	59
5.3.1.	Anatomical location	59
5.3.2.	Age	60
5.4.	Technical limitations	60
5.4.1.	Fascicle alignment in other planes	60
5.4.2.	Scanning depth and gel pad	60
5.4.3.	Scanning site within the muscle	61
5.4.4.	Ultrasound processing software	61
5.5.	Reflection of intramuscular connective tissue content in echo intensity	62
5.6.	Comparability to human muscle in-vivo	63
5.7.	Clinical implications and potential clinical use	64
5.8.	Conclusion	65
5.9.	Outlook	65
6.	REFERENCES	67
7.	APPENDIX	77
7.1.	List of figures	77
7.2.	List of tables	77
8.	PRE-PUBLICATION OF RESULTS	78

List of Abbreviations

α	pennation angle
DLR	Deutsches Zentrum für Luft- und Raumfahrt (German Aerospace Center)
ECM	extracellular matrix
ECR	extensor carpi radialis muscle
EDC	extensor digitorum communis muscle
EDL	lateral digital extensor muscle
EI	echo intensity
FCR	flexor carpi radialis muscle
FCU	flexor carpi ulnaris muscle
FHL	flexor hallucis longus muscle
FL	fibularis longus muscle
FPA	fascicle probe angle
FT	fibularis tertius muscle
GA	gel pad angle
IMAT	intramuscular adipose tissue
IMCT	intramuscular connective tissue
MGV	mean gray value
MGV_00	mean gray value at 0° fascicle probe angle
MRI	magnetic resonance imaging
PSO	psoas major muscle
RF	rectus femoris muscle
ROI	region of interest in ultrasound images
ROICy	scanning depth or y-coordinate of the region of interest center
SAT	subcutaneous adipose tissue
SCH	infraspinatus muscle
SSP	supraspinatus muscle
TEG	tilt echo gain
ϑ	insonation angle and angle of reflection at the fascicle

1. Summary

The breadth of functions attributed to muscle has only recently been grasped, augmenting it from mere body locomotor to important metabolic and endocrine organ. Its structure, supported by intramuscular connective tissue, is cause and consequence of many functional changes in the muscle. Each muscle fiber is surrounded by endomysium; perimysium in turn engulfs several muscle fibers forming a fascicle. Epimysium forms the outermost layer of a muscle and is also known as fascia in clinical contexts. In pennate muscles, fascicles are not parallel to the epimysium but lie at an angle allowing for more force to be generated per muscle cross-sectional area. Changes of intramuscular connective tissue are difficult to track in a non-invasive and inexpensive way. While ultrasound offers a chance to do so, it lacks reliability as each measurement is highly dependent on operator and subject variables such as probe tilt, ultrasound device settings, muscle pennation angle and subcutaneous fat layer.

Ultrasound waves are emitted from a probe and travel through connective tissue and muscle at different speeds of sound. At each tissue interface a portion of them is reflected to the probe. B-mode ultrasound images consist of pixels of different gray values determined by the sound energy received at the probe, which is also called *echo intensity*.

Echo intensity in muscle increases with age and immobilization, but also in muscular dystrophy, which may be attributed to muscle atrophy and denser intramuscular connective tissue under these circumstances. This relationship allows for tracking muscle quality with ultrasound and eventually could help with early detection of muscle pathology. However, echo intensity decreases with increasing pennation angle if not corrected for. Similarly, different probe tilts lead to differing echo intensities, i.e., a low inter-rater reliability. This study aimed to establish a relationship between the insonation angle and echo intensity in order to mathematically integrate this relationship in future measurements or even implement it in future devices.

From the laws of specular reflection, we hypothesized (1) that the highest echo intensity would result from a perpendicular insonation of muscle fascicles, i.e., with the probe parallel to the fascicle. The mean gray value (MGV) of the ultrasound image at 0° of fascicle probe angle (FPA) would then be comparable between muscles without the bias of probe tilt or pennation angle. Next, we hypothesized (2) that the relationship between MGV and FPA could be mathematically modeled and (3) that this would result in a trigonometric function.

51 muscles of *Bos taurus* from overall 10 different anatomical locations were scanned post-mortem at 5 different insonation angles using an angulated ultrasound gel pad. The ultrasound scans were obtained in longitudinal orientation to the fascicles with the skin, subcutaneous fat and the superficial fascia removed. All ultrasound settings remained constant throughout measurements. Pennation angle, tilt angle of the probe and mean gray value in a region of

interest were measured, the relationship between FPA and MGV was analyzed and the slope of the linear function for each muscle was calculated (*tilt echo gain*; TEG).

Computation of FPA to MGV revealed a sinusoidal fit, confirming hypotheses 2 and 3. At smaller FPAs the relationship could be modeled with a linear fit with high enough accuracy. The linear fit was used for further calculations as it would be more user-friendly in the clinical setting. We found that MGV was indeed highest at an FPA of 0° for every muscle aligning with our first hypothesis. Both MGV at 0° FPA (MGV_00) and TEG showed muscle-specific differences. They also behaved differently across muscles indicating that they reflect different features of muscle architecture. In mixed effect models age was significant for MGV_00.

Limitations of this study include the unknown effect of internal image processing of the ultrasound software which is inherent to all commercial scanners. Changes in echo intensity could also have been caused by employing an ultrasound gel pad resulting in a slight variability in scanning depth. However, no significant muscle-specific effects were detected for the depth of the region of interest suggesting that scanning depth did not affect the results. While new parameters for measuring echo intensity were found in this study, it cannot be determined whether MGV_00 and TEG correlate with the amount of IMCT, which is a topic of ongoing research. Finally, age could only be made available for part of the animals resulting in limited validity of the data regarding the relationship between age and MGV_00.

This study established and validated a new method to quantitatively measure echo intensity in muscles using angulation, from here on referred to as *spatial gain sonography*. MGV_00 and TEG serve as more objective parameters than echo intensity alone, especially with regards to probe tilt, and might serve as new muscle-specific variables to compare between or track muscle echo intensity over time. This will allow for future muscular ultrasound studies to be more comparable and is one step in the necessary standardization towards reliable ultrasound diagnostics of musculoskeletal pathologies.

2. Zusammenfassung

Das breite Spektrum der Funktionen von Muskulatur wurde erst kürzlich erfasst und deren Stellenwert damit von simplem Bewegungstreiber zu metabolisch und endokrin aktivem Organ angehoben. Die strukturelle Architektur des Muskels, unterstützt durch intramuskuläres Bindegewebe, ist dabei Ursache und Folge vieler funktioneller Anpassungen. Jede Muskelfaser ist von sogenanntem Endomysium umgeben, während Perimysium mehrere Muskelfasern umschließt und damit ein Faszikel bildet. Epimysium, auch als Faszie bezeichnet, bildet die äußerste Schicht des Muskels. In gefiederten Muskeln liegen die Faszikel nicht parallel zum Epimysium, sondern in einem Winkel, der eine größere Kraftgenerierung bei gleicher anatomischer Querschnittsfläche erlaubt. Veränderungen von intramuskulärem Bindegewebe lassen sich nicht-invasiv und kosteneffizient mittels Ultraschall quantifizieren. Jedoch ist die Zuverlässigkeit solcher Messungen bisher kompromittiert, da jene stark von Variablen wie Schallkopfneigung, Geräteeinstellungen, Fiederungswinkel und subkutaner Muskelschicht abhängen.

Ultraschallwellen werden von einer Ultraschallsonde emittiert und setzen sich in Bindegewebe und Muskel mit jeweils unterschiedlichen Schallgeschwindigkeiten fort. An jeder Grenzfläche zweier Gewebe wird daher ein Teil der Wellen zur Sonde zurück reflektiert. Ein B-Mode Ultraschallbild besteht aus Pixeln unterschiedlicher Grauwerte in Abhängigkeit von der empfangenen Schallenergie, der sogenannten *Echointensität*.

Die Echointensität von Muskel steigt mit höherem Alter und Immobilisierung an, aber auch im Rahmen neuromuskulärer Krankheiten, wie zum Beispiel bei Muskeldystrophie, was in Muskelfaseratrophie und Verdichtung des intramuskulärem Bindegewebes begründet liegen könnte. Diese Abhängigkeit erlaubt, Aussagen über die Muskelqualität mithilfe von Ultraschall zu treffen und könnte in Zukunft die Früherkennung von Muskelerkrankungen erleichtern. Allerdings muss beachtet werden, dass die Echointensität mit einem zunehmenden Fiederungswinkel aufgrund simpler akustischer Gesetzmäßigkeiten sinkt. Ebenso führt variable Sondenneigung zu unterschiedlichen Echointensitäten, das heißt auch zu einer niedrigen Interrater-Reliabilität. Das Ziel dieser Studie war, eine mathematische Beziehung zwischen Schallwinkel und Echointensität zu etablieren und diese dann in zukünftigen Messungen zu verwenden.

Anhand des Reflexionsgesetzes stellten wir die Hypothese auf, (1) dass die höchste Echointensität bei senkrechter Beschallung der Faszikel auftreten würde, das heißt mit einer zu den Faszikeln parallel gehaltenen Sonde. Der *mittlere Grauwert* (MGV) des Ultraschallbildes bei einem *Faszikelsondenwinkel* (FPA) von 0° wäre anschließend zwischen verschiedenen Muskeln und ohne den Einfluss der Sondenneigung vergleichbar. Als nächstes stellten wir die Hypothese auf, (2) dass das Verhältnis zwischen MGV und FPA mathematisch zu rekonstruieren sei und (3) dass dies in einer trigonometrischen Funktion resultieren würde.

51 Muskeln von *Bos taurus* insgesamt 10 verschiedener anatomischer Lokalisationen wurden dafür post-mortem mit fünf verschiedenen Schallwinkeln mittels einer geneigten Vorlaufstrecke mit Ultraschall untersucht. Haut, subkutanen Fettgewebe und die oberflächliche Faszie wurden zuvor entfernt. Die Geräteinstellungen wurden über alle Messungen hinweg unverändert gehalten. Der Fiederungswinkel, der Sondenneigungswinkel und der mittlere Grauwert wurden in longitudinaler Richtung zu den Faszikeln gemessen und anschließend das Verhältnis zwischen FPA und MGV analysiert sowie der Anstieg der linearen Funktion jedes Muskels berechnet (*Tilt Echo Gain*; TEG).

Die Aufzeichnung von MGV über FPA ergab eine sinusoidale Regression, was Hypothese 2 und 3 bestätigt. Für kleinere FPA war es möglich, eine lineare Regression mit ausreichender Genauigkeit zu erhalten. Zur Vereinfachung in der klinischen Anwendung wurde diese lineare Funktion für die weiteren Berechnungen verwendet. Entsprechend unserer ersten Hypothese konnte der höchste MGV bei einem FPA von 0° (MGV_00) gemessen werden. MGV_00 und TEG zeigten zudem muskel-spezifische Unterschiede. Sie verhielten sich über verschiedene Muskeln hinweg nicht gleichgerichtet, repräsentierten also unterschiedliche Eigenschaften der Muskelinnenstruktur. Das Alter der Tiere war signifikant für MGV_00 in der Berechnung in gemischten Modellen. Eine Limitierung dieser Studie ist die unklare Bildverarbeitung durch die interne Ultraschallsoftware, über die jedes kommerzielle Ultraschallgerät verfügt. Veränderungen der Echointensität könnten zudem durch die Vorlaufstrecke und damit unterschiedliche Schalltiefen entstanden sein. Es konnten jedoch keine signifikanten muskelspezifischen Effekte für die Tiefe der Messregion festgestellt werden, was eine Beeinflussung der Ergebnisse durch die Schalltiefe nahezu ausschließen lässt. Mit MGV_00 und TEG konnten neue Parameter für die Beschreibung von Echointensität ermittelt werden, jedoch kann nicht beurteilt werden, ob diese mit dem Gehalt an intramuskulärem Bindegewebe korrelieren, was weiterhin Gegenstand der Forschung ist. Schließlich ist die Validität der Aussagen zum Verhältnis von Alter und MGV_00 eingeschränkt, da das Alter nur für einige der Tiere verfügbar war.

In dieser Studie wurde eine neue Methode zur quantitativen Messung der Echointensität von Muskeln mittels Sondenneigung, ab hier als *Spatial Gain Sonography* bezeichnet, etabliert und validiert. MGV_00 und TEG sind objektivere Parameter als Echointensität allein, vor allem in Bezug auf die Sondenneigung, womit sie als neue muskelspezifische Variablen zum Vergleich zwischen Muskeln oder Messzeitpunkten dienen können. Dies führt zukünftig zu besser vergleichbaren Ultraschallstudien des Muskels und ist ein wichtiger Schritt der Standardisierung auf dem Weg zu zuverlässiger Ultraschalldiagnostik muskuloskelettaler Pathologien.

3. Introduction

3.1. Outline of the dissertation

The musculoskeletal system allows humans to stand, walk, breathe, grasp, speak and much more. The consequences of muscle deterioration become apparent during rehabilitation of patients after long hospitalization or of astronauts returning from microgravity. Either can lead to lasting pathology or accidents which explains a clinician's interest in quantification of these changes. Muscle is composed of muscle cells and connective tissue and both change during training and immobilization. This dissertation looks at the interface of ultrasonic images with the objective to render intramuscular connective tissue more accurately quantifiable and trackable over time and between patients.

The introduction will give an overview of muscle anatomy and physiology and take a closer look at the function of *intramuscular connective tissue* (IMCT). An overview of the methods to analyze IMCT that are already established will be given with an emphasis on ultrasound. Basic principles of ultrasound will briefly be discussed leading up to the main parameter used in this study: *echo intensity* (EI). The introduction will outline how this value changes under different physiological conditions and how it links to IMCT. Parameters confounding with EI measurements will also be introduced and their significance for this study subsequently dissected in the discussion.

The publication that resulted from this dissertation describes the critical step of standardizing the measurement of EI in 'Material and Methods'. The results of the study can also be found in the publication. In turn, a separate and in-depth introduction and discussion are to follow in this dissertation.

The objective of this study was to derive an equation that models the relationship between EI and insonation angle in order to then determine more objective parameters than pure EI to quantitatively assess internal muscle structure.

3.2. Anatomy of intramuscular connective tissue

3.2.1. Gross anatomic organization of muscle

Muscle is composed of muscle cells surrounded by connective tissue which in turn consists of fibroblasts and extracellular matrix (ECM). Skeletal muscle cells are also called muscle fibers due to their long and threadlike appearance. A muscle fiber is composed of several hundred rod-like organelles, the myofibrils.

In the past the majority of research on changes regarding function and pathology in skeletal muscle has been focused on the remodeling of muscle fibers only.¹ However, in recent years it was found that IMCT plays a similarly crucial role in muscle growth, repair, and functionality.² Muscle ECM and IMCT are both being used in the literature. The term intramuscular

connective tissue will be employed here, as the focus lies (a) on the entire tissue surrounding muscle cells including muscle ECM and connective tissue cells and (b) on the intramuscular part of connective tissue, i.e., endo- and perimysium rather than epimysium. IMCT serves as a scaffold for muscle fibers, organizing them into subunits increasing in size. Each muscle fiber is surrounded by endomysium (**Figure 1**).¹

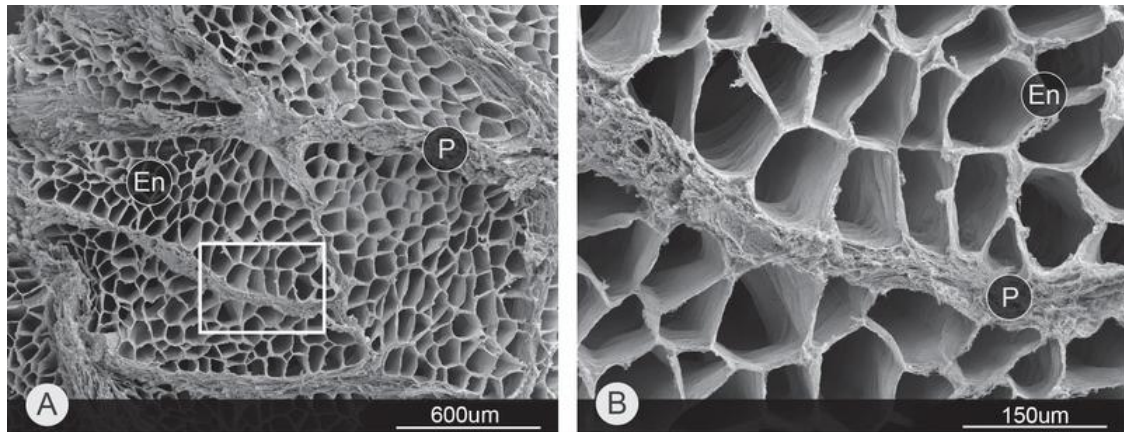


Figure 1: Scanning electron microscopic images of a domestic turkey's lateral gastrocnemius muscle. **A** Cross-section that shows morphological distinction between endomysium (En) and perimysium (P) and **B** close-up view of the white rectangle in A. (adapted from Sleboda et al.³ and used with permission)

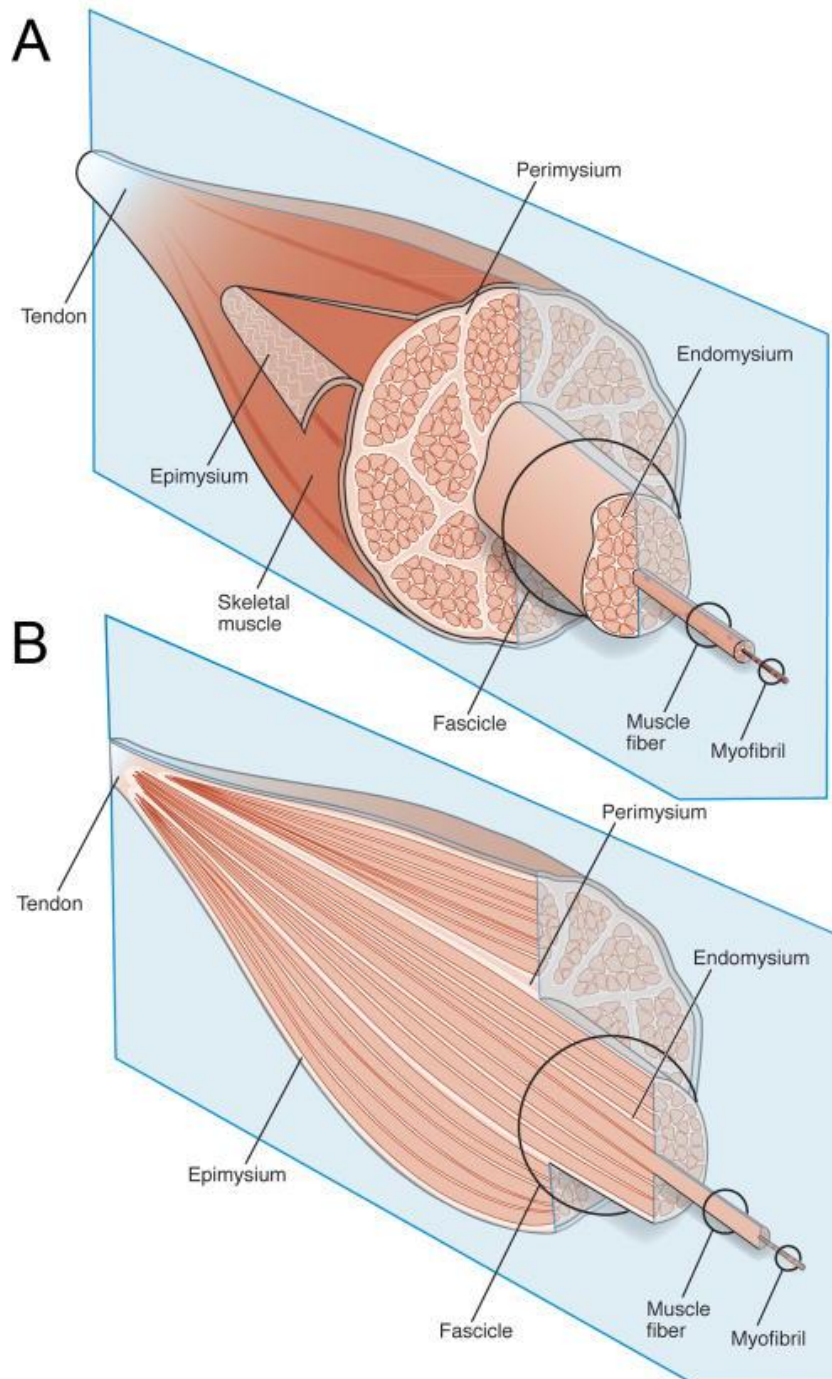


Figure 2: **A** Schematic drawing of the macroscopic organization of muscle fibers and IMCT and **B** its cross-section. Myofibrils make up muscle fibers which are surrounded by endomysium. Several muscle fibers form a fascicle which is in turn encompassed by perimysium. Many fascicles form a muscle enclosed by epimysium. The cross-sectional image is a simplification: in reality, not all perimysial strands reach the tendon. (From Gillies and Lieber et al.¹ and used with permission).

Multiple endomysial strands are organized as perimysium forming a muscle fascicle (**Figure 1, Figure 2**). The structure of the perimysium has notoriously been difficult to study as it is too large for microscopic quantification and too small for macroscopic analysis. Another reason for the paucity of studies on the perimysium lies in its uncertain delineation. In contrast to the endomysium which is found exclusively and ubiquitously between muscle fibers, fascicles

surrounded by perimysium are harder to discern in any imaging method and perimysium is often seamlessly connected to the tendon.¹ Several muscle fascicles are held together by epimysium (**Figure 2**). This thickest form of connective tissue of the muscle is identical to the outer muscle “fascia”, a term that is usually adopted by clinicians and physiotherapists. Rather than being part of its internal structure, the epimysium surrounds a full muscle. While dividing IMCT into the above entities allows for didactic clarity, it seems that these subunits have been defined rather arbitrarily and that the organization of IMCT is much more complex when examined under the microscope.¹

In addition to the hierarchy of IMCT, it is important to understand that muscle fibers in most muscles are oriented in an oblique fashion.⁴ With the fibers not being parallel to the fascia, a so-called *pennation angle* is created that will be of importance in this work.

3.2.2. Microscopic structure

Järvinen et al. was able to distinguish between endomysium and perimysium in qualitative scanning electron microscopic analysis.⁵ Even though the main direction of fiber in perimysium is often hard to distinguish, three distinct networks can be discerned, of which the longitudinal and orthogonal can be seen in **Figure 3**.

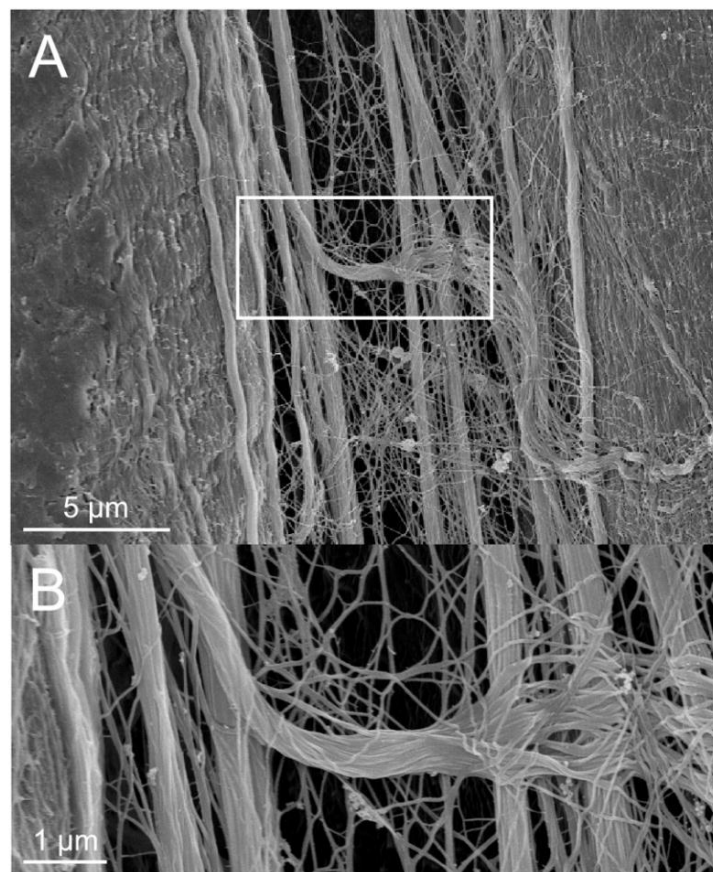


Figure 3: **A** Scanning electron micrograph of mouse EDL showing longitudinal perimysial strands. A cross-linking strand in the white box is enlarged in image **B**, showing it fraying

across several longitudinal strands when connecting to a neighboring muscle fascicle. (from Gillies and Lieber et al.¹ and used with permission).

In endomysium, the main collagen fiber orientation is longitudinal to the muscle fiber. These fibers lie directly on the surface of the muscle fiber. The second layer consists of collagen fibers that run orthogonally to the long axis of the muscle fiber and attach to adjacent muscle fibers. The third part of the network is formed by collagen fibers that surround intramuscular nerves and blood vessels.

Collagen fibers are built of many collagen fibrils, which in turn are polymers of helical tropocollagen. Under the microscope the wavy structure of collagen fibers becomes apparent, a feature that allows for compliance in IMCT, i.e., avoiding rupture upon acute stretching. The curvature of the collagen fiber, the so-called *crimp angle*, differs between muscles and can change depending on the type and frequency of the muscle's use⁵ (**Figure 4**).

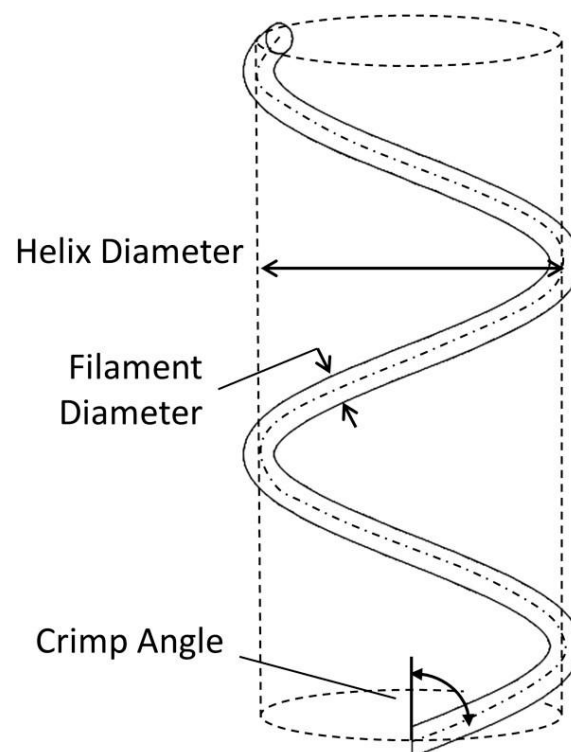


Figure 4: Schematic diagram of a crimped collagen fiber. Collagen fibers form a helix with a crimp angle that allows for compliance when the fiber is stretched, e.g., due to muscle extension. (From Vorhees et al.⁶ with permission to use according to the terms of the Creative Commons Attribution License (<http://creativecommons.org/licenses/by/2.0>))

3.2.3. Molecular composition of intramuscular connective tissue

Extracellular matrix in muscle is composed of collagens, glycoproteins, proteoglycans and elastin. Collagen forms the central fibers of IMCT and is produced by dedicated IMCT

fibroblasts. The endomysium, its adhesions to the myofibrils, the perimysium and the epimysium are composed of different types and ratios of the 28 collagens so far described.⁷ The fibril-forming type I and III collagen represent the majority of collagens in all entities of muscular connective tissue. Type I collagen consists of strong parallel fibers which are responsible for the tensile strength and rigidity of the muscle. Type III collagen forms a looser fiber network allowing for compliance of the tissue.⁸ Perimysium consists primarily of type I collagen and the proteoglycan decorin, a composition distribution it shares with tendon tissue (Gillies und Lieber 2011). The basement membrane of muscle cells, predominantly consisting of collagen IV, is intimately connected to the endomysium which highlights the role of IMCT in force transmission from the muscle tissue to the tendon.⁹

3.3. Physiological function of intramuscular connective tissue

Movement generated by muscles stems from the interaction of myosin and actin molecules converting chemical energy from ATP into kinetic energy. The minimal quantity of these forces becomes relevant only at the level of the muscle where thousands of muscle fibers¹⁰ are joined to one another and to the tendon, namely by connective tissue. This section shall briefly highlight the relevance of IMCT in structural organization, force transmission and muscle elasticity to underline the importance of studying it.

3.3.1. Organization of intramuscular structures

IMCT lends muscle its structure in order to function as a unit. It also embeds blood vessels and neurons for both the muscle as a whole and each individual muscle fiber.¹¹ In fast twitch fibers which use (anaerobic) glycolysis for energy transformation, capillaries can be found on each corner of the polyhedral muscle fiber. In contrast, in slow twitch muscle which transforms chemical energy aerobically using oxygen, there are additional capillaries along the endomysial sheath between the corners.

Besides accommodating blood vessels and nerves, IMCT, especially the perimysium, serves as a deposit for intramuscular fat.¹² Increased *intramuscular adipose tissue* (IMAT) - which can be a consequence of immobilization, injury and systemic disease - leads to decreased contractile strength of the muscle as a whole.¹³ With regard to imaging studies, it is important to recognize that both IMCT and IMAT undergo quantitative changes under these conditions and are sometimes hard to distinguish.

3.3.2. Force transmission

IMCT serves as a scaffold and glue for the contractile portion of the muscle. It is not an active contractile element itself, but is connected to muscle fibers at focal adhesions, which allow for its crucial role in force transmission during muscle contraction. Contractile forces in the

myofibrils are transmitted through the muscle fiber directly to the tendons that connect to bones in order to move joints. However, it has been observed that a significant percentage of muscle fibers end within the fascicle and never reach the tendon.^{14,15} This suggests that the longitudinal transmission is not the only pathway of force transmission in the muscle. It was shown (a) in mice that force is transmitted equally well longitudinally and laterally through shear of the endomysium¹⁶ and (b) in a mathematical model that even more than 50% of the force transmission in muscle occurs laterally.¹⁷ The idea of force transduction from one muscle fiber to another via endomysium can be expanded into the concept of lateral load sharing. This mechanism also allows for sustained function during repair of damaged sarcomeres and muscle growth: The IMCT network keeps the strain uniform across fibers and avoids loss of function of a whole contractile strand while the torn muscle fiber is repaired or new sarcomeres are added during muscle lengthening.¹⁸

3.3.3. Elastic energy storage capacity of intramuscular connective tissue

In addition, IMCT contributes to the elastic properties of muscle, i.e., the capability to return to its original shape after strain is applied.¹² In 1949, Hill proposed that the mechanical properties of a muscle can be described with three elements: a contractile element and an elastic element in series in addition to an elastic element in parallel to these.¹⁹ This became known as the “Hill-type three element model”.¹² In part this has been proven by demonstrating the parallel tensile strength of the endomysium: In an experiment correlating stress and strain in human muscle, the tensile load bearing capacity of an endomysium and muscle fiber bundle was significantly higher than that of muscle fibers alone.²⁰

3.4. Methods to quantify intramuscular connective tissue

As a structure-lending force transmitter, elastic load bearer and metabolic influencer, IMCT has gained academic importance in the past two decades thus various methods were developed to evaluate its quality and quantity for fundamental research and diagnostic purposes.

On the molecular level, IMCT can be explored via proteomics, quantifying proteins involved in ECM organization.^{21,22} Likewise, biochemical studies of collagen have been performed for quantification of changes, although these solely reveal content, not structural features.^{23,24} Microscopically, the morphology of stained muscle cross section can be analyzed (**Figure 5**) as well as composite distribution through immunohistochemical staining.^{25,26} All these methods require a biopsy or post-mortem muscle. Due to their invasiveness, they are neither rapidly available nor infinitely repeatable. Next to physiological metrics that can be obtained in compliant volunteers, macroscopic imaging tools have been used increasingly in the past years due to their non-invasiveness. These include the very readily available and cost-efficient

ultrasonography²⁷⁻³⁰ and shear wave elastography to examine muscle stiffness^{31,32}, as well as computed tomography, conventional magnetic resonance imaging and diffusion tensor imaging^{33,34}.

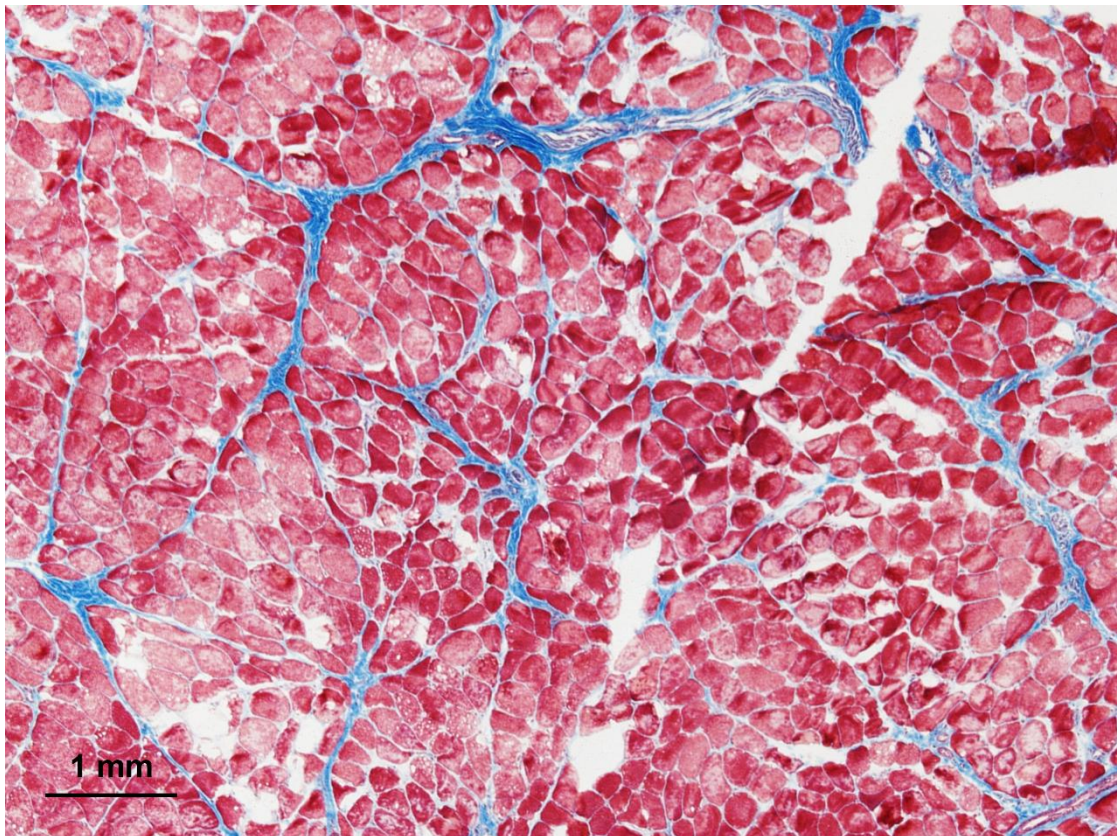


Figure 5: Trichrome stain of bovine muscle, 5-fold enlargement. Modified Masson stain (adapted from Sigma-Aldrich Procedure No. HT15, revised 11/2016) using Bouin's solution, iron hematoxylin, Biebrich scarlet-acid fuchsin and aniline blue. Muscle cells are stained pink, IMCT fibers surrounding muscle, nerves and blood vessels are stained blue. Dark purple staining of nuclei was unsuccessful in this stain for unknown reasons. Large white areas are shearing artefacts. While perimysium is well visible, endomysium is not stained in all regions, which might indicate loss of it during freezing, cutting or staining. Even though perimysium can be made visible under the microscope, its size relative to the image and irregularity in thickness suggests that one section of this size is not representative of its content in the whole muscle or even muscle region. (Image by the author in collaboration with the research laboratory of Prof. Dr. Bent Brachvogel of the University Hospital Cologne)

3.5. Principles of muscle ultrasound analysis

3.5.1. Advantages of ultrasound compared to other modalities

Ultrasound has some advantages compared to other modalities for muscle and IMCT evaluation. First of all, it is non-invasive which makes it more patient-friendly and suitable for tracking a person's muscle quality at multiple time points without lasting damage. Its rapidness

and lack of contraindications render it even more suitable for point-of-care use.³⁵ Devices can still be relatively large, but are more easily transportable compared to an MRI or CT scanner. Increasingly, handheld ultrasound probes linked to mobile devices as screens and control units are being tested in the clinical context and even in remote environments such as the International Space Station.³⁶

Finally, ultrasonography can provide real-time and high resolution images which is especially important in the study of muscle physiology and architecture as the direct changes during muscle contractions become quantifiable.³⁵

3.5.2. Ultrasound wave generation

Ultrasound waves are longitudinal waves with a frequency greater than 20 kHz, i.e., above the threshold for human hearing.³⁷ They are formed by an alternation of compression and relaxation of molecules in a medium. This is often depicted as a unidirectional wave for simplicity (**Figure 6**). The cells or molecules in a tissue or liquid serve as coupled oscillators. The speed of propagation of sound c through the tissue depends on the characteristics of their bonds and is defined as the frequency multiplied by the wavelength of the sound waves. For example, the speed of sound in muscle ($c = 1580 \text{ m/s}$) is higher than in water at body temperature ($c = 1524 \text{ m/s}$)³⁸.

In an ultrasound transducer, ultrasound waves are generated by piezoelectric crystals. These crystals change their conformation upon application of an electrical current (inverse piezoelectric effect) generating a wave, and create a change in voltage upon mechanical impact (piezoelectric effect). This means that in an ultrasound probe the piezoelectric crystals serve both as emitter and receiver of the ultrasound waves.

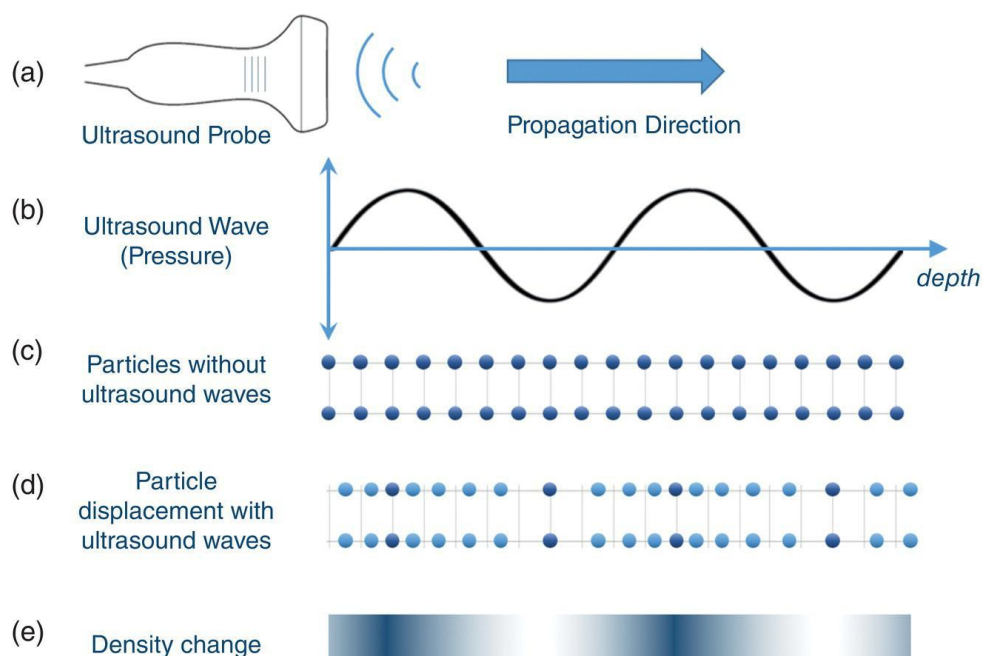


Figure 6: Schematic model illustrating ultrasound wave propagation in a medium. Ultrasound leads to an alternation of compression and rarefaction in a medium, depicted as particles in a network here (c, d). The change in local density (e) leads to a pressure change in the medium that can be modeled with a wave (b). (From Harput et al.³⁹ and used with permission)

Apart from frequency and wavelength, a sound wave emitted from an ultrasound probe is defined by its amplitude which in turn depends on sound intensity. Brighter ultrasound images may be obtained through increasing the voltage to the crystals, thereby increasing the output power. Intensity is defined by the power over the cross-sectional area of the sound waves and is proportional to the square of the wave's amplitude.³⁷

3.5.3. Ultrasound image generation

While in computer tomography and magnetic resonance imaging tissues are directly depicted, it is the interactions at boundaries of tissues with differing properties that are visualized in ultrasound.³⁷ Different ultrasound modes exist that generate images in different manners:

B-mode (for brightness) was used in this study and is used in many clinical settings for identification and scaling of bodily structures. Each pixel in the image is assigned a brightness value according to the energy received at the probe. Traveling time of the ultrasound waves determines the location of the pixel. In A-mode (for amplitude), the amplitudes of waves are computed over time as they travel back to the probe (**Figure 7**). This mode is hardly used anymore. In M-mode (for motion), one longitudinal band of the image is shown over time, so that moving structures, such as heart valves, can be examined more closely.

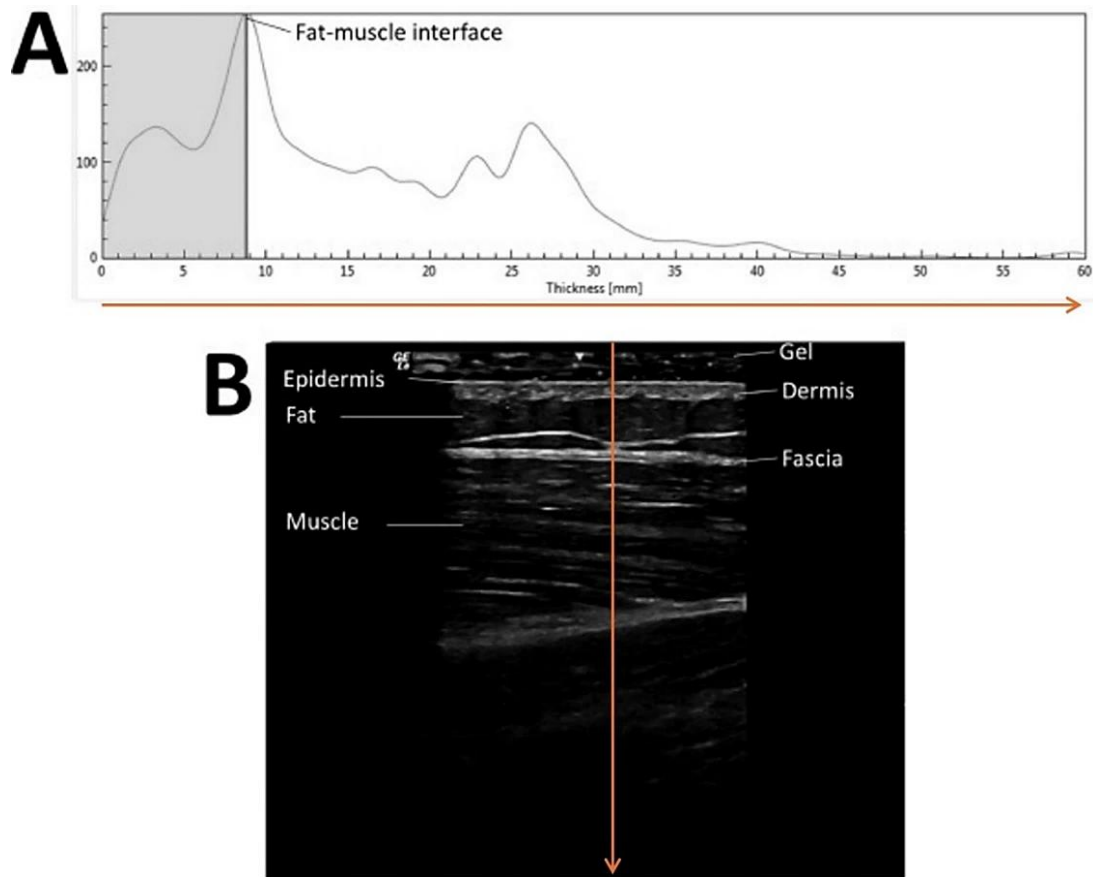


Figure 7: Comparison of A-mode and B-mode ultrasound images. In A-mode the amplitude of received ultrasound waves in one line is displayed. In B-mode, these amplitudes from several lines (orange line as an example) are converted into pixels with the respective brightness and displayed as an image. (From Wagner et al.⁴⁰ and used with permission)

All modes have in common that they derive from soundwaves modified at tissue interfaces converted into images. The depiction of these interfaces is determined by acoustic impedance which itself depends on the densities and the speeds of sound in the respective tissues:

$$Z = \rho \cdot c$$

Z = acoustic impedance

ρ = density of medium

c = speed of sound in medium

Tissue	Speed of sound (m/s) (Average across studies)
Muscle	1588.4
Connective Tissue	1545.0
Tendon/Ligament	1750.0
Bone (cortical)	3514.9
Brain	1546.3
Fat	1440.2
Water (20°C)	1482.3

Table 1: Speeds of sound in different tissues. (Adapted from: Hasgall et al.⁴¹)

The reflected intensity at an interface of two tissues can be calculated using their specific acoustic impedances³⁸ derived from the speeds of sound within them (**Table 1**):

$$\frac{I_R}{I_0} = \left(\frac{Z_2 - Z_1}{Z_1 + Z_2} \right)^2$$

I_R = reflected intensity

I_0 = insonation intensity (at perpendicular insonation)

Z_1 = acoustic impedance of tissue 1

Z_2 = acoustic impedance of tissue 2

Connective tissue and muscle have different acoustic impedances leading to a tissue interface that reflects sound waves, which becomes apparent in an ultrasound image of a muscle scanned transversally to the fascicles: hypoechoic parts represent muscle tissue and hyperechoic parts IMCT due to the difference in impedance at their interfaces⁴² (**Figure 8**).

With increasing acoustic impedance of a tissue, attenuation of ultrasound waves increases. Within a whole muscle, the acoustic impedance stays constant. Interestingly, due to its anisotropic structure, muscle as a whole has different attenuation coefficients from different scanning angles: perpendicular fibers have an attenuation coefficient of 0.96 and parallel fibers of 1.40 dB/cm at 1 MHz⁴³.

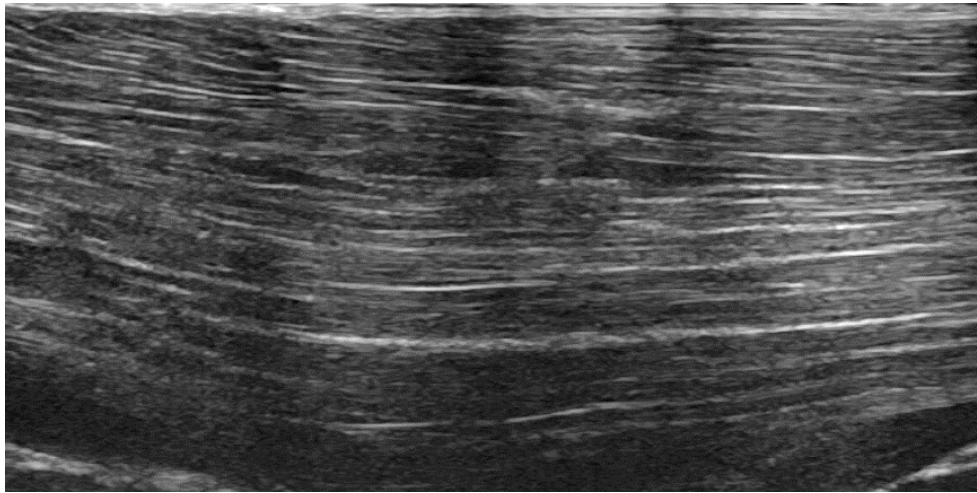


Figure 8: Ultrasound image of a bovine muscle (extensor digitorum communis; EDC) in fascicle-aligned orientation which highlights the anisotropic nature of muscle. IMCT is represented by hyperechoic and muscle fiber by hypoechoic lines.

At tissue interfaces four phenomena occur: reflection, absorption, refraction and scattering (**Figure 9**, and Figure 1 of publication)

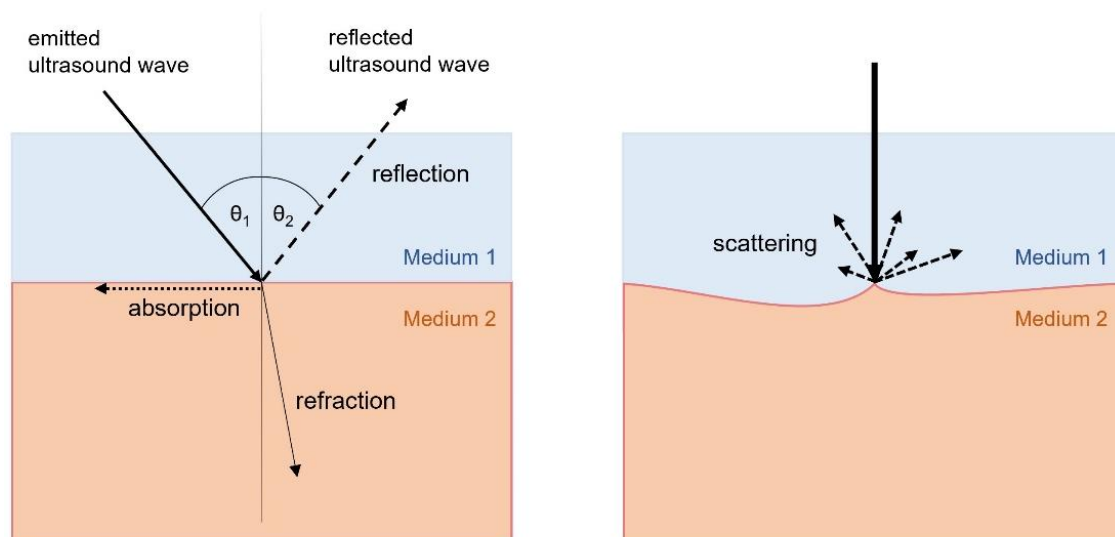


Figure 9: **A** Reflection and refraction of an ultrasound ray at the interface of two media of different acoustic impedance. The insonation angle θ_1 is equal to the reflection angle θ_2 while the refraction angle is larger or smaller depending on the direction of impedance change. Part of the ultrasound wave energy is absorbed by the tissue leading to an increase in tissue temperature. **B** If surface irregularities within the range of the ultrasound wavelength are encountered, the ultrasound ray is scattered in many, but unpredictable directions.

At defined and clear borders of two surfaces with differing acoustic impedance, part of the ultrasound waves is reflected - with the incident angle equal to the reflection angle as shown in **Figure 9**, part is transmitted through the medium at a different angle (refraction) and part is absorbed by the tissue. If the medium surface has inconsistencies that are in the range of the

wavelength of the ultrasound wave, the waves are scattered, i.e., their energy is passed on in various directions.⁴⁴ Ultrasound images are a mixture of signals from reflected and scattered waves.³⁷ Reflected energy will be represented in a determined location on a B-mode ultrasound image while scattering has a more probabilistic distribution. Hence, structures that merely scatter elevate EI but cannot be visually identified. Both phenomena affect the brightness of the tissue behind them in the direction of the ultrasound beam.³⁸

The question arising is how to predict whether an ultrasound wave is reflected or scattered, i.e., whether the interface will be distinguishable on a B-mode image. One could also ask: what is the minimal thickness of a strand of IMCT for ultrasound to still detect it?

This question can be answered by calculating the axial resolution. In ultrasound, axial and lateral resolution determine to what degree of detail the tissue can be pictured. The axial resolution depends on the wavelength. A higher ultrasound frequency allows for a higher resolution, but the maximum reachable depth will simultaneously decrease due to attenuation. Theoretically, the highest reachable resolution is half the wavelength.³⁷

This means that if the emitted frequency were 10 MHz in muscle ($c = 1580 \text{ m/s}$), the wavelength would be $\lambda = \frac{c}{f} = \frac{1580 \frac{\text{m}}{\text{s}}}{10 \cdot 10^6} = 158 \cdot 10^{-6} \text{ m} = 158 \mu\text{m}$. The maximum reachable resolution would therefore be $\frac{158 \mu\text{m}}{2} = 79 \mu\text{m}$. The thickness of endomysium in healthy young humans is approximately $9 \mu\text{m}$.²⁶ With a frequency of 15 MHz the resolution is $52.5 \mu\text{m}$. This means that in the longitudinal direction, endomysium muscle fiber interfaces would hardly lead to reflection with either frequency. The wavelength is too high. Perimysium in bovine muscle as was examined in this study can range in thickness between 30 to $120 \mu\text{m}$ ⁴⁵ depending on which hierarchical level the perimysium is measured at. Therefore, parts of perimysium will cause reflection of ultrasound when using a frequency of 10 or 15 MHz.

Lateral resolution describes the ability to discriminate between objects in the plane perpendicular to the ultrasound wave and depends on the width of the wave.³⁷

3.5.4. Current methods to quantify echo intensity in ultrasound

EI is the sum of the ultrasound wave energy received by the piezoelectric ceramics in the probe, both from reflected and scattered beams. Acoustic energy is transformed into electricity and then translates into brightness of the respective pixel on the B-mode image. EI has not been described quantitatively for a very long time. A first approach was the Heckmatt scale, a four-level scale based on the visual appearance of the muscle and bone distal to it in ultrasound.⁴⁶ A more quantitative approach uses gray values. The mean gray value can be calculated in the whole image or a region of interest, with black represented by a gray value of 0 and white by 255.³⁰ Interventional studies have also grouped these gray values into EI bands, looking at the increase or decrease of the number of gray value pixels, for instance, in the 0-

50 or 200-255 EI band, arguing that these changes offer different and perhaps more tissue content specific information than the mean gray value.⁴⁷

3.5.5. Influence of pennation angle on echo intensity in muscle

In muscle, EI alteration through reflection is of particular significance because unlike in tissue consisting of near round cells that have the same properties from any direction, muscle does not possess this characteristic. Due to its long cylindric muscle fibers, it is anisotropic meaning its reflection will differ if scanned from different directions even though the tissues' acoustic impedance remains unchanged.^{38,42} This anisotropy leads to the characteristic depiction of skeletal muscle in ultrasound with layers of long fascicles visible in the longitudinal scanning plane.

For this work it is important to understand that ultrasound beams are reflected most when they encounter a surface perpendicularly.³⁷ At a different angle, less energy is directed back to the ultrasound probe leading to a lower EI and a lower brightness on the image (**Figure 10**). This is a phenomenon that was exploited and characterized in this dissertation.

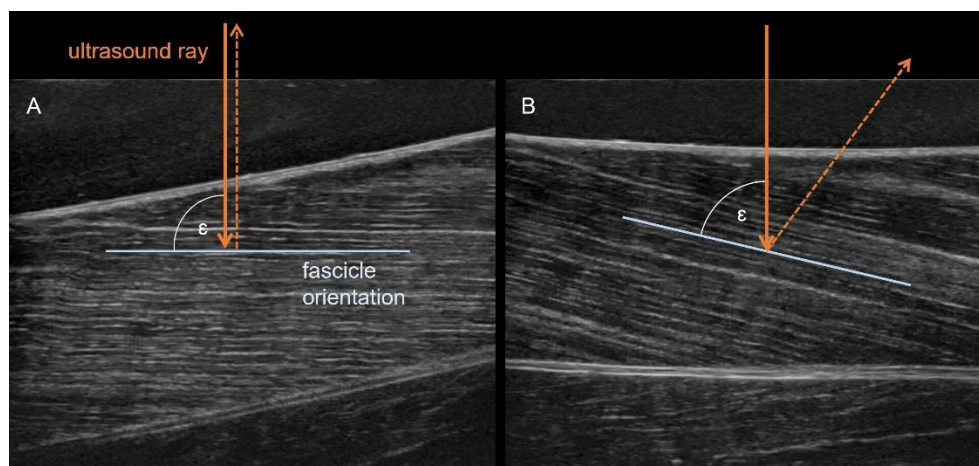


Figure 10: A Bovine muscle scanned perpendicularly to the fascicle orientation versus **B** at a different angle. Scanning at 90° leads to an overall brighter image, i.e., an increased echo intensity.

In addition, the fascicles in many muscles lie at an angle to the epimysium or the aponeurosis as demonstrated in an ultrasound image in **Figure 11**. This angle is called pennation angle. It allows for more and shorter muscle fibers instead of few long ones to be arranged in a muscle, thereby increasing the potential force that can be produced in a given muscle area (**Figure 12**).⁴

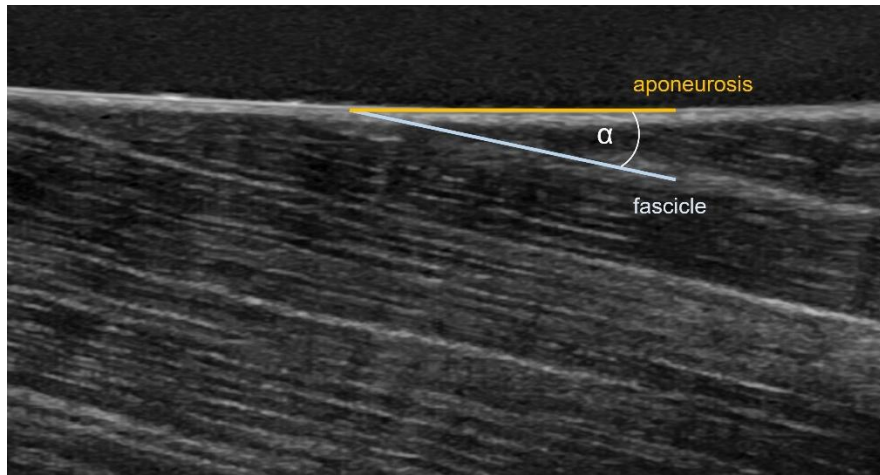


Figure 11: Ultrasound image of an infraspinatus muscle in fascicle-aligned orientation showing an angle α between aponeurosis and fascicle, called pennation angle.

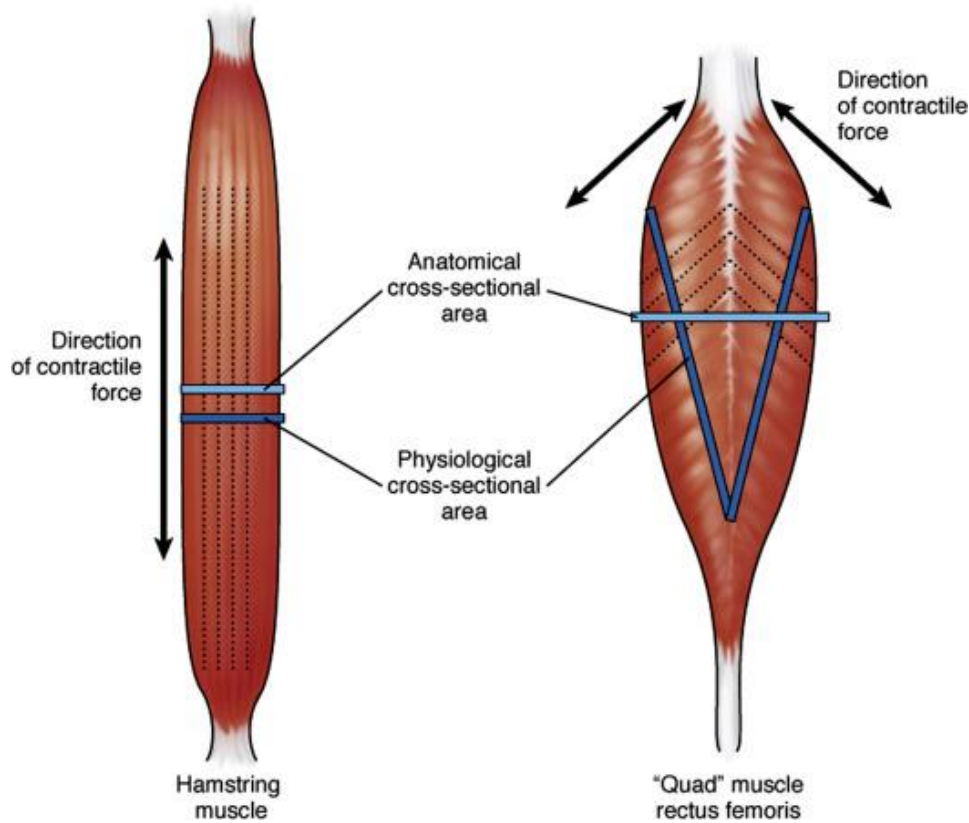


Figure 12: Schematic demonstration of the function of the pennation angle as shown in a comparison of a non-pennate human hamstring muscle and a pennate rectus femoris muscle. The pennation allows for a larger physiological cross-sectional area in reference to the anatomical cross-sectional area. The pennate muscle can therefore create more force over the same size. (From Carlson et al.⁴⁸ and used with permission)

As each muscle fascicle is surrounded by perimysium creating echo interfaces, EI will depend on pennation angle. Oftentimes, it is therefore not possible to compare echo intensities of muscles that are scanned perpendicularly to the skin since their pennation angle differs and

affects EI. It has become common practice to obtain ultrasound images at the angulation that yields the highest EI visually.^{49,50} This practice is of course highly subjective and leads to variability between examiners, a problem the method presented in this work aims to solve. Besides pennation angle, other physiological factors such as physical exercise and aging can affect EI which shall be introduced in the next section.

3.6. Physiological changes affecting echo intensity and intramuscular connective tissue

It has been shown in a study of dogs with muscular dystrophy that increased EI correlates with a higher amount of fibrous tissue in the muscle which can be explained by an increased amount of ultrasound energy being reflected due to more tissue interfaces causing a jump in acoustic impedance.³⁰ Alterations of the muscle do not have to be as drastic as in muscular dystrophy – changes of EI can already be observed with physiological changes in aging, unloading and exercise. Awareness to these changes as additional factors influencing EI in muscle ultrasound studies shall be raised in this section. The effects of aging and training status on IMCT will be intercalated and finally both compared in **Table 2**.

3.6.1. Echo intensity with age

With age, IMCT content per area increases²⁵ and muscle fibers are lost or atrophy⁵¹ leading to a smaller muscle diameter^{25,52,53}. This would lead to an increase in EI since more reflecting structures are located within the same area compared with younger muscle. Indeed, studies have shown that EI increases with age^{29,54}, the correlation was found to be muscle-specific and non-linear.²⁷ Referring to the prior section, it should be noted that pennation angle decreases with age. According to ultrasound physics, this could automatically lead to an increased EI. A study showed however, that even after statistically correcting for this decrease in pennation angle, older subjects still had higher EI in the gastrocnemius muscle, suggesting that a change in intramuscular tissue composition could be responsible.⁵⁵

Bali et al. proposed that strength instead of age is the better predictor of EI since muscle strength had a much stronger correlation with EI than age.⁵⁶ The studies included only untrained subjects, i.e., with less than 4 sessions of lower-extremity exercise in a month. There was still a positive if weak correlation between age and EI, though this highlights the importance of stratification into trained and untrained subjects in ultrasound studies.

Fukumoto et al. attempted this by grouping elderly subjects into higher and lower physical activity group in a longitudinal 4-year-study.⁵⁷ Interestingly, they found a decrease in EI over 4 years in the highly active group and no change in EI in the group with low physical activity. This implies that some of the effects of aging could be “reversed” by physical activity. Certainly,

caution should be taken when interpreting EI values relating to age without any information on physical strength or activity level.

3.6.2. Echo intensity with immobilization

As physical training seems to play an important role in muscle EI in ultrasound, the next two sections shall illuminate the effects of immobilization and exercise.

Although the effects of immobilization are easily measurable in bedridden patients or in immobilized extremities after injury, very few studies exist on the matter. One study showed that after knee joint immobilization in young volunteers, vastus lateralis muscle but not rectus femoris muscle EI increased.⁵⁸ Of note, the *cross-sectional area* (CSA) of the muscle decreased with immobilization suggesting that increases in EI are a direct effect of muscle atrophy paired with a relative increase of IMCT per CSA. It had been thought for a long time that absolute IMCT content increases during immobilization, after tenotomy or after denervation of a muscle.^{59–62} However, no increase in endomysium thickness could be observed during immobilization but only an increase in IMCT content per CSA due to muscle atrophy, i.e., a relative increase.²⁶ Nevertheless, it has been observed that endomysium forms more fibers, especially more perpendicular cross-links between muscle fibers during unloading⁵ (**Figure 13**) and perimysium becomes more disorganized (**Figure 14**) suggesting that new reflection and scattering of ultrasound waves due to an altered IMCT structure on the fiber level could cause an increase in EI.

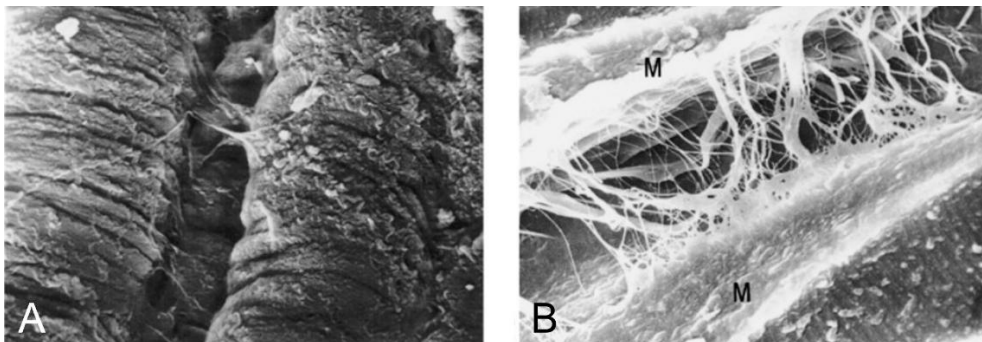


Figure 13: A Normal soleus muscle. **B** Immobilized soleus muscle. The number of endomysial collagen fibers running perpendicularly to the muscle fiber increases in immobilized muscle. (From Järvinen et al.⁵ and used with permission)

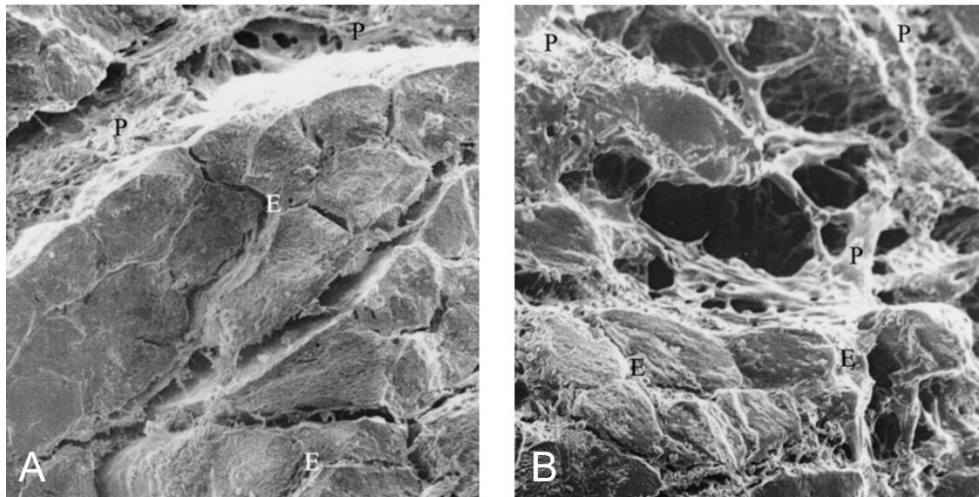


Figure 14: **A** Normal gastrocnemius muscle **B** Immobilized gastrocnemius muscle. The amount of connective tissue is visibly increased in immobilized muscle with the perimysium becoming more disorganized. (From Järvinen et al.⁵ and used with permission)

Microgravity and bed rest studies offer an ideal testbed especially for lower extremity unloading. However, while muscle ultrasound has been performed to measure muscle thickness⁶³, EI of muscle has not yet been measured in these settings.

3.6.3. Echo intensity with exercise

In a review of the existing literature, Wong et al. found nine studies in which EI decreased after repeated resistance exercise, nine with no significant change and three with an increase in EI.⁶⁴ The data are as heterogeneous as the speculation on the reasons for this. Potentially influential factors could be the length of the training period and timepoints of measurement that varied widely between studies ranging from one day⁶⁵ (acute effects) to 24 months⁶⁶ (chronic effects). It should be noted of course that the differences in findings could also be caused by differing technical parameters during ultrasound examination; this shall be discussed in the next section. Finally, it could be hypothesized that the type of muscle, for example antigravity muscles that support maintaining posture vs. non-antigravity muscles or muscles with more slow-twitch vs. fast-twitch fibers, could show a different reaction to acute and chronic training affecting EI. The heterogeneity of data continues into histological and biochemical IMCT studies where an increase in collagen content was found in pennate but not in non-pennate muscles in rabbits⁶⁷ and thickness of IMCT remained unchanged between sedentary and physically active mice⁶⁸. Immediately after training, collagen synthesis increases but long-term effects of endurance training on IMCT remain unknown.^{68,69} This highlights the challenges, but also the chances in detailed mapping of IMCT and EI. This study aims to propose a new method setting measurement standards to reduce heterogeneity in EI studies for more definitive results.

Condition	Intramuscular connective tissue (IMCT)	Echo Intensity (EI)
Age	<p>Denser and more regular IMCT (fewer cross-connections) but smaller area percentage and smaller total amount of collagen⁷⁰</p> <p>IMCT content per area increases²⁵</p>	<p>Increased EI with higher age^{29,54}, Caution: Correlation probably compromised by training status⁵⁶</p>
Immobilization	<p>IMCT content increases during immobilization, after tenotomy or after denervation of a muscle⁵⁹⁻⁶²</p> <p>Increase in IMCT fiber number especially in endomysium connecting muscle fibers perpendicularly⁵</p> <p>Increased relative amount of endomysium due to muscle fiber atrophy while absolute amount of endomysium measured by thickness remains unchanged after 55 days of bed rest²⁶</p> <p>Long-term: muscle fibers degrade and are replaced by fibrous tissue and fat⁶²</p>	<p>Increase in EI with immobilization^{58,71}</p> <p>Higher EI in subjects with less physical activity⁷²</p>
Exercise	<p>Resistance: 15-week jump training in rabbits increased muscle stiffness and collagen content only in pennate muscles EDL and RF (rectus femoris) but collagen content decreased in psoas major muscle⁶⁷</p>	<p>9 studies with decrease in EI, 9 with no change, 3 with increase in EI⁶⁴ with long-term exercise in most studies.</p> <p>Thereof one study with short-term effect (up to 72h after resistance exercise) showing an increase in EI⁶⁵</p>

	<p>IMCT thickness in sedentary mice compared to 10 week voluntary wheel running unchanged⁶⁸</p> <p>Endurance: Immediately after training with a peak at 24h, collagen synthesis increases in humans⁶⁹</p> <p>Structural effects and effects of habitual training unknown⁶⁸</p>	
--	---	--

Table 2: Overview of studies on effects of age, immobilization and exercise on IMCT structure vs. echo intensity. This table is not comprehensive but rather serves as a basis in the attempt to link IMCT structure and echo intensity.

3.7. Measurement variables affecting echo intensity

Given its high dependability on the examiner, ultrasound imaging naturally has some disadvantages in quantification and diagnostics compared to other tools. Similar to MRI, muscle thickness and cross-sectional area, pennation angle, fascicle length and EI can be measured using ultrasound.⁷³ These data can be used to broadly characterize muscle atrophy for example. However, some of these parameters, especially EI, have not been linked to clinical conditions with certainty.⁶⁴ One big challenge with ultrasound in regards to quantification is reliability between operators, evaluation methods and devices. A high degree of standardization is necessary for measurements by two different operators to yield the same results, for example in terms of experience in musculoskeletal ultrasound⁷⁴ or probe tilt⁷⁵. Moreover, ultrasound software has evolved to include complex algorithms to optimize images for clinical use so that comparison between devices is virtually impossible.⁷⁶ These variables limiting quantitative muscle ultrasonography shall be discussed in more detail and approaches for necessary standardization will be reviewed here.

3.7.1. Device settings and processing

Reliable measurements of EI in ultrasound require a set of constant device settings, e.g., frequency and gain. A higher frequency leads to better resolution but shallower penetration of the tissue and vice versa. A higher gain will increase the gray value in either the whole image or an image band chosen by the operator. Time Gain Compensation increases the gray value behind a structure that particularly attenuates or reflects ultrasound waves in order for it to be

visible in the clinical setting. These settings directly affect EI and should not be changed in between measurements.⁷⁷

Unfortunately, even if these settings were equal in two different ultrasound devices, two different values for EI can result. This is in part due to the postprocessing changes performed automatically. As all commercially available ultrasound devices use postprocessing software and raw data are hard to obtain due to restrictions by the manufacturers, this study will not be able to address this problem beyond keeping all device settings constant across all muscles.

3.7.2. Insonation angle

This study originated in the idea that the insonation angle takes an influence on EI by simple geometric consideration as demonstrated in **Figure 10**. Only two studies have quantified this effect before. Ishida et al. reported a decrease in EI of 7.8 % with a transducer tilt from 0 to 9° in the rectus femoris muscle.⁷⁵ Dankel et al. measured EI at -8 to 8° in 2° increments rolling the probe around its longitudinal axis and scanning the muscle transversally.⁷⁸ The greatest change in EI was detected in the tibialis anterior muscle, with 10.5% in a 2° tilt and a 29.5% change in EI with a 6° tilt. This underlines the importance of standardizing the probe tilt as the smallest changes in scanning angles inadvertently made by the examiner can lead to relevant changes in EI.

Another challenge in this regard involves the pennation angle. Even if the probe were to be held exactly perpendicular to the muscle, different pennation angles across muscles would still bias the results for EI. With EI being only measured at one angle, it is also hard to correct for pennation angle later on. Hence, this study proposes a method to avoid the influence of different angles between probe and fascicles altogether. This required taking measurements at a minimum of two different angles in the sagittal plane of the muscle, i.e., fascicle-aligned. Different insonation angles can be achieved by the machine's internal feature called *beam steering* (**Figure 15**, left). Beam steering results in a fixed insonation angle of 12°. In order to achieve higher angles manual probe tilt was adopted in addition in this study using an angulated ultrasound gel pad (**Figure 15**, right).

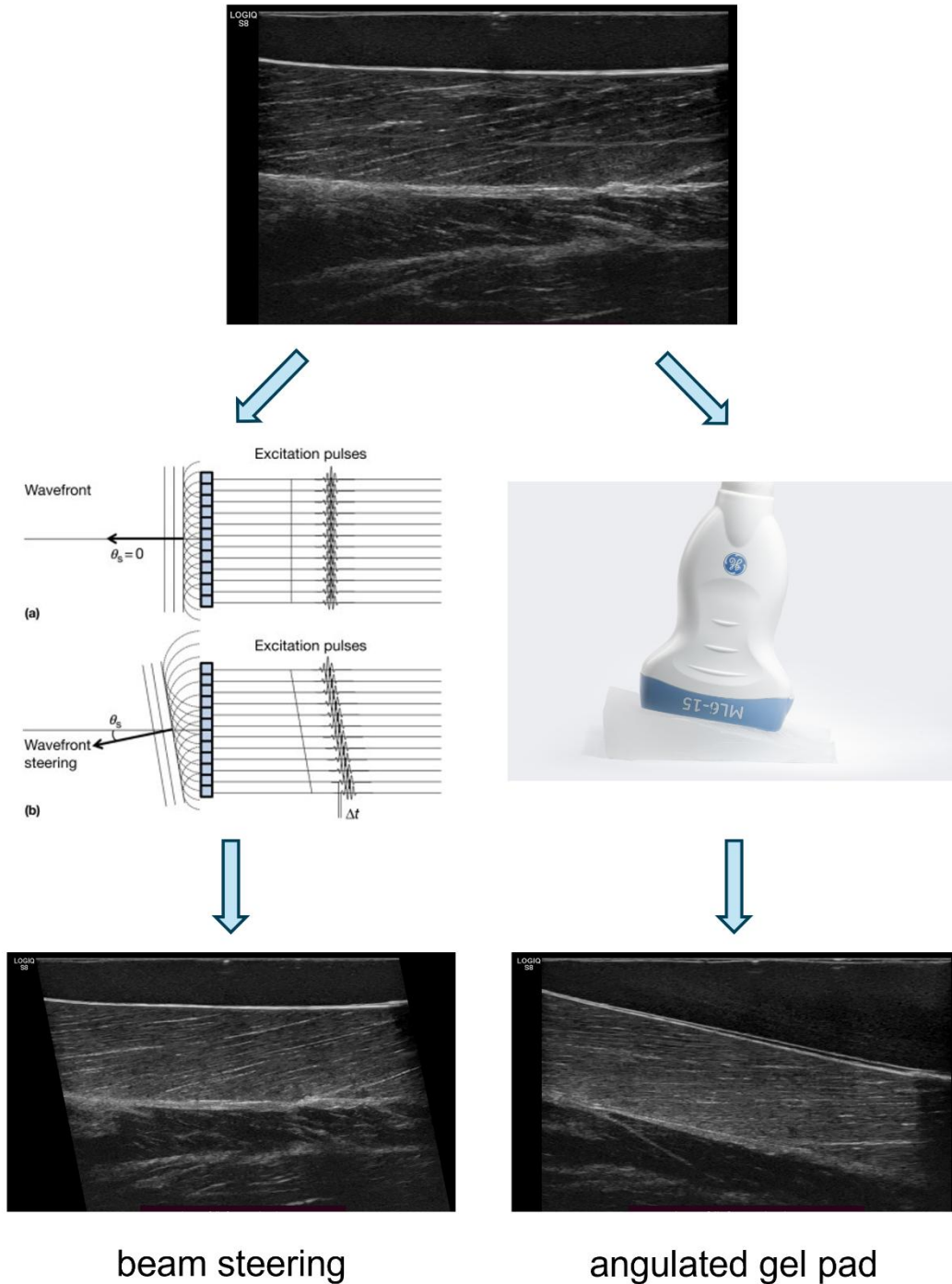


Figure 15: Changing the insonation angle via beam steering versus probe tilt with an angulated gel pad. **Top:** non-modified ultrasound image of a bovine *flexor hallucis longus* (FHL) muscle with visible layers of a flat gel pad, epimysium, muscle, aponeurosis (from the top). **Left:** Diagram of the mechanism behind beam steering. The ultrasound waves are emitted at different time points from the probe thereby creating a tilted wave front. This results in an angulated ultrasound image and an altered insonation angle, in this case by 12°. **Right:** Demonstration of an angulated ultrasound gel pad with a tilted probe on top of it and with the probe holder removed. This technique similarly results in an angulated ultrasound image and a new insonation angle. (middle left image from Thijssen et al.⁷⁹, middle right image by DLR, both used with permission)

3.7.3. Pressure

Pressure on the probe leads to deformation of muscle and will therefore change EI in ultrasound. One study showed that with increased probe pressure between 1.5 and 10 N, EI increased linearly. Additionally, inter-rater reliability for EI values was higher with near maximum pressure.⁸⁰ This implies that EI measured with minimal force, as is standard practice, increases variation in results. Ensuring higher pressure during examination for higher reliability poses a significant challenge as force applied can vary among examiners, and exerting maximum pressure may compromise patient comfort. Nevertheless, it is crucial to acknowledge and understand this relationship.

3.7.4. Size of region of interest

A region of interest (ROI) must be set either manually or automatically in the muscle on the ultrasound image in order to calculate a mean gray value within and to avoid confounding by vessels, nerves and epimysium. Studies have determined that the size of this ROI affects EI consistency between scans with a trend towards higher consistency with greater ROI as would be expected for an average value, however, this relationship was non-linear.^{81,82} Importantly, one of these studies also found that the minimum ROI for a reliable evaluation of EI is about 15% of the maximal rectangular ROI.⁸² It is therefore not necessary to employ the maximum ROI for reliable EI values. The discussed study has limited applicability for the present project as the former used transverse muscle scanning while this work uses longitudinal (fascicle-aligned) scans. Nonetheless, we expect some convertibility to longitudinal scanning in terms of reliability. The ROI had to be kept relatively small in order to fit it in all images including those with extreme angulation. The ROI was always kept in the same location of the muscle, i.e., it was adjusted to the angulation of the probe accordingly.

3.7.5. Subcutaneous adipose tissue

Subcutaneous adipose tissue (SAT) absorbs a portion of the ultrasound wave energy, thus a thicker fat layer may decrease EI.^{28,83} Some studies nowadays match⁸⁴ or correct for subcutaneous tissue⁵⁶ using a coefficient experimentally determined by Young et al. which, however, neglected IMCT.^{85,86} In this study, ex-vivo muscles were conveniently scanned without a fat layer. Even the outer layer of epimysium was removed for minimal confounding.

3.7.6. Scanning depth

Similar to an additional layer of tissue, ultrasound waves are attenuated more the deeper they travel into the tissue. Hence, EI decreases with increasing depth.⁸⁷ It is therefore important to keep the scanning depth constant across measurements. In many studies, depth is allowed to be varied between subjects aiming to include the whole muscle in the image.^{27,56,81} This was

not necessary in this study as the ROI had to be small enough to avoid it from being placed outside of the muscle after angulation any way. Care was taken in the planning of the study so that the constant depth would lead to an ROI within the muscle in every type of muscle scanned. As mentioned before, it is also not necessary to include the whole muscle in the ROI for high reliability so that scanning depth could actually be kept constant across measurements in many more studies to avoid bias.

3.7.7. Scanning site in the muscle

Finally, it should be considered that ultrasound never results in a scan of the full muscle but only produces an image of a cross section at one site. This leads to the question whether EI is constant throughout the muscle. One study comparing two measurement sites in the rectus femoris muscle found that EI significantly differed between the two concluding that two muscle regions should not be used interchangeably for a reliable EI analysis.^{77,88} In this study the scanning site was constant within one muscle as no movement other than that of a robotic axis (**Figure 16**) was undertaken between scans. Between muscles however, scanning site may not have always been the same as priority was given to lack of vessels and large epimysial strands as well as large enough thickness of the muscle to be able to take appropriate images in all angle setting.

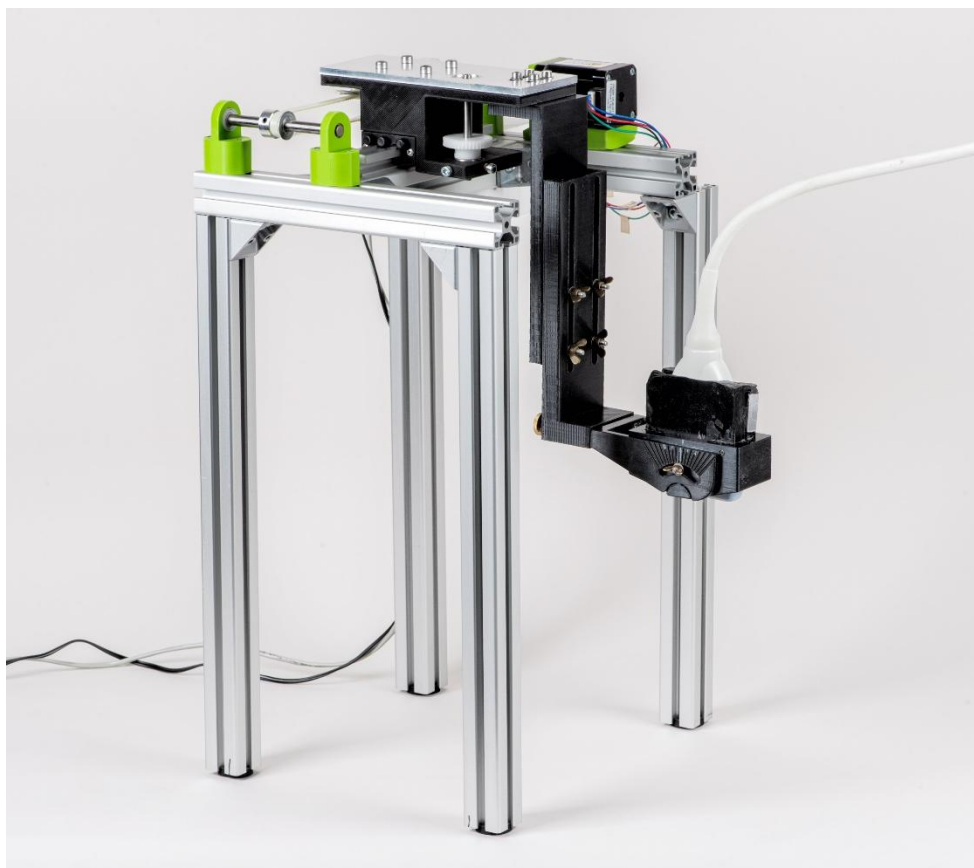


Figure 16: Robotic axis controlled by an Arduino UNO unit (*Arduino*, Monza, Italy) to perform small and precise movements and keep the probe in the same location during sequence recording for each angle. The set-up translates the probe in one direction only. A probe holder is attached to the axis, the gel pad was fixed to the probe and probe holder and placed between the probe and the bovine muscle. (Image by DLR)

The breadth of variables with potential to confound with EI highlights that standardization is a necessity in muscle ultrasonography. In in-vivo and diagnostic studies clinicians' skills, patient anatomy, especially varying layers of fat and skin, types of devices and device settings require particular attention. Hardly any degree of standardization will lead to results free of confounders, but in this ex-vivo animal study, many of the above-mentioned parameters were standardized in order to produce the most reliable data possible.

3.8. Hypotheses and objective of this study

The idea of this study originated in the phenomenon that EI of muscle will vary depending on the insonation angle. The angle between the probe and the insonated fascicles was named *fascicle probe angle* (FPA). The probe was placed in a longitudinal orientation to the fascicles. When FPA is 0° , i.e., the probe parallel to the fascicles, ultrasound rays hit the fascicles perpendicularly.

It was hypothesized (1) that echo intensity, represented by the mean gray value (MGV), would reach its maximum at an FPA of 0° . We also predicted (2) that the relationship between MGV and FPA could be mathematically modeled and (3) that this model would follow a trigonometric function.

This hypothesis is based on the laws of specular reflection that also apply to ultrasound. Changing the FPA from 0° by angulating the probe results in a change of the angle of reflection at the fascicle (ϑ). This displaces the reflected ultrasound ray by $\Delta x \propto \sin(2\vartheta)$ (**Figure 17**).

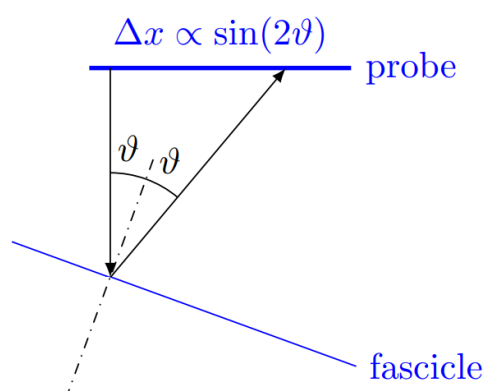


Figure 17: Schematic diagram of the reflection of an ultrasound ray at a fascicle with an insonation angle ϑ . Δx is the length of the probe. ϑ is the insonation and the reflection angle.

Since all reflected rays will be displaced by that amount, the MGV decreases. The more the angle approaches 0° again, the higher the MGV becomes, meaning there is a “gain in echo intensity”. We hypothesized that a function of the form $y = \beta_0 - \left(\frac{\beta_1}{2}\right) \sin(2x)$ would model this relationship, with x being ϑ and y being MGV. The coefficient β_0 represents scattering that does not depend on the individual fascicle’s reflection. Next, we hypothesized that for small FPAs, a simpler linear fit ($y = \beta_0 - \beta_1 \cdot x$) would be sufficiently accurate. We defined the slope of this function β_1 as *tilt echo gain* (TEG) and predicted that it would be muscle-specific depending on the respective IMCT architecture.

The aim of this study was to model the relationship between EI and insonation angle and to create two new valid parameters for EI quantification in muscle, namely the MGV extrapolated to an FPA of 0° (MGV_00) and TEG in order to surpass mere EI in independence of confounding parameters.

4. Publication



OPEN

Ex-vivo validation of spatial gain sonography for the quantification of echo intensity in fascicle-aligned ultrasound images in ten anatomical muscles in *Bos taurus*

Sophie C. Rosahl¹✉, Philipp Rauschendorfer¹, Lukas Arndt¹, Thomas Voigtmann^{2,3}, Uwe Mittag¹ & Jörn Rittweger^{1,4}

This study aimed to validate the concept of spatial gain sonography for quantifying texture-related echo intensity in B-mode ultrasound of skeletal muscle. Fifty-one bovine muscles were scanned postmortem using B-mode ultrasonography at varying fascicle probe angles (FPA). The relationship between mean gray values (MGV) and FPA was fitted with a sinusoidal and a linear function, the slope of which was defined as tilt echo gain (TEG). Macroscopic muscle cross sections were optically analyzed for intramuscular connective tissue (IMCT) content which was plotted against MGV at 0° FPA (MGV_00). MGV peaked at FPA 0°. Sine fits were superior to linear fits (adjusted r^2 -values 0.647 vs. 0.613), especially for larger FPAs. In mixed models, the pennation angle was related to TEG ($P < 0.001$) and MGV_00 ($P = 0.035$). Age was relevant for MGV_00 ($P < 0.001$), but not TEG ($P > 0.10$). The correlation between the IMCT percentage and MGV_00 was significant but weak ($P = 0.026$; adjusted $r^2 = 0.103$). The relationship between fascicle probe angle and echo intensity in B-mode ultrasound can be modeled more accurately with a sinusoidal but more practically for clinical use with a linear fit. The peak mean gray value MGV_00 can be used to compare echo intensity across muscles without the bias of pennation angle.

Keywords Intramuscular connective tissue, Fascia, Musculoskeletal ultrasonography, Spatial gain ultrasonography, B-mode ultrasound

Abbreviations

α	Pennation angle
DLR	Deutsches Zentrum für Luft- und Raumfahrt (German Aerospace Center)
ECR	Extensor carpi radialis muscle
EDC	Extensor digitorum communis muscle
EDL	Lateral digital extensor muscle
FCR	Flexor carpi radialis muscle
FHL	Flexor hallucis longus muscle
FL	Fibularis longus muscle
FPA	Fascicle probe angle
FT	Fibularis tertius muscle
GA	Gel pad angle
IMCT	Intramuscular connective tissue
MGV	Mean gray values
MGV_00	Mean gray value at 0° fascicle probe angle
MRI	Magnetic resonance imaging

¹Institute of Aerospace Medicine, German Aerospace Center (DLR), Cologne, Germany. ²Institute of Material Physics in Space, German Aerospace Center (DLR), Cologne, Germany. ³Institute of Theoretical Physics, Heinrich-Heine-Universität, Düsseldorf, Germany. ⁴Department of Pediatrics and Adolescent Medicine, University Hospital Cologne, Cologne, Germany.

PSO	Psoas major muscle
ROI	Region of interest in ultrasound images
ROI _{Cy}	Scanning depth or y-coordinate of the region of interest in ultrasound images
SCH	Infraspinatus muscle
SSP	Supraspinatus muscle
TEG	Tilt echo gain

The role of connective tissue in muscle

Intramuscular connective tissue (IMCT) is essential to the functioning of the muscle. The smallest entity of IMCT is endomysium which surrounds muscle fibrils in interconnected tubular sheaths¹. Several muscle fibers forming a fascicle are engulfed in perimysium. The whole muscle is surrounded by epimysium. Together, these IMCT entities tightly connect the contractile components of the muscle, organize and uphold the structure of the muscle², transmit forces generated by the myofibrils³, and allow for plasticity during growth or injury of the muscle⁴. They also connect to other connective tissues, which have been referred to as 'fascia' in the recent past⁵.

Quantification of intramuscular connective tissue

Evidence suggests that IMCT composition, structure and quantity are altered with age^{6–8}, by muscle loading^{9,10}, by immobilization^{11–14} and in diseases such as spastic cerebral palsy¹⁵ and Duchenne muscular dystrophy¹⁶. Therefore, analyzing IMCT is of diagnostic, therapeutic and prognostic value. Microscopic analyses reveal the structure mainly of endomysium^{12,13} and do not allow for perimysium content assessment. In addition, ex-vivo observations require a muscle biopsy, hence are not feasible for rapid assessment or long-term tracking. A non-destructive, non-invasive, simple, and objective method is desirable for assessment of IMCT quantity and structure. While magnetic resonance imaging studies allow for an overview and volume analysis⁶, a more readily available and more cost-effective method is muscle ultrasonography¹⁷. Pillen et al. found that the ultrasound echo intensity increases in dystrophic muscle¹⁸. On physical grounds it can be expected that the structure of IMCT leaves an imprint on echo intensity. Our study aims to explore and exploit this connection further.

Ultrasonography of intramuscular connective tissue

Ultrasound waves are reflected at surfaces where materials of differing acoustic impedance adjoin¹⁹. The border between perimysium and muscle fibers comprises one of the main differences in acoustic impedance.

The angle of insonation influences echo intensity (Fig. 1A). The measured reflection is strongest when the ultrasound rays hit the surface perpendicularly and the ultrasound probe is oriented parallel to the surface¹⁹.

We hypothesize that echo intensity is highest at a fascicle probe angle (FPA) of 0°—when probe and fascicle are parallel (hypothesis 1). We further hypothesize that the relationship between echo intensity and FPA can be mathematically modeled (hypothesis 2). It is also hypothesized that this model is best described by a trigonometric function that can be derived from the laws of specular reflection at the fascicles (hypothesis 3). Lastly, we suggest that this model can be well approximated with a linear relationship between MG_V and FPA.

Therefore, we propose that the rate of change in echo intensity per change in FPA will differ for each muscle depending on the architecture of its IMCT. This ratio will be termed tilt echo gain (TEG) here. Notably, a similar technique utilizing angulation in ultrasound has proven useful in detecting experimental inflammation in tendons^{20,21}, albeit without mathematical foundation and analysis.

We have conceptualized these above ideas and submitted them for patent (Deutsches Marken- und Patentamt, 10 2019 118 823.7). The present study aimed to validate tilt echo gain by testing our hypotheses 1 to 3.

Materials and methods

Provenience and preparation of sample muscles

Ultrasound images of 51 limb and torso muscles of *Bos taurus* were obtained. All animals were female and of either one of the breeds "Rotbunt" and "Schwarzbunt". Due to the availability of samples only of different age for female and male cattle (only older bulls or young calves) at the abattoir, an un-biased sex comparison was not possible and therefore an analysis of solely female cattle was performed. To emulate in-vivo analyses in humans, post-mortem muscles of domestic cattle were used. The bovine limbs and torso muscles were obtained within 24 h after slaughter from the abattoir *Schlachthof Frenken* in Düren, Germany, where they were cooled at 6 °C, and brought to the lab at the Institute of Aerospace Medicine at the German Aerospace Center (DLR), Cologne, in cooled state. The limbs and muscles were then stored in a refrigerator at 5 °C until their examination zero to two days after retrieval. Before ultrasound scanning was started all muscles were allowed to warm to room temperature (20 °C) to allow for comparability. The animals' age could be made available by the abattoir only in 12 out of 24 animals.

Ten different muscles were analyzed. From the forelimb, extensor carpi radialis (ECR), flexor carpi radialis (FCR), and extensor digitorum communis (EDC) muscle were scanned. Muscles from the hindlimb included the lateral digital extensor (EDL), fibularis longus (FL), fibularis tertius (FT) muscle and the deep digital flexor muscle with the flexor hallucis longus muscle (FHL) as part of it. Torso muscles included the supraspinatus (SSP), infraspinatus (SCH) and psoas major (PSO) muscle. For ultrasound measurements, the superficial fascia was removed and limb muscles remained attached to the bone.

Ultrasound scanning procedures

Ultrasound images were obtained using the linear-array probe ML6-15 of a GE LOGIQ S8 ultrasound device (GE Healthcare, Milwaukee, WI, USA) in B-mode with a center frequency of 15 MHz. Ultrasound device settings were kept constant between all measurements, using a scanning depth of 3.5 cm and a gain of 50 dB. Time gain control and CrossXBeam were turned off to avoid corrections to individual images by the ultrasound software.

The limbs or muscles were affixed onto a board. Ultrasound video sequences were obtained with the ultrasound probe placed on the epimysium—which can also be referred to as the aponeurosis—where the muscle fascicles insert. The probe was in longitudinal alignment with the muscle fascicles (Fig. 1A).

Using a 3D-printed probe holder, the probe was mounted to a robotic axis run by an Arduino UNO (Arduino, Monza, Italy). The robotic axis allowed for translation of the probe holder by 14.04 mm in a single direction during an ultrasound video sequence (Fig. 1B). Three images from each sequence were used later in order to increase internal validity. The probe holder facilitated to keep the manually adjusted angulation setting of the probe consistent in relation to the epimysium and the longitudinal axis of the fascicles. The robotic axis allowed for consistency of the scanning site between measurements at different angles. An ultrasound gel pad (Vorlaufstrecke SONOKIT soft, 200 × 100 × 40 mm, Co. Sonogel, Bad Camber, Germany; ultrasound velocity $c = 1460 \frac{\text{m}}{\text{s}}$, absorption coefficient $a = 0.053 \frac{\text{dB}}{\text{MHz mm}}$) cut to angles of 0°, 12° and 24° was used for each measurement. Ultrasound video sequences were obtained at 0°, 12°, 24°, -12°, and -24° probe angle in relation to the epimysium (Fig. 1A).

Preparation of muscle sections and imaging

Muscles were subsequently cut transversally into three parts equal in length and frozen at -25 °C. Muscle cross sections of 1 mm thickness were obtained from each of the three parts using a cutting machine (Slicer Master M20, Graef, Arnsberg, Germany). After fixation in a 1:10 37%-formaldehyde/tenfold-PBS buffer solution for four hours, each muscle section was photographed according to a standardized procedure with constant camera and lighting parameters using a digital single-lens mirrorless camera with a macro lens. These images were then segmented via thresholding using the machine learning software *ilastik: Interactive Learning and Segmentation Toolkit* (ilastik Team, 2011) that was initially fed with data from manual segmentation differentiating between IMCT and muscle visually. The images were then evaluated for IMCT content using the percentages of pixels above and below that threshold determined by the machine learning algorithm for all images (Fig. 1D).

Image processing

A three-step custom-made Python algorithm (Python 3, <http://www.python.org>), QuantICUS (Quantification of Intramuscular Connective tissue with Ultrasound) in version 1.0, was developed to extract single images from the ultrasound video sequences at the same locations in each muscle and to determine the pennation angle α , FPA (Fig. 1c) and mean gray value (MGV) in a region of interest (ROI) of the same rectangular size and orientation in each image (for further details see Supplementary Material “Image Processing: Calculation of Pennation Angle and Fascicle Probe Angle”).

Data processing

Output data from the QuantICUS tool were further processed and analyzed with R (<http://www.r-project.org>) in its version 4.2.2 by merging data obtained from separate muscles into one database. Homogeneity of frames within sweeps was verified by statistically testing for the effect of frame number (i.e. of probe translocation) upon epimysium angle and MGV, which both were found to be non-significant (linear mixed effect models from R-package ‘nlme’, all $P > 0.20$). Accordingly, all frames were included in the analysis.

Next, we assessed the relationship between FPA and MGV, hypothesizing that a trigonometric function would serve this purpose (s. Figure 1A). Fitting was effectuated with the basic R-function ‘lm’, with a prior sine-transformation of the independent variable ($y = \beta_0 - (\beta_1/2) \cdot \sin(2x)$ where x is the absolute value of FPA). For comparison and simplicity reasons, we also tried a linear fit ($y = \beta_0 - \beta_1 \cdot x$) which can be derived from the trigonometric function for smaller angles when $\sin(2x)$ approximates $2x$. To compare between both fitting results, we used residual plots and quantile–quantile plots to judge residual deviation from normality, and also Akaike’s information criterion.

To finally obtain spatial gain sonography results, we then fitted a linear relationship between FPA and MGV for all individual muscle specimens, in order to arrive at estimates for the expected gray value at FPA 0° ($\text{MGV}_{00} = \beta_0$). Tilt echo gain (TEG) was then computed as $100 \cdot \beta_1 / \beta_0$, to give the % change in MGV per FPA change (s. Table 2).

Statistical analyses

Correlations between TEG values were performed with the R-function ‘lm’ after visual inspection of the plots. The following criteria were adopted to interpret the magnitude of the correlations: $r < 0.1$, trivial; $0.1 < r \leq 0.3$, small; $0.3 < r \leq 0.5$, moderate; $0.5 < r \leq 0.7$, large; $0.7 < r \leq 0.9$, very large; and $r > 0.9$, almost perfect²⁰.

Linear mixed effect models were run with the R-function ‘lme’ to compare differences in pennation angle α with ‘Muscle’ as fixed factor and animal ID as random effect. Similarly, differences in MGV_{00} , TEG, and in ROI_{Cy} (y-coordinate of the region of interest in the ultrasound scans) were tested with setting Muscle and α as fixed effects. Separate models were run, once excluding Age and once including Age. From the mixed models, we extracted β coefficients, i.e. the offset and slope for each fixed factor, as well as the contribution from fixed effect variables towards the overall r^2 -value, using the function ‘rsq.lmm’ from the library ‘rsq’. All models were scrutinized with residual plots and quantile–quantile plots, and residuals were found to be well-behaved for all models.

Data are presented as means (standard deviation) if not stated otherwise. The level of significance was set to 0.05.

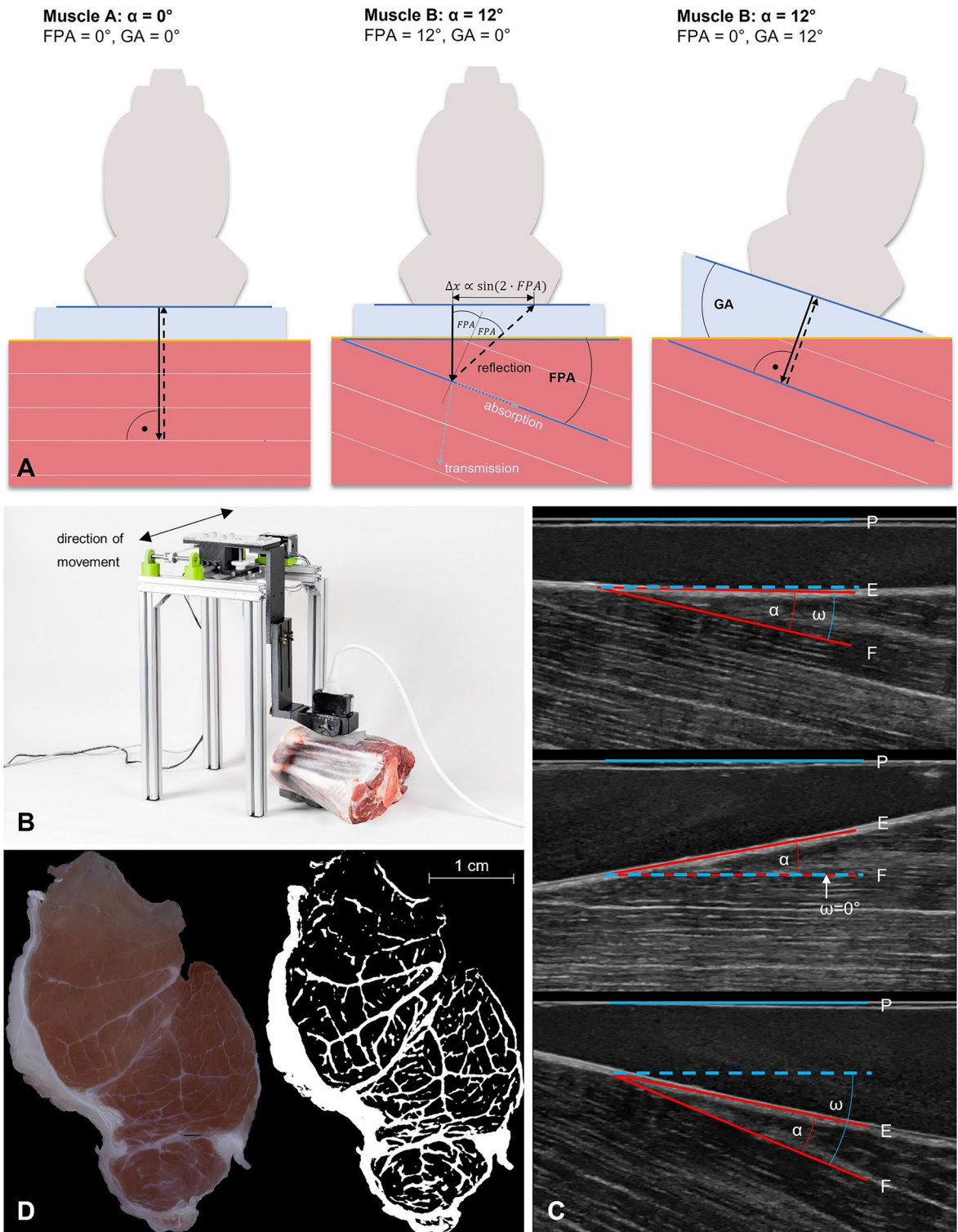


Figure 1. Visualization of ultrasound image acquisition and analysis. (A) The fascicle probe angle (FPA) is subject to variation in both the pennation angle (α , middle) and the gel pad angle (GA, right). Only GA can be controlled by the operator, while α stays constant in a resting muscle. The ultrasound gel pad enables angulation affording minimal ultrasound attenuation prior to coupling into the tissue. At a muscle/IMCT interface, reflection, transmission, absorption, and scattering (not indicated) occur and change with the FPA. A change in FPA causes a change in the angle of reflection $x=|FPA|$, and hence causes the reflected ultrasound ray to be displaced by $\Delta x \propto \sin(2 \cdot |FPA|)$ in the probe. Thus, a change in FPA will cause all reflected rays within a detector area of fascicle-transverse length Δx to be reflected away from the probe, and thus the MGV decreases by an amount $\propto \Delta x$. The image in the middle exemplifies the trigonometric relationship between the probe angle and the amount of ultrasound waves being reflected back to the probe. The echo intensity detected is determined by the function $y = \beta_0 - (\beta_1/2) \cdot \sin(2|FPA|)$ where β_0 is the mean gray value at 0° FPA (MGV_00) and β_1 is the tilt echo gain (TEG). (B) Set-up for ultrasound image acquisition: The linear probe is held in place by a probe holder that is attached to a robotic axis translating the probe in the shown direction. (C) Representative ultrasound images of an infraspinatus muscle scanned with a 0° (left), $+12^\circ$ (middle) and -2° (right) gel pad. α is the pennation angle, between fascicle (F) and epimysium (E). ω is the fascicle probe angle (FPA), between fascicle and probe (P). The mean gray value is visibly higher at a smaller FPA (middle < top < bottom). (D) Segmentation of macroscopic photo of muscle cross section (left) with *ilastik* (right).

Results

Animals were between 3.34 and 8.22 years old (mean 5.90 years). There were no missing datasets from the image processing, and no data were excluded during data processing, so that all data could be subjected to statistical analysis. Table 1 gives an overview of the number of tested muscle specimens.

MGV peaked for FPA = 0° (Fig. 2A,B). When comparing the results for fitting a sine function $y = \beta_0 - (\beta_1/2) \cdot \sin(2|FPA|)$ (Fig. 2A) with results for a linear fitting $y = \beta_0 - \beta_1 \cdot |FPA|$ (Fig. 2B), the former was superior both in terms of adjusted r^2 -values (0.647 vs. 0.613) and Akaike's information criterion (7846 vs. 7942). For greater values of FPA residuals were larger for the linear plot (Fig. 2D), thus with slightly greater deviation from normal distribution (Fig. 2F) than for the sine fit (Fig. 2C,E). This demonstrates the correctness of the assumed sine function, but also that the function can conveniently be linearized as long as the range of observation is not too far from 0° . Therefore, the spatial gain sonography parameters were calculated with the linear fit (Fig. 3A), as this will be more practicable in the clinical setting. The adjusted r^2 -values were > 0.7 for 48 out of 51 specimens (see Fig. 3B). TEG was found to be entirely unrelated to MGV_00 ($P = 0.33$, Fig. 3C) (Table 2).

Visual inspection of MGV_00 and TEG suggested muscle-specific variation in MGV_00 and TEG across the different anatomical muscles (Fig. 4) That impression was confirmed by statistical testing with mixed effect models, which revealed muscle-related differences with regards to α ($P = 0.043$), MGV_00 ($P = 0.041$) and TEG ($P = 0.01$). The pennation angle α was also related to TEG ($P < 0.001$) and MGV_00 ($P = 0.035$) across Muscle. No effects of Muscle or α were observed for ROICy (both $P > 0.1$), suggesting that variation in scanning depth does not explain the former findings. When including age as fixed factor into these mixed effect models, it was significant for MGV_00 ($P < 0.001$) but not for TEG ($P > 0.10$). Of note, Muscle remained significant for MGV_00 and TEG after including age into the mixed models, and the amount of variation that was explained by fixed factors (r^2 fixed in Table 3) increased. The percentage of IMCT in a muscle cross section measured optically significantly affected MGV_00 but the amount of variance accounted for by the regression was low ($r^2 = 0.103$).

Discussion

All three initial hypotheses were confirmed: Echo intensity is generally peaking at a fascicle probe angle of 0° (hypothesis 1). Echo intensity decreases with increasing deviation from a 0° fascicle probe angle which can be modeled with a sinusoidal function and approximated with a linear function (hypothesis 2 and 3).

TEG, i.e. the slope of this linear function for each muscle, and MGV_00 did not show a strong correlation. MGV_00 can be seen as an extensive measure describing the echo intensity (quantity) of echo-reflecting texture within the muscle tissue. As a second, independent descriptor, TEG can be regarded as a more 'qualitative' variable that probably assesses the order of 'directionality' of the tissue-textures. MGV_00 and TEG were differently expressed between different anatomical muscles. The pennation angle was related to MGV_00 and TEG across muscle groups. Age increased the amount of variance explained by anatomically different muscles and pennation angle in the mixed models. Increased echo intensity at FPA 0° in ultrasound correlated with an increased percentage of IMCT in a macroscopic muscle cross section when measured optically, suggesting that echo intensity could at least in part reflect the amount of IMCT.

Tilt echo gain fit

Echo intensity was found to be dependent on fascicle probe angle, with the maximum echo intensity measured at 0° FPA. We originally assumed that a sinusoidal function would prove a better fit than a linear function due to trigonometric laws underlying the physics of reflection, and that was indeed the case. Other factors such as differences in acoustic impedance between muscles may influence echo intensity but the angle-dependency clearly dominates, hence a trigonometric regression could be derived. Interestingly however, a linear function showed almost equal performance, in particular at smaller fascicle probe angles. This can be explained by the fact that deviations of $y = 2 \times$ from $y = \sin(2x)$ amount to approximately 10% at an angle of 20° . For an angle of 0° (MGV_00) which was of particular interest in this study, results obtained from a linear fit compared to the trigonometric fit showed almost no difference. A linear variation of the intensity with FPA approaching zero can be taken as the most generic model-free expectation, and thus suggests itself as a robust analysis method for

Muscle	A0	B8	C0	C5	D8	F1	G2	H0	H7	J1	J6	K9	N6	O2	P0	P3	R6	S7	S9	T8	U1	V5	V9	Y8	Sum
ecr	0	0	0	1	1	0	0	0	1	0	1	0	1	1	1	0	0	0	0	1	0	0	0	0	8
edc	0	0	0	1	1	0	0	0	1	0	1	1	1	1	1	0	0	0	0	1	1	0	0	0	10
edl	0	0	0	0	0	0	0	0	0	1	0	0	0	0	0	0	0	0	0	0	0	0	0	0	1
fcr	0	0	0	1	1	0	0	0	1	0	1	1	1	1	1	0	0	0	0	1	1	0	0	0	10
fhl	0	0	0	0	0	0	0	1	0	0	0	0	0	0	0	1	1	0	0	0	0	0	1	0	4
fl	0	0	0	0	0	0	0	1	0	1	0	0	0	0	0	1	1	0	0	0	0	0	1	0	5
ft	0	0	0	0	0	0	0	1	0	0	0	0	0	0	0	1	1	0	0	0	0	0	1	0	4
pso	0	0	1	0	0	0	0	0	0	0	0	0	0	0	0	0	0	1	0	0	1	0	0	0	3
sch	1	0	0	0	0	1	1	0	0	0	0	0	0	0	0	0	0	0	0	0	0	0	0	0	3
ssp	0	1	0	0	0	0	0	0	0	0	0	0	0	0	0	0	0	0	0	0	0	1	0	1	3
Sum	1	1	1	3	3	1	1	3	3	2	3	2	3	3	3	3	3	1	3	2	1	1	3	1	51
Age					6.08			3.34	8.22	5.52	6.34		6.42	4.99		5.11	4.43		8.22	6.97			5.11		

Table 1. Overview of specimens tested. Highlighted in bold is the sum of analyzed muscles per animal in each column and the sum of different anatomical muscles analyzed overall in each row.

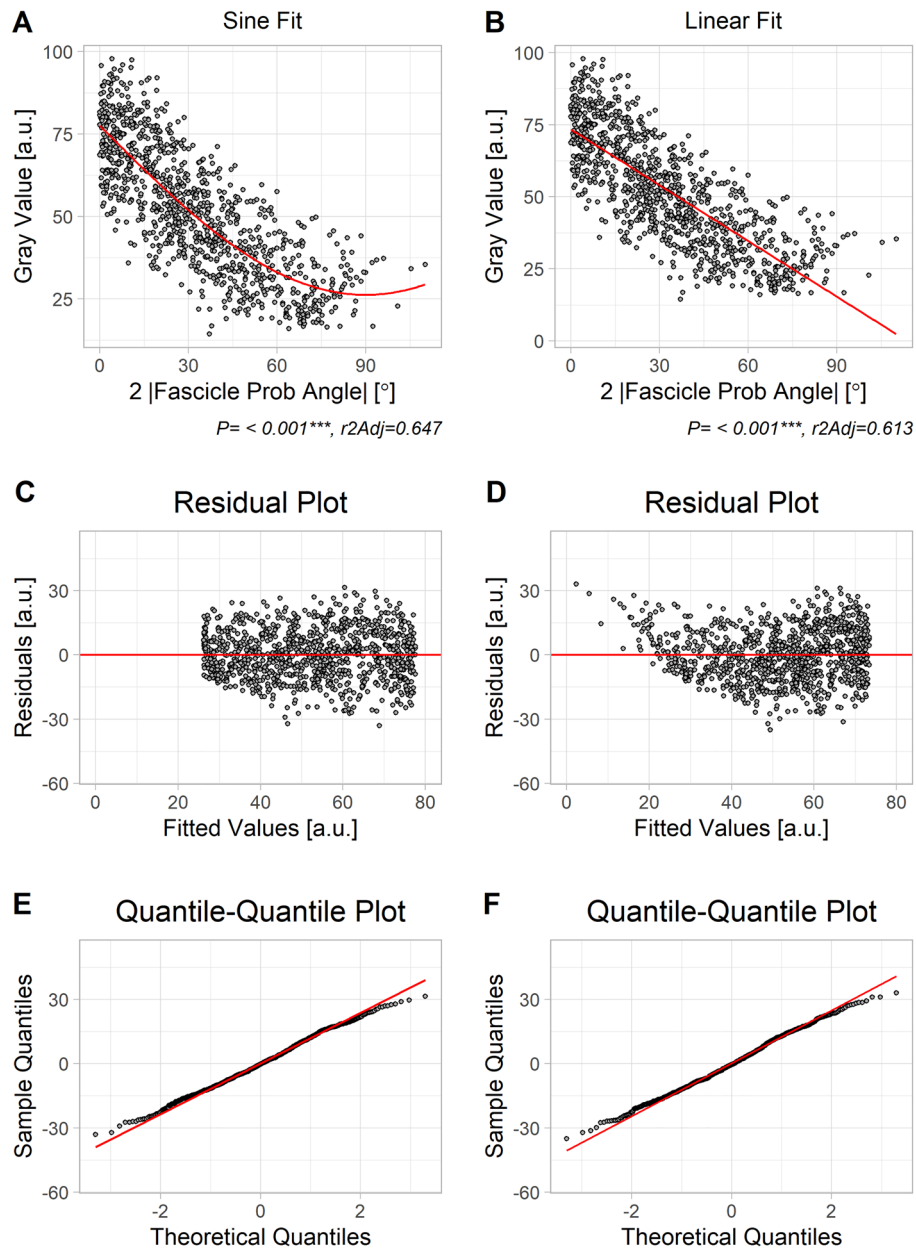


Figure 2. Comparing results for fitting a sine function (left column) *versus* a linear function (right column) for the grand ensemble of all data. Note that both fits were performed with absolute FPA as independent variable. (A, B) Scatter plot of raw data with fitted function curves. As can be seen, gray values peaked at FPA = 0°. (C, D) Residuals (i.e. vertical distance of data point from fitted line in upper row) plotted vs. fitted values (i.e. y-coordinate of fitted curve in A and B, upper row). As can be seen, residuals at extreme ends of x-axis deviate more from 0 in D than in C. (E, F) Observed quantiles plotted *versus* expected quantiles. A straight line would indicate normal distribution of residuals. Although residuals from both fittings seem to be reasonable, they seem slightly closer to normal distribution at extreme ends for the sinusoidal fit.

small enough FPAs. In consequence, we opted to work with the linear function for practicality and suggest that use of this function and clinical ultrasound measurements be restricted to an FPA range between -30° and 30° .

It should be noted though that the ultrasound software might have affected the gray values in the images via post-processing. It was ensured that time gain control was kept constant at all levels, and that other correction features were turned off to avoid intrinsic correction of the images. Nonetheless, insight into the complete ultrasound post-processing algorithm is probably needed to fully comprehend and exclude the possibility of interference with the acquired data.

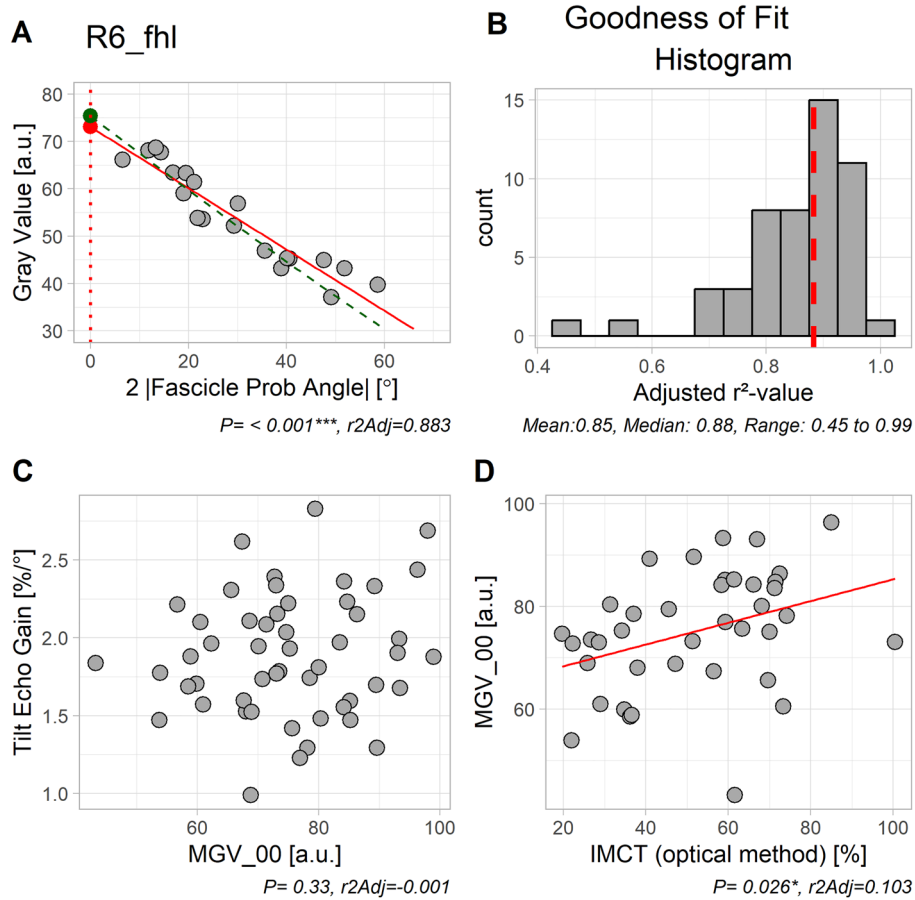


Figure 3. Illustration of spatial gain parameters. **(A)** The green line indicates the sinusoidal fit and the red line the linear fit. The green and red circle represent the predicted MGv₀₀ (gray value at FPA 0°) for each fit. Estimates for MGv₀₀ were directly derived from the fitted line at x-value 0° and the negative slope was defined as tilt echo gain in percent MGv₀₀ per degree (TEG). For this plot, we used data from fhl muscle in animal R6, since the adjusted r²-value for that specimen coincided with the median of all adjusted r²-values. **(B)** Distribution of all adjusted r²-values, with the median marked as vertical dashed line in red. **(C)** Correlation between TEG and MGv₀₀ was very weak. **(D)** Correlation between MGv₀₀ and IMCT ratio measured optically in cross sections was significant, but weak.

Variable	<i>pso</i>	<i>edc</i>	<i>ecr</i>	<i>ft</i>	<i>fcr</i>	<i>fhl</i>	<i>sch</i>	<i>fl</i>	<i>edl</i>	<i>ssp</i>	<i>P.α</i>	<i>P. Muscle</i>	<i>post-hoc</i>
<i>N</i>	3	10	8	4	10	4	3	5	1	3	–	–	–
α	11.1 (0.5)	7.4 (5.2)	13.1 (3.9)	17 (6.9)	11.6 (4.9)	10.2 (2.3)	15.2 (4.9)	10 (10.3)	14.3 (NA)	1.6 (0.4)	–	0.043*	fit–ssp (<i>P</i> =0.017)
<i>MGv₀₀</i>	66.8 (5.7)	68.9 (13.7)	72.1 (13.1)	72.3 (4.7)	72.5 (10.9)	75.4 (12.6)	83.1 (11.2)	84.8 (7.1)	93.1 (NA)	94.1 (7.7)	0.035*	0.041*	No significant post-hoc findings
<i>TEG</i>	2.1 (0.01)	1.98 (0.35)	1.68 (0.27)	1.31 (0.26)	2.16 (0.31)	1.89 (0.21)	1.65 (0.33)	1.9 (0.49)	1.9 (NA)	2.01 (0.62)	<0.001***	0.01**	fit–fcr (<i>P</i> =0.019)
<i>ROI_{Cy}</i>	410.14 (16.69)	449.67 (61.02)	420.93 (39.68)	380.42 (13.97)	419.31 (47.01)	402.23 (42.72)	414.67 (37.65)	438.53 (41.78)	431.82 (NA)	439.14 (43.38)	0.17	0.24	–

Table 2. Descriptive statistics (given as means and their standard deviation in brackets) for the different anatomical muscles tested, and results of testing with mixed effect models and Dunn’s post hoc test, using the entire data set and not including Age into the models.

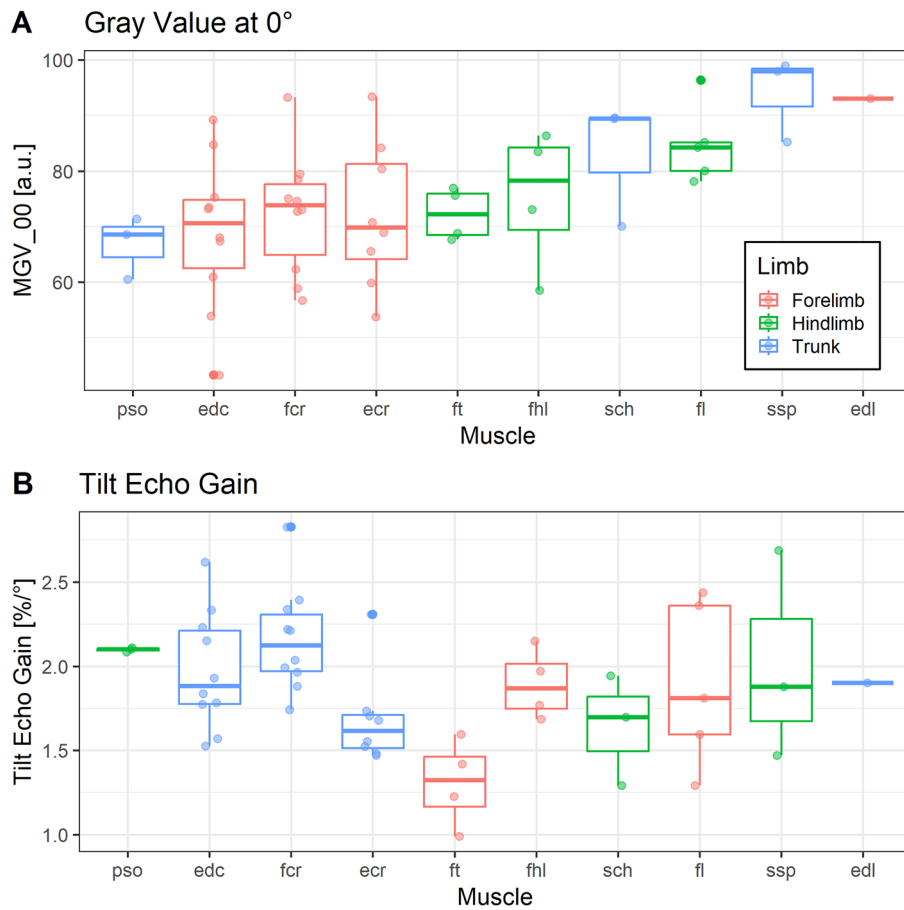


Figure 4. Box plots for MGV_00 and TEG across all analyzed muscles, shown by identical anatomical muscles (x axis) and grouped by forelimb, hindlimb and trunk muscles via color. **(A)** Forelimb muscles (edc, ecr, fcr, edl), hindlimb muscles (ft, fhf, fl) and trunk muscles (pso, sch, ssp) can hardly be distinguished by MGV_00, rather, differences exist between each muscle. **(B)** TEG is distributed differently across muscles compared with MGV_00.

Variable	Age excluded				Age included				
	Offset	P (Muscle)	β (α)	r^2 fixed	Offset	P (Muscle)	β (α)	β (Age)	r^2 fixed
MGV_00	74.6*** (60.8 to 88.4)	0.041	-0.7* (-1.29 to -0.11)	0.43	27.6*** (7.7 to 47.5)	0.013	-0.61* (-1.12 to -0.1)	6.5*** (3.8 to 9.2)	0.68
TEG	2.48*** (2.1 to 2.86)	0.01	-0.034*** (-0.051 to -0.017)	0.55	1.99*** (1.3 to 2.68)	0.007	-0.032** (-0.049 to -0.015)	0.04 (-0.05 to 0.13)	0.63

Table 3. Comparison of linear mixed model results with excluding or including Age as fixed effect. Beta denotes the regression coefficient, and r^2 fixed the contribution from fixed factors to the overall r^2 value. Values for Offset and Beta are given as means (95% confidence interval). Asterisks denote significance as follows: * $P < 0.05$, *** $P < 0.001$.

Comparison of different anatomical muscles

The muscle specimens tested in this study yielded systematic variation with regard to MGV_00 and TEG across the different anatomical muscles. This was more evident for TEG than for MGV_00, as the latter failed to yield any significant post hoc results. For TEG, a significant post hoc difference was found between fibularis tertius muscle (hindlimb) and the supraspinatus muscle (torso). However, there was no general trend for trunk, hindlimb or forelimb muscles.

It should be considered that this study was not designed to find IMCT differences across anatomical muscles, but rather included a variety of different muscles to validate the concept of spatial gain sonography. Moreover, two factors need to be considered here. First, muscles from different breeds of *Bos taurus* were analyzed and literature suggests that muscle architecture varies between different breeds^{22,23}. However, that group also found that the variation in the density of slow muscles fibers had greater variation within the muscle than across breeds which

relativizes the problem of different breeds but reveals another obstacle for the comparison between muscles. The scanning site was not always the exact same in every anatomically equal muscle. Rather, attention was given to choosing an area with parallel fascicles without blood vessels and sufficient muscle thickness to scan across all angles. In order to make anatomical observations across different muscles, the muscle structure varying within a muscle needs to be considered^{24,25}.

It is apparent from Fig. 4, however, that variation in TEG and in MGV_00 was different across different anatomical muscles, further corroborating that these two measures are independent and convey diverging information.

Influence of pennation angle on spatial gain parameters

We also observed an effect of pennation angle α on spatial gain sonography parameters independent of FPA. Muscles are pennated in order to increase force per unit muscle mass²⁶. Because muscles differ in their function and size, their pennation angles vary likewise as observed in this study. The pennation angle might therefore depend on the function of the specific muscle, e.g. load-bearing antigravity muscles versus non-antigravity muscles, which in turn could influence IMCT architecture and hence spatial gain parameters.

Influence of age on spatial gain parameters

Age was significant for MGV_00 when included as a fixed factor into mixed models. Other studies have confirmed increased echo intensity at higher age^{27–29}. However, as clearly demonstrated in this study, echo intensity is subject to fascicle probe angle changes. Therefore, and as much as pennation angle systematically decreases with aging^{30–32}, reporting age-related effects without adjusting echo intensity for fascicle probe angle, surely has potential to over-estimate age and immobilization-related changes. In that sense, our new parameter MGV_00 can be regarded as a standardized and more robust version of ‘echo intensity’ as it was used in literature for characterizing perimysium in skeletal muscle.

Correction for pennation angle in echo intensity measurements

Former clinical studies have suggested that increases in muscular echo intensity can be utilized in the diagnostic approach to muscle atrophy and dystrophy^{33,34}. However, dystrophy and atrophy have a bearing on pennation angle. Whilst pennation angle decreases with immobilization-related atrophy³⁵ it was found to be increased in Duchenne muscular dystrophy³⁶. Again, such effects will lead to bias, and to systematic under- or over-estimation of skeletal muscle echo intensity, unless adjustment is performed. One group researching neuromuscular disorders in children visually corrected for pennation angle by adjusting the probe over the muscle until the echo intensity was highest^{37,38}. Another study even measured echo intensity alteration with a probe tilt up to 6° in both directions in relation to the skin and proposed that the operator shall minimize the probe tilt during muscle examination³⁹. While both strategies are in line with the presented evidence, they are less quantitative than our approach, raising issues of intra- and inter-operator reproducibility. Moreover, whilst those proposed ‘work-arounds’ for echo intensity could be regarded as precursors for MGV_00, we are not aware of any former attempt to model and assess TEG functions.

Reflection of perimysium content in echo intensity

Upon optical analysis of muscle cross sections, higher IMCT percentages were measured for higher values of MGV_00 from ultrasound analysis. This finding is in line with a previous study that showed that histological fibrous tissue content in dogs with muscular dystrophy linearly correlates with echo intensities in the respective muscles¹⁸. As opposed to that study, we took samples from healthy bovine muscles and analyzed macroscopic cross sections of the whole muscle instead of microscopic images. We presumed that the perimysium measured in ultrasound would be better represented by these large sections as perimysium is too vast to be estimated reliably in one microscopic field. This approach in turn relies on the assumption that solely perimysium, and not endomysium, is reflected in ultrasound echo intensity measurements. Axial resolution, the resolution longitudinal to the ultrasound beam, depends on the length of an ultrasound pulse and the wavelength. A smaller wavelength will also lead to a shorter pulse length thus allowing for better discrimination between objects that are closer together. An ultrasound wave with a frequency of 15 MHz traveling through bovine muscle, in which the average speed of sound is 1580 m/s⁴⁰, has a wavelength of 105 μm . The best axial resolution that can be achieved is half the pulse length⁴¹. Under optimal conditions, if the pulse length is only one wavelength and hence axial resolution is 52.5 μm , bovine perimysium with a thickness between 30 and 120 μm will contribute to an echo alteration^{42,43}. However, endomysium with a thickness of 5 to 15 μm depending on the muscle⁴³ is probably not represented in current B-Mode ultrasound images and at most contributes to scattering of ultrasound waves which occurs when the wavelength is considerably greater than the size of the encountered object⁴⁴.

In addition, in this study we were careful not to include planes with visible adipose tissue, blood vessels or nerves that might cause increases in echo intensity. Nonetheless, for in-vivo studies this is sometimes unavoidable and it therefore remains a matter of discussion whether echo intensity truly reflects the amount of IMCT in a muscle^{45,46}.

Discussion of implementation in the clinical setting

Beam steering is one tool already implemented into ultrasound software which would allow for implementation of spatial gain sonography into clinical practice. The clinician would have to obtain an ultrasound image of a muscle longitudinally with no angulation first. Second, an image of the exact same location using beam steering is needed. In one of these images, the pennation angle would need to be measured, which is possible on most ultrasound devices or can be measured using computer software. Using the linear function, MGV_00 would

result from the regression fit of mean gray value and fascicle probe angle. The measurement can be repeated at any given time point and MGV_00 tracked over time for a muscle echo intensity evaluation without the influence of a potentially changing layer of subcutaneous fat or an altered muscle volume in patients.

Limitations

Although our study did find significant effects by anatomical muscle in age and pennation angle, the study was not designed to find such effects. Therefore, the interpretation of these effects must remain on a somewhat speculative level. It should also be noted that our photographic image analysis of the perimysium assessed quantity, but not structural or textural information. However, conducting such an assessment would constitute a considerable undertaking, and we therefore decided to demonstrate the viability of spatial gain sonography in principle before making larger investments into potentially moot and certainly costly perimysium assessments.

Also, one needs to consider that our specimens stem from older female cattle only, and did not contain younger or very old animals, and also no male cattle. The next step will be a larger human study to validate our novel approach, and to further explore the effects of age, sex, immobilization and exercise training.

The potential effects on echo intensity from using an ultrasound gel pad should also be discussed. Different scanning angles required gel pads of varying thickness, which lead to a varying amount of sound wave energy absorption in each angle setting. This may have biased our results, which is placed into a relative context again by (1) the absorption coefficient of the gel pad being only half that of muscle (0.053 vs. $0.11 \frac{dB}{MHz \cdot mm}$ respectively⁴⁷) and (2) the proportions of the gel pad: the gel pad for 0° was 1 cm in thickness while the gel pad for 12° was 0 cm on one end and 2 cm on the other allowing for some amount of averaging out of the mentioned distortion. Due to these circumstances, a complex calculation of the minor effects of the gel pad on echo intensity in each image was not included in this analysis.

Another limitation arises from the fact that we used a commercial ultrasound scanner, and that the image processing therefore contains elements unknown to us⁴⁸. For example, ultrasound images may be displayed using a logarithmic scale instead of linear which would influence the model. However, this device-internal information could not be verified and therefore remains a limitation of the study which can only be circumnavigated using hard to obtain raw ultrasound data in future studies. For example, there is a possibility that brightness is adjusted for depth by the machine, and that the observed effects by pennation angle could be a by-product of our study scanning deeper tissue portions for muscles with greater pennation angle^{49,50}. To rule that possibility out, we examined whether pennation angle was related to scanning depth (ROICy). This was not the case, which enhances our confidence in the results related to pennation angle, as well as the viability of spatial gain sonography in general.

Conclusions

The present study has validated the concept of spatial gain sonography in principle by demonstrating that echo intensity peaks when the probe is parallel to skeletal muscle fascicles. Hereby, we can derive MGV_00 as an estimate of perimysium content that is not biased by concomitant variation in pennation angle. Our method can also work in cases where the ultrasound cannot be aligned parallel to the fascicle orientation, e.g. in muscles with large pennation angle or with an anatomical axis that is oblique to the skin. For these reasons MGV_00 constitutes an improvement of the currently used 'echo intensity' that could be readily adopted for making medical diagnoses.

Perhaps even more importantly, we showed that through introduction of TEG as a new variable, another tissue property can be captured that assesses systematic and meaningful effects that are largely independent of MGV_00. Future fundamental research will be required to develop a better understanding of what this variable reflects where it is clinically relevant. If the outcome of that future research demonstrates viability of the spatial gain approach to yield clinically relevant information, then the scanning analysis procedures would have to be standardized for clinical usage, e.g. by replacing the gel pads with a more time-efficient method. Eventually, automated computation of TEG and MGV_00 into the scanner software would further facilitate the applicability.

Data availability

All data analyzed during this study are available from the corresponding author on reasonable request.

Received: 1 October 2023; Accepted: 6 February 2024

Published online: 15 February 2024

References

1. Sleboda, D. A., Stover, K. K. & Roberts, T. J. Diversity of extracellular matrix morphology in vertebrate skeletal muscle. *J. Morphol.* **281**, 160–169 (2020).
2. Purslow, P. P. The structure and functional significance of variations in the connective tissue within muscle. *Comp. Biochem. Physiol. Part A Mol. Integr. Physiol.* **133**, 947–966 (2002).
3. Ramaswamy, K. S. *et al.* Lateral transmission of force is impaired in skeletal muscles of dystrophic mice and very old rats. *J. Physiol.* **589**, 1195–1208 (2011).
4. Purslow, P. P. Muscle fascia and force transmission. *J. Bodywork Mov. Therap* **14**, 411–417 (2010).
5. Wilke, J., Krause, F., Vogt, L. & Banzer, W. What is evidence-based about myofascial chains: A systematic review. *Arch. Phys. Med. Rehabil.* **97**, 454–461 (2016).
6. Csapo, R., Malis, V., Sinha, U., Du, J. & Sinha, S. Age-associated differences in triceps surae muscle composition and strength—An MRI-based cross-sectional comparison of contractile, adipose and connective tissue. *BMC Musculoskeletal Disord.* **15**, 209 (2014).
7. Fede, C. *et al.* The effects of aging on the intramuscular connective tissue. *Int. J. Mol. Sci.* **23**, 11061 (2022).
8. Wojtysiak, D. Effect of age on structural properties of intramuscular connective tissue, muscle fibre, collagen content and meat tenderness in pig longissimus lumborum muscle. *Folia Biol. (Krakow)* **61**, 221–226 (2013).
9. Williams, P. E. & Goldspink, G. Connective tissue changes in surgically overloaded muscle. *Cell Tissue Res.* **221**, 465–470 (1981).

10. Mendias, C. L., Schwartz, A. J., Grekin, J. A., Gumucio, J. P. & Sugg, K. B. Changes in muscle fiber contractility and extracellular matrix production during skeletal muscle hypertrophy. *J. Appl. Physiol. (Bethesda, Md.: 1985)* **122**, 571–579 (2017).
11. Haus, J. M., Carrithers, J. A., Carroll, C. C., Tesch, P. A. & Trappe, T. A. Contractile and connective tissue protein content of human skeletal muscle: Effects of 35 and 90 days of simulated microgravity and exercise countermeasures. *Am. J. Physiol. Regul. Integr. Comp. Physiol.* **293**, R1722–7 (2007).
12. Järvinen, T. A. H., Jozsa, L., Kannus, P., Jarvinen, T. L. N. & Jarvinen, M. Organization and distribution of intramuscular connective tissue in normal and immobilized skeletal muscles. An immunohistochemical, polarization and scanning electron microscopic study. *J. Muscle Res. Cell Motil.* **23**, 245–254 (2002).
13. Mayer, W. P., Baptista, J. D. S., Oliveira, F., de Mori, M. & Liberti, E. A. Consequences of ankle joint immobilisation: Insights from a morphometric analysis about fibre typification, intramuscular connective tissue, and muscle spindle in rats. *Histochem. Cell Biol.* <https://doi.org/10.1007/s00418-021-02027-3> (2021).
14. Williams, P. E. & Goldspink, G. Connective tissue changes in immobilised muscle. *J. Anat.* **138**(Pt 2), 343–350 (1984).
15. Booth, C. M., Cortina-Borja, M. J. F. & Theologis, T. N. Collagen accumulation in muscles of children with cerebral palsy and correlation with severity of spasticity. *Dev. Med. Child Neurol.* **43**, 314 (2001).
16. Desguerre, I. *et al.* Endomysial fibrosis in Duchenne muscular dystrophy: A marker of poor outcome associated with macrophage alternative activation. *J. Neuropathol. Exp. Neurol.* **68**, 762–773 (2009).
17. Lee, J. C. & Healy, J. Sonography of lower limb muscle injury. *AJR. Am. J. Roentgenol.* **182**, 341–351 (2004).
18. Pillen, S. *et al.* Skeletal muscle ultrasound: correlation between fibrous tissue and echo intensity. *Ultrasound Med. Biol.* **35**, 443–446 (2009).
19. Li, J. *et al.* (eds) *Ultrasound Fundamentals* (Springer, 2021).
20. Hinkle, D., Wiersma, W. & Jurs, S. G. *Applied Statistics for the Behavioral Sciences* 5th edn. (Houghton Mifflin, 2003).
21. Lehtinen, A., Bondestam, S. & Taavitsainen, M. Use of angulation in the detection of tendinitis with US. *Eur. J. Radiol.* **18**, 175–179 (1994).
22. Albrecht, E., Teuscher, F., Ender, K. & Wegner, J. Growth- and breed-related changes of muscle bundle structure in cattle. *J. Anim. Sci.* **84**, 2959–2964 (2006).
23. Albrecht, E., Lembcke, C., Wegner, J. & Maak, S. Prenatal muscle fiber development and bundle structure in beef and dairy cattle. *J. Anim. Sci.* **91**, 3666–3673 (2013).
24. Oranchuk, D. J., Stock, M. S., Nelson, A. R., Storey, A. G. & Cronin, J. B. Variability of regional quadriceps echo intensity in active young men with and without subcutaneous fat correction. *Appl. Physiol. Nutr. Metabol.* **45**, 745–752 (2020).
25. Rabello, R. *et al.* Echo intensity reliability between two rectus femoris probe sites. *Ultrasound (Leeds, England)* **27**, 233–240 (2019).
26. Roberts, T. J. *et al.* The multi-scale, three-dimensional nature of skeletal muscle contraction. *Physiology (Bethesda, Md.)* **34**, 402–408 (2019).
27. Ryan, E. D. *et al.* Pennation angle does not influence the age-related differences in echo intensity of the medial gastrocnemius. *Ultrasound Med. Biol.* **41**, 618–621 (2015).
28. Ota, M., Ikezoe, T., Kato, T., Tateuchi, H. & Ichihashi, N. Age-related changes in muscle thickness and echo intensity of trunk muscles in healthy women: Comparison of 20–60s age groups. *Eur. J. Appl. Physiol.* **120**, 1805–1814 (2020).
29. Kobayashi, K. *et al.* Effect of age on shear modulus, muscle thickness, echo intensity of the upper limb, lower limb, and trunk muscles in healthy women. *Eur. J. Appl. Physiol.* <https://doi.org/10.1007/s00421-022-05099-8> (2022).
30. Morse, C. L., Thom, J. M., Reeves, N. D., Birch, K. M. & Narici, M. V. In vivo physiological cross-sectional area and specific force are reduced in the gastrocnemius of elderly men. *J. Appl. Physiol. (Bethesda, Md.: 1985)* **99**, 1050–1055 (2005).
31. Strasser, E. M., Draskovits, T., Praschak, M., Quittan, M. & Graf, A. Association between ultrasound measurements of muscle thickness, pennation angle, echogenicity and skeletal muscle strength in the elderly. *Age (Dordrecht, Netherlands)* **35**, 2377–2388 (2013).
32. Jacob, I., Johnson, M. I., Jones, G., Jones, A. & Francis, P. Age-related differences of vastus lateralis muscle morphology, contractile properties, upper body grip strength and lower extremity functional capability in healthy adults aged 18 to 70 years. *BMC Geriatr.* **22**, 538 (2022).
33. Pillen, S. *et al.* Quantitative skeletal muscle ultrasound: Diagnostic value in childhood neuromuscular disease. *Neuromuscul. Disord.* **17**, 509–516 (2007).
34. MacLennan, R. J. *et al.* Declines in skeletal muscle quality versus size following two weeks of knee joint immobilization. *PeerJ* **8**, e8224 (2020).
35. Seynnes, O. R., Maganaris, C. N., de Boer, M. D., Di Prampero, P. E. & Narici, M. V. Early structural adaptations to unloading in the human calf muscles. *Acta Physiologica (Oxford, England)* **193**, 265–274 (2008).
36. Bulut, N. *et al.* Ultrasonographic assessment of lower limb muscle architecture in children with early-stage Duchenne muscular dystrophy. *Arquivos de neuro-psiquiatria* **80**, 475–481 (2022).
37. Scholten, R. R., Pillen, S., Verrips, A. & Zwarts, M. J. Quantitative ultrasonography of skeletal muscles in children: Normal values. *Muscle Nerve* **27**, 693–698 (2003).
38. Pillen, S. *et al.* Skeletal muscle ultrasonography: Visual versus quantitative evaluation. *Ultrasound Med. Biol.* **32**, 1315–1321 (2006).
39. Dankel, S. J. *et al.* The impact of ultrasound probe tilt on muscle thickness and echo-intensity: A cross-sectional study. *J. Clin. Densitom.* **23**, 630–638 (2020).
40. Ludwig, G. D. The velocity of sound through tissues and the acoustic impedance of tissues. *J. Acoust. Soc. Am.* **22**, 862–866 (1950).
41. Lieu, D. Ultrasound physics and instrumentation for pathologists. *Arch. Pathol. Lab. Med.* **134**, 1541–1556 (2010).
42. Torrecano, G. (ed.). *Determination of Perimysium and Endomysium Thickness in Bovine, Ovine and Caprine Semimembranosus and Semitendinosus Muscles by Video Image Analysis* (2001).
43. Dubost, A., Micol, D., Meunier, B., Lethias, C. & Listrat, A. Relationships between structural characteristics of bovine intramuscular connective tissue assessed by image analysis and collagen and proteoglycan content. *Meat Sci.* **93**, 378–386 (2013).
44. Costello, J. R., Arif, H., Kalb, B. & Martin, D. R. In *An Introduction to Medical Physics* (ed. Maqbool, M.) 329–370 (Springer, 2017).
45. Reimers, K., Reimers, C. D., Wagner, S., Paetzke, I. & Pongratz, D. E. Skeletal muscle sonography: A correlative study of echogenicity and morphology. *J. Ultrasound Med.* **12**, 73–77 (1993).
46. Stock, M. S. & Thompson, B. J. Echo intensity as an indicator of skeletal muscle quality: Applications, methodology, and future directions. *Eur. J. Appl. Physiol.* **121**, 369–380 (2021).
47. Nassiri, D. K., Nicholas, D. & Hill, C. R. Attenuation of ultrasound in skeletal muscle. *Ultrasonics* **17**, 230–232 (1979).
48. Pillen, S. & van Alfen, N. Muscle ultrasound from diagnostic tool to outcome measure—Quantification is the challenge. *Muscle Nerve* **52**, 319–320 (2015).
49. Girts, R. M. *et al.* The influence of ultrasound image depth and gain on skeletal muscle echo intensity. *Appl. Physiol. Nutr. Metabol.* **47**, 839–846 (2022).
50. Schlegel, W., Karger, C. P. & Jäkel, O. *Medizinische Physik* (Springer, 2018).

Author contributions

S.R. planned and conducted the data collection, wrote the main manuscript text and prepared figure 1. J.R. provided the statistical analysis and prepared figures 2–6. P.R. helped with the conceptualization of the study

and improved the methods. L.A. conducted the data collection for the macroscopic image analysis and wrote the text on this section. U.W. wrote and together with S.R. optimized the software for ultrasound image analysis. T.V. provided the mathematical model and the physical concepts as a basis for the hypothesis and interpretation of results. All authors have read and approved the final manuscript.

Funding

Open Access funding enabled and organized by Projekt DEAL.

Competing interests

The authors declare no competing interests.

Additional information

Supplementary Information The online version contains supplementary material available at <https://doi.org/10.1038/s41598-024-53852-0>.

Correspondence and requests for materials should be addressed to S.C.R.

Reprints and permissions information is available at www.nature.com/reprints.

Publisher's note Springer Nature remains neutral with regard to jurisdictional claims in published maps and institutional affiliations.



Open Access This article is licensed under a Creative Commons Attribution 4.0 International License, which permits use, sharing, adaptation, distribution and reproduction in any medium or format, as long as you give appropriate credit to the original author(s) and the source, provide a link to the Creative Commons licence, and indicate if changes were made. The images or other third party material in this article are included in the article's Creative Commons licence, unless indicated otherwise in a credit line to the material. If material is not included in the article's Creative Commons licence and your intended use is not permitted by statutory regulation or exceeds the permitted use, you will need to obtain permission directly from the copyright holder. To view a copy of this licence, visit <http://creativecommons.org/licenses/by/4.0/>.

© The Author(s) 2024

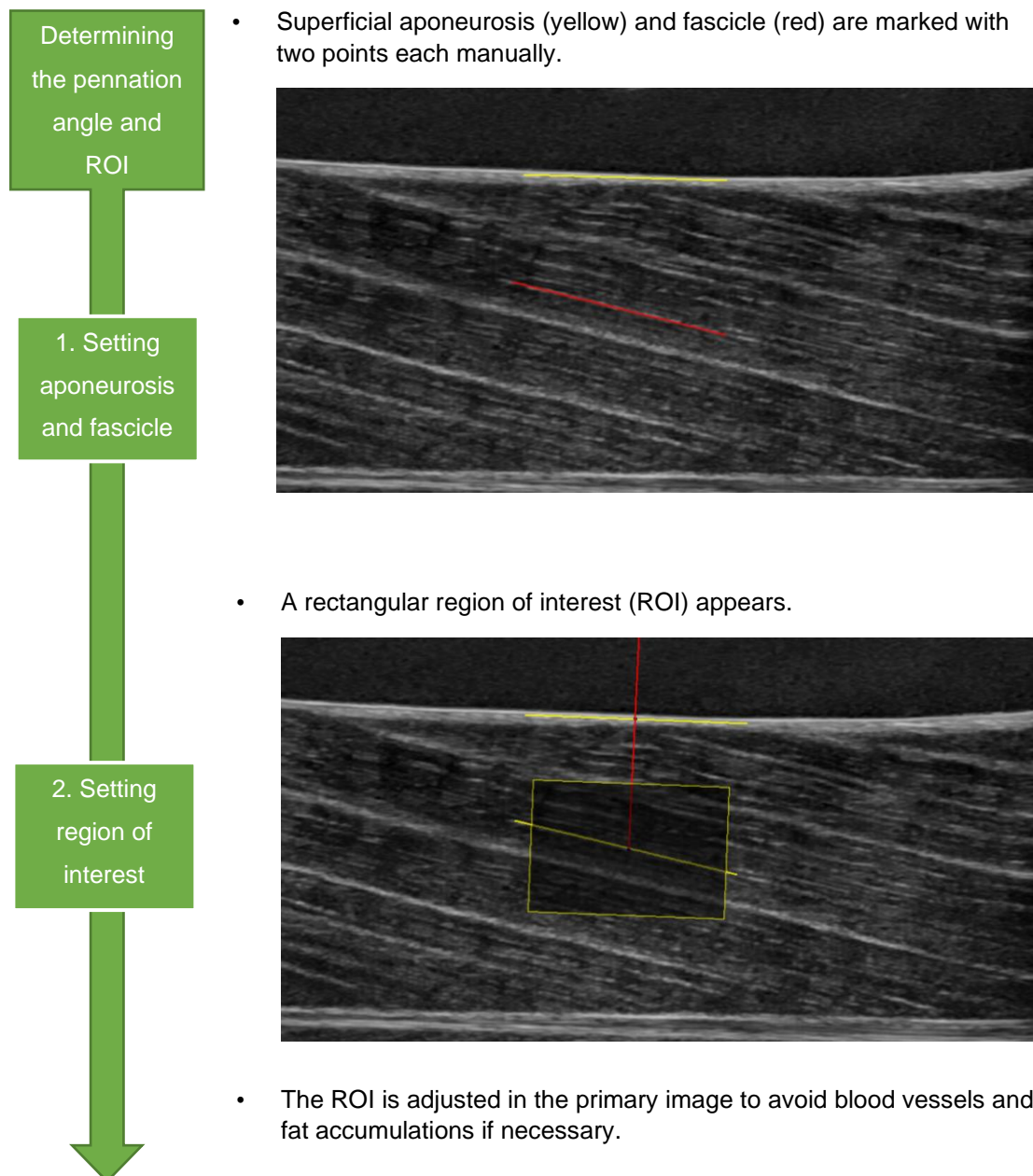
Supplementary Files

Image Processing: Calculation of Pennation Angle and Fascicle Probe Angle

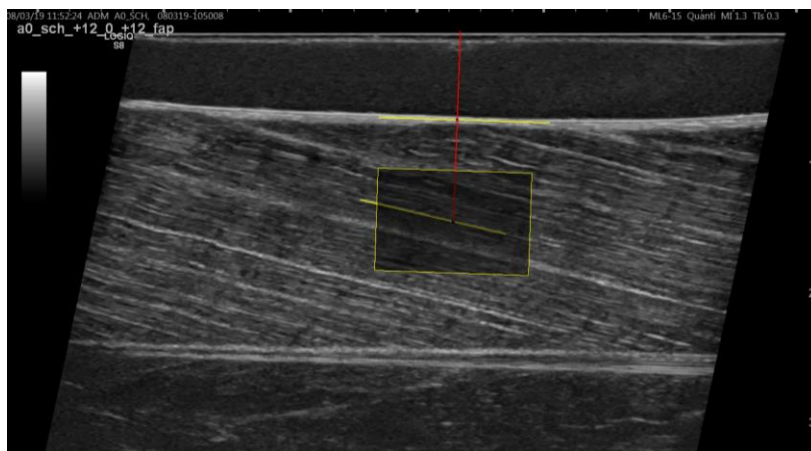
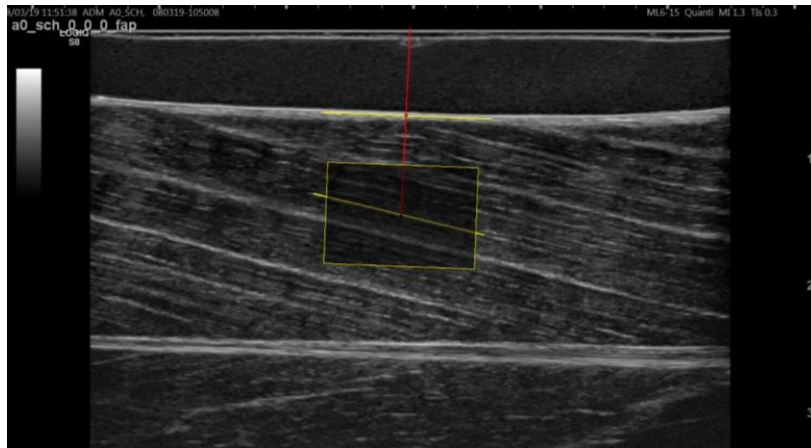
1. Pennation Angle

The pennation angle was indicated manually on each ultrasound image and calculated using the custom-made *Python* script “QuantICUS” (Quantification of Intramuscular Connective Tissue with Ultrasound).

Supplementary Figure 1: Workflow for Ultrasound Image Angle Calculation in *Python*



- In all subsequent scans of that muscle, the ROI is computed by the script according to the angulation in the respective images. Example 0° vs. 12° beam steering angle:

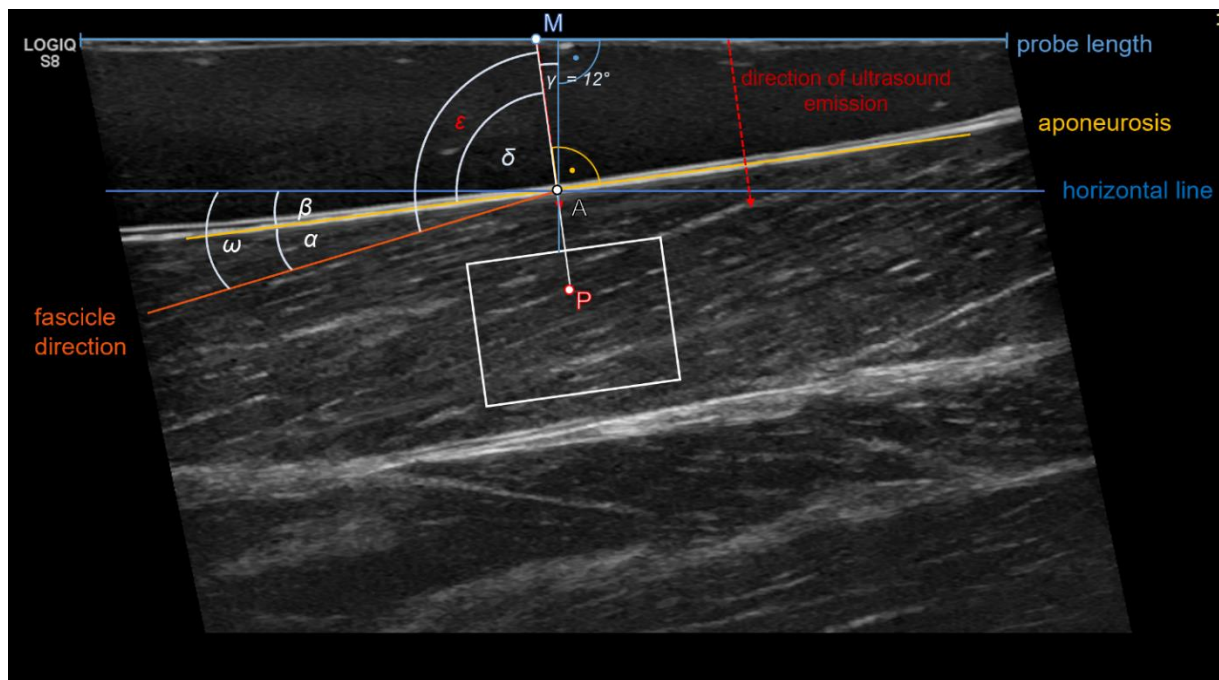


3.
Measuring
angles and
echo
intensity

- The examiner does not move the ROI anymore, unless it is outside of the ultrasound image.
- Results: The aponeurosis probe angle and mean gray value inside the ROI are measured.
- The pennation angle is calculated.

2. Fascicle Probe Angle

The fascicle probe angle was calculated in R using the appropriate equation derived from the geometric outline as shown below. This image serves as an example and will differ slightly for each angle and gel pad configuration.

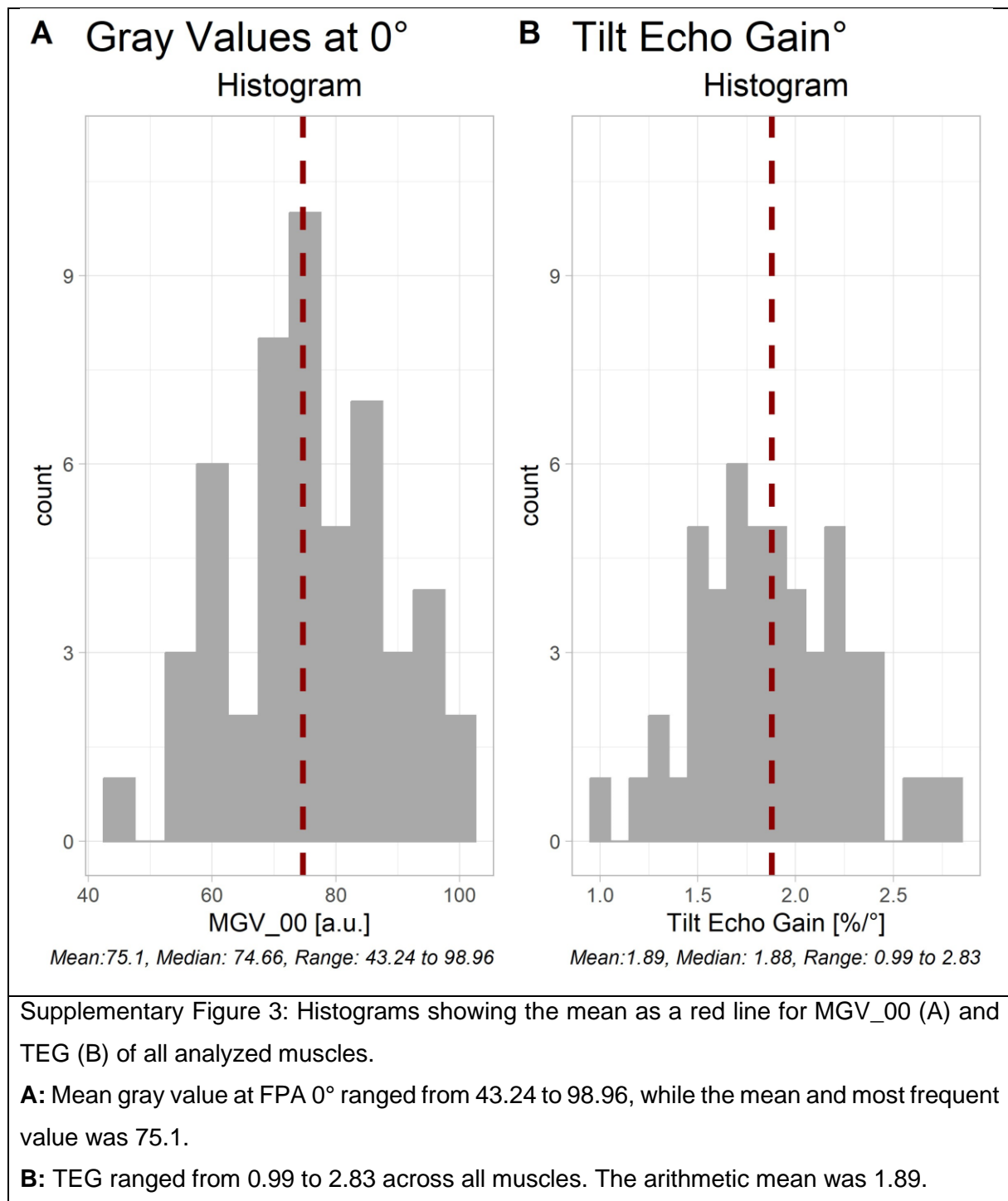


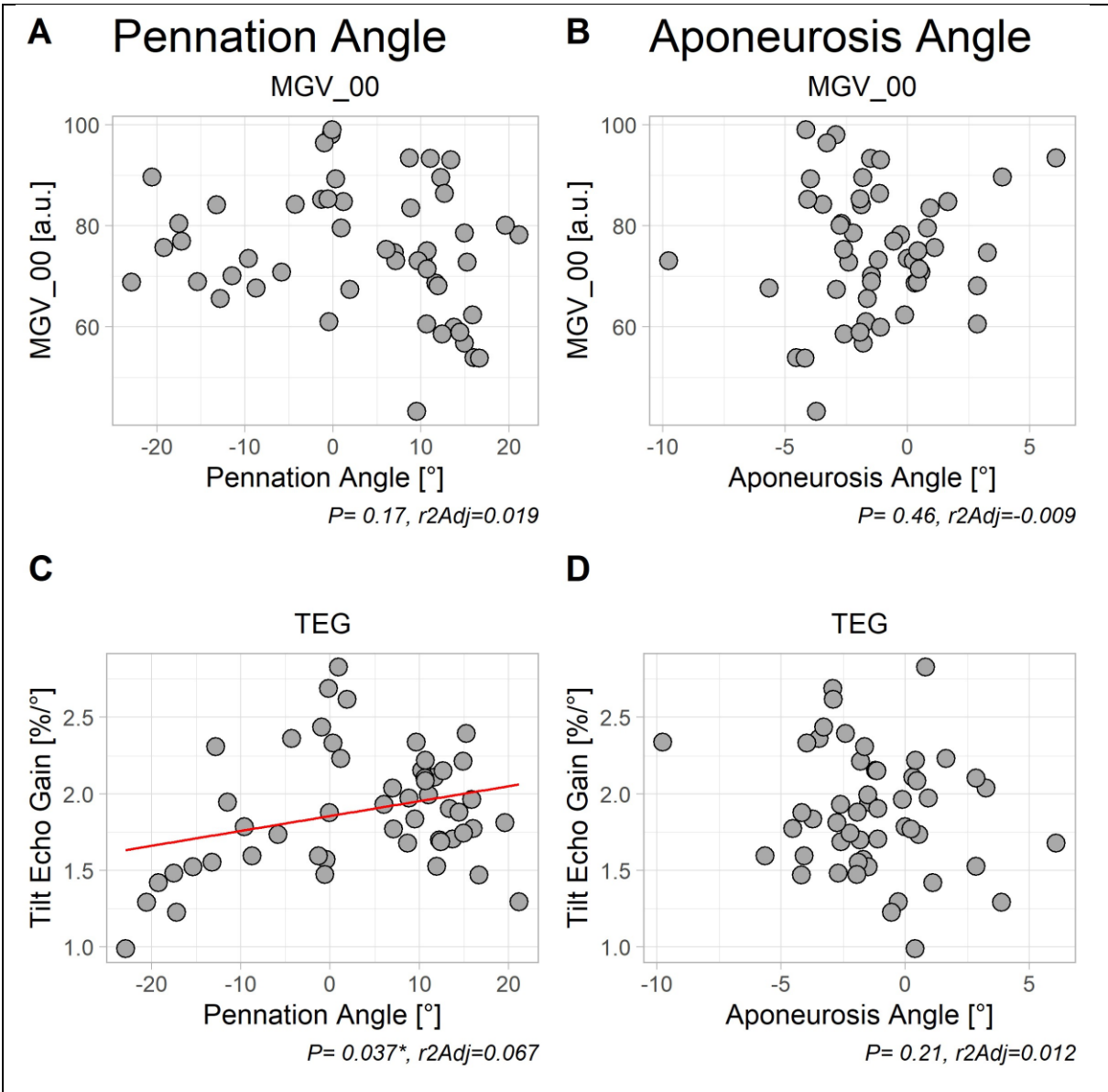
Supplementary Figure 2: Ultrasound image with angles α through ϵ used in image analysis.

Greek Letter in Suppl. Figure 2	Angle Name	Values or Equation
α	Pennation Angle	$\alpha = \omega - \beta$
β	Aponeurosis Probe Angle/ Measured Gel Pad Angle	see α
γ	Beam Steering Angle	+12/0/-12°
δ	Aponeurosis Insonation Angle	$\delta = \varepsilon - \alpha $
ε	Fascicle Insonation Angle	If $\alpha > 0^\circ$ ($\omega > \beta$), then $\varepsilon = 90^\circ + \omega - \gamma$ If $\alpha < 0^\circ$ ($\omega < \beta$), then $\varepsilon = 90^\circ - \omega - \gamma$
ω	Fascicle Probe Angle	see ε
-	Given Gel Pad Angle	+24/+12/0/-12/-24°

Supplementary Table 1: Angle descriptions displayed in ultrasound image in *Supplementary Figure 2* and their mathematical relationship.

Supplementary diagrams





Supplementary Figure 4: Relationship of pennation and aponeurosis angle to MGV_00 and tilt echo gain (TEG).

A/B: Pennation angle and aponeurosis angle did not significantly affect MGV_00.

C/D: Pennation angle had a significant influence on TEG, however with a very weak correlation and aponeurosis angle had no significant influence on TEG.

5. Discussion

5.1. Summary of results

All three hypotheses were confirmed in this study. First, echo intensity was indeed highest when ultrasound waves were directed perpendicularly to the fascicle, i.e., at a fascicle probe angle of 0° . After EI was confirmed to depend on insonation angle in muscle, the relationship between echo intensity and FPA could be mathematically modeled. This model showed a trigonometric function, confirming hypotheses 2 and 3. These experimental results were utilized to establish simplified approaches for potential clinical application.

First, it was observed that at smaller FPAs the trigonometric function approaches a linear function, which would be much more convenient for clinical use. Hence, this function was employed for further data analysis. MGV_00, i.e. the highest EI at the point where fascicles are scanned perpendicularly showed significant variation between muscles allowing for it to be used as a distinctive parameter in muscle studies. Tilt Echo Gain (TEG), the other novel parameter introduced in this study, was also found to be a muscle-specific value, and hence provides a more objective means to compare echo intensities between different muscles.

5.2. Relevance of mean gray value and tilt echo gain

TEG can be calculated by obtaining echo intensities at a minimum of two different FPAs, i.e., by tilting the probe between two measurements. The more data points, the more valid the function and its slope TEG will be. Using this method, the probe angle is no longer a confounding variable when comparing echo intensities between muscles or time points, which has been a considerable inter-rater validity problem in former studies. Other groups have tried to circumnavigate this problem by visually correcting the probe tilt until the echo intensity was highest^{49,50}, or by quantifying the change in EI with a probe tilt of 6° .⁷⁸ It was suggested that probe tilt should be minimized by the ultrasound operator. While this increases awareness of the problem it does not necessarily heighten validity considering that holding an ultrasound probe at a certain angle while looking at a screen is rather unreliable. The method presented in this work uses 3D-printed probe holders to keep the probe in place. It has additionally been tested on human gastrocnemius muscle holding the probe in place with straps on the lower leg.⁸⁹

When adopting spatial gain parameters for echo intensity *comparisons*, the subcutaneous fat layer and pennation angle become less relevant as a confounder, as they are the same in both measurements taken and hence filtered out to a large degree. In longitudinal or comparative studies of muscles, MGV_00 as an absolute variable and even more so TEG as a relative variable are highly useful to increase internal and external validity of echo intensity measurements.

5.3. Factors affecting mean gray value and tilt echo gain

While not the main objective of this study, the standardized approach taken grants the possibility to compare between muscles of different anatomical location, and determine the influence of age and pennation angle on TEG measurements.

5.3.1. Anatomical location

Muscles of ten different anatomical locations from forelimb, hindlimb and torso of *Bos taurus* were analyzed. As these muscles serve different functions and are therefore thought to contain different amounts of IMCT, a comparison of their TEG and MGV_00 was warranted. It was especially of interest to determine any difference between the muscle groups “stabilizing trunk muscle” and “mobilizing limb muscle”.

Their differences in IMCT content are known from studies in the meat industry, which examine beef tenderness and compare it to IMCT content. The distal muscles of the limbs are long muscles with a pennate structure and therefore a high connective tissue content.⁹⁰ This structural feature could be explained by the higher amount of shear strain they have to accommodate during movement compared to trunk muscles.^{91–93} The meat from the distal limb is tough, but very lean due to the constant activity of these muscles in the live animal.⁹⁴ More proximal “trunk” muscle such as the supraspinatus or the psoas major muscle (known as filet) are very tender parts of beef which could indicate a lower IMCT content.⁹³

Extrapolating from studies by Pillen et al. it can be hypothesized that the trunk muscles which contain less IMCT have lower echo intensities.³⁰

A systematic variation of TEG between muscles was observed with a significant post hoc difference between the fibularis tertius muscle (hindlimb) and the supraspinatus muscle (trunk) showing that TEG is most likely a muscle-specific value. However, this study showed no general trend in TEG or MGV_00 difference for forelimb, hindlimb and trunk muscles. Factors that may have influenced these results include the use of different breeds of *Bos taurus* between which muscle architecture may vary^{95,96} and different scanning sites in each muscle aiming for an unobstructed ultrasound image.

One could argue that the data is consistent with the expectation for the psoas major muscle showing the lowest MGV_00 as it is one of the most tender and fine-grained parts of the beef.⁹¹ However, this study was not designed to find such specific differences. Their detection would require a higher number of specimens per muscle and an endpoint dedicated to the difference in MGV_00 between anatomical muscles or muscle groups.

Of note, the distribution of MGV_00 and TEG does differ across muscles implying that these two values contain different information derived from echo intensity.

5.3.2. Age

In muscles of older adults, higher EI values can be observed compared to younger subjects.^{29,54,55} Additionally, muscles have lower pennation angles in older subjects.^{53,97,98} This suggests that the lower pennation angle may be the cause for the increased EI in older people when not corrected for fascicle insonation angle in ultrasound studies. However, in a study comparing EI values of 24 young men (age 19.8 ± 1.7 y) and 21 older men (69.3 ± 3.3 y), EI values were still higher in the older group after statistically correcting for pennation angle.⁵⁵ In a mixed model analysis of our data, age as a fixed factor was significant for MG_V_00. Unfortunately, only the ages of the cattle for the limb muscle were known so a more comprehensive analysis is warranted in the future. Notably, when using spatial gain sonography performing a statistical correction for pennation angle is no longer necessary and comparable values can be obtained immediately.

5.4. Technical limitations

5.4.1. Fascicle alignment in other planes

In this study, changing fascicle alignment in the sagittal plane was done on purpose by probe angulation and addition of an ultrasound gel pad. Both, alignment in the transversal and coronal plane were kept constant. However, potential fascicular angles in these planes and differences between muscles were not quantitatively accounted for. They, too, could influence the echo intensity of a muscle, especially if it is considered that IMCT runs in bands and not merely round strings that reflect equally into all directions. As IMCT angles in these other planes are not as simple to measure as the pennation angle, it will be difficult to include or correct for them in future studies. Hence, for now the only option in the planes not shown in the ultrasound image is visual correction to reach maximum echo intensity. One could also argue that if standardization by quantification of these angles is not possible, another reference needs to be used. This was done in one study by aligning the probe in transverse image until the underlying bone had the highest echo intensity, which is however also a visual correction method.⁹⁹

5.4.2. Scanning depth and gel pad

Ultrasound waves are constantly attenuated as they travel through tissue, so that an increased scanning depth and a thicker gel pad could have led to lower EI. While some degree of accuracy may have been lost due the gel pad, a look at the absorption coefficients of the gel pad, $a_g = 0,053 \frac{dB}{MHz \cdot mm}$, compared to muscle tissue, $a_m = 0,11 \frac{dB}{MHz \cdot mm}$, reveals that their difference in magnitude probably prevented any relevant attenuation by the gel pad.¹⁰⁰ Compared to in-vivo studies, an advantage in this study was the lack of a subcutaneous fat

layer allowing for a constant scanning depth across muscles. Merely, manual angulation led to some systematic variation in scanning depth compared to no angulation or angulation using beam steering. In an analysis of the relationship between the distance of the center of region of interest from the probe (ROICy) and EI, neither anatomical muscle nor pennation angle had an effect for ROICy. This suggests that scanning depth did not have a systematic influence on results in this study.

5.4.3. Scanning site within the muscle

The scanning site between different muscles of the same anatomical location varied in this study, e.g., when scanning the supraspinatus muscle of two different animals the location of the probe on the muscle may not have been the same on each muscle. The only standardization in this regard was visual in that the largest area of uniform fascicles with no blood vessels or intramuscular aponeuroses was chosen. This limits the possibility to draw conclusions about differences between muscles since it has been shown that different scanning sites within some muscles can result in different EIs.^{101,102} Once these in-vivo measurements had been corrected for SAT layer the variability was reduced which in turn is in favor of the presented data. Nonetheless, muscle-specific differences in this study shall be interpreted with caution, and it should be noted again that the study was not designed to find these differences. The objective was to model a mathematical relationship. The described limitation therefore has no impact on the validity of the equation or the new parameters since within each muscle the location was kept constant using the precision of a robotic axis.

5.4.4. Ultrasound processing software

As discussed in the introduction, many internal settings of the ultrasound device, such as gain and depth have an influence on EI. These manually adjustable settings were kept constant across all measurements to rule out any confounding effect. However, modern ultrasound software often enhances the image automatically. This ensures optimal visibility of structures in a clinical setting when visual detection of organs and tissues is key. In a scientific setting, these corrections can lead to biased results. For example, if brightness is automatically increased by the software in a darker image, EI at perpendicular insonation of the aponeurosis will be elevated in all muscles with a greater pennation angle. Again, all controls related to gain were turned off, but in order to rule out any internal corrections, one would need to dissect the ultrasound software or access raw ultrasound data which are hard to obtain with commercial ultrasound scanners.

Other studies have attempted two different approaches to address this problem:

Pillen et al. measured echo intensity in images of animal muscles and human subjects from two devices and then created a conversion equation for the echo intensities.¹⁰³ This ensured

that all hardware and software changes were incorporated into the conversion. The availability of such equations would lower the threshold for examiners using quantitative muscle ultrasound compared to them having to devise a conversion scale themselves. However, phantom measurements would need to be taken with all ultrasound devices available and all on the same phantom muscles.

O'Brien et al. were able to design a portable ultrasound device without any postprocessing software.¹⁰⁴ This is the ideal machine for quantitative echo intensity analysis. At the same time, clinical imaging requiring image adjustment and high resolutions is not supported by the device which would therefore require a clinician to acquire both devices. The optimal solution would be an ultrasound device that features both, a postprocessing algorithm for use in the acute clinical setting and the possibility to turn it off for precise quantitative diagnostic measurements in muscles.

5.5. Reflection of intramuscular connective tissue content in echo intensity

The discussed experimental series was initiated with the objective to map and quantify connective tissue within the muscle. Using ultrasound, this would pertain primarily to perimysium as the wavelength of a common clinical ultrasound device does not permit detection of the delicate endomysium.¹⁰⁵

The assumption that echo intensity serves as an indicator for echo intensity stems from a study performed on seven muscles each of two dogs with muscular dystrophy by Pillen et al.³⁰ The group found that in muscle with increased fibrous tissue echo intensity was higher. Little interstitial fat was present in all muscles so most of the effect can be attributed to fibrosis, i.e., increased connective tissue.

However, an earlier study comparing ultrasound and biopsies showed that IMAT has a greater influence on echo intensity than IMCT.¹⁰⁶ It is questionable whether microscopic studies can reflect what is seen in an ultrasound image, however. In the present project, several Sirius Red-stained muscle cross sections were studied under the microscope after spatial gain sonography was performed. Since mostly endomysium and merely parts of perimysium were represented in these, it was concluded that a comparative study with ultrasound would not lead to internally valid results. Another study demonstrated that higher echo intensity in ultrasound correlates with an increased IMAT content in MRI and an increased extramyocellular lipid content as determined in magnetic resonance spectrometry.¹⁰⁷ In yet another study, a thicker layer of subcutaneous fat lead to an increase in echo intensity implying that correspondingly increased IMAT leads to an increase in EI.²⁸ The authors rightfully stated that attenuation by a thicker fat layer may have lead to a more pronounced correction by the ultrasound device accounting for the increased EI.

Both IMCT and IMAT appear hyperechogenic compared to skeletal muscle tissue in ultrasound images leading to an almost impossible discrimination between the two.¹⁰⁸

Therefore, a first step was taken in reviewing the literature on how age, immobilization and training affect echo intensity and comparing this to the effects on IMCT structure and content (Table 2 in Introduction). The comparison shows that for some conditions such as age and immobilization, correlations between EI and IMCT structure can be drawn. However, studies examining the effects of exercise are not as homogenous and IMCT structure in this setting has not been well studied showing that a major gap in the research has yet to be filled.

In summary, without IMAT present, echo intensity can be an indicator of IMCT content, however when present, IMAT seems to have a pronounced effect on echo intensity. This means that echo intensity may well be used as an indicator of muscle quality, though it is highly individual whether an elevated echo intensity represents IMAT or IMCT.

It shall be noted, however, that TEG in this study emphasizes the anisotropic features of muscle, namely IMCT organizing muscle into parallel bundles. The confounding effect of evenly distributed, isotropic IMAT would be eliminated to a certain degree using TEG based on this method. A comparative study between muscles of the same IMCT content with differing IMAT content would be required in order to validate this assumption.

5.6. Comparability to human muscle in-vivo

Quantifiable muscle ultrasound is developing into a valuable diagnostic tool in humans, especially due to its wide availability and time and cost efficiency. The question naturally arises whether beef muscle is comparable to human muscle in ultrasound and if spatial gain parameters can be used in human in-vivo studies.

Human and beef muscle both consist of muscle fibers surrounded by IMCT which is hierarchically structured into endomysium, perimysium and epimysium.^{12,93} Pennate muscles can be found in both species suggesting that the proposed method will lead to an increased level of standardization and therefore validity in human muscle studies as well.

Regarding in-vivo versus ex-vivo analysis, it is important to note that changes in meat post-mortem can be observed. Almost immediately after slaughter myofibril diameter and myofibril spacing decrease. A change in muscle fiber diameter and spacing can be observed within 24 hours, e.g., for the breed “Hereford” an increase by 5% and a decrease by 0.04% respectively.¹⁰⁹ Since the samples were collected within 24 hours after slaughter and analyzed within 48 hours, muscle fiber structure had indeed already been affected. This could potentially have influenced the echo intensity in ultrasound measurements. However, the differences would have been subtle as demonstrated in the aforementioned example from a bovine muscle study.¹⁰⁹ In addition, the entirety of any muscle was analyzed within a few hours so that no bias is to be expected within measurements of one muscle.

Other challenges in the transition to in-vivo studies pertain to rest duration and participant positioning. With current measurement methods, a standardization is necessary as fluid shifts in different positions and with different rest times affect EI.^{56,108}

Finally, SAT thickness will influence echo intensity in in-vivo studies. Of note, TEG is designed as a relative value examining the rate of change of EI over the angulation, so that the value may not be impacted by a constant layer of SAT as much as EI. If this can be validated in human studies, employing TEG would set an important step for reliable in-vivo measurements. In conclusion, beef muscle is highly comparable to human muscle regarding its architecture. Use of the spatial gain methods in humans in-vivo will necessitate minor changes in study design compared to this ex-vivo study in animals, however, they are feasible to implement. Before spatial gain parameters are used for tracking purposes in humans, they should be validated in a methodological experimental series, studying the effects of pennation angle, rest duration, subject positioning and subcutaneous fat layer in humans.

5.7. Clinical implications and potential clinical use

While qualitatively described in other studies before, the data presented here quantitatively prove that the tilt of the probe affects echo intensity.^{49,50,78} Therefore, any methods that did not use a fixed probe tilt or did not correct for it in the data evaluation should not be employed for quantitative echo intensity tracking in muscle.

Beyond merely highlighting the importance of standardized alignment, spatial gain sonography has the potential to serve as a tool for tracking muscular changes in athletes, in the elderly, in bedridden patients, and in astronauts. Once the above-mentioned challenges for measurements in humans have been resolved it also promises to offer an objective parameter in the diagnosis and tracking of neuromuscular disorders.

Previous studies already offer data, if limited, on these topics. Echo intensity decreases with muscle strengths¹¹⁰, while it increases with inactivity in elderly test subjects⁷². A study in young women showed an increase in echo intensity in the vastus lateralis after two weeks of knee joint immobilization.⁵⁸ Consistent with the present study, muscle echo intensity increases with age as shown in a multiple regression analysis of 95 healthy volunteers.⁹⁹ Echo intensity is not only subject to change in a physiological range of parameters such as activity and age, but also shows alterations in disease. In Duchenne muscular dystrophy, echo intensity increases indicating replacement of muscle fibers by other tissues.¹¹¹ Likewise, multiple sclerosis patients showed increased echo intensity in affected muscles compared to volunteers.¹¹² While by no means representing a comprehensive overview of muscle echo intensity studies, this excerpt highlights the potential of ultrasound echo intensity measurement for tracking intramuscular changes in various physiological and pathological conditions. However, as of now the absence

of absolute EI cut-offs for presence of disease limits the use of the method for diagnosing neuromuscular diseases.

Lastly, in clinical application inter-rater comparison is challenged by different ultrasound devices and by the lack of standardization of ultrasound settings. Both can be mitigated by going further than solely measuring absolute EI and calculating MGV₀₀ and TEG instead.

5.8. Conclusion

Ultrasonography is an increasingly relevant tool in musculoskeletal diagnostics. Muscle thickness and cross-sectional area have been measured for many years but these do not reflect muscle quality. Hence, echo intensity of ultrasound images has been used increasingly. Echo intensity could be used for tracking training and deterioration processes as well as serving as a diagnostic tool for neuromuscular diseases. However, quantification still presents a challenge due to lack of standardization in image acquisition and because IMCT and IMAT can hardly be distinguished on current ultrasound images. This study aimed to circumnavigate the former by establishing that the relationship between MGV and FPA can be modeled with a trigonometric function. Moreover, for small FPAs a linear function is a good enough fit which led to the definition of MGV₀₀, the MGV at perpendicular insonation of the fascicle, and TEG, the rate of change of MGV over FPA, as muscle-specific values in this study. Both could be used in clinical practice for tracking and diagnostic purposes once validated in human in-vivo studies. Impeding factors to the quantification of IMCT via ultrasound remains the impossibility to distinguish IMCT from IMAT with this imaging modality as well as image postprocessing by internal ultrasound software. Despite this, the method presented in this dissertation, spatial gain sonography, advances the standardization and applicability of quantitative ultrasound of the muscle structure.

5.9. Outlook

Next steps in the application of spatial gain sonography entail studying the feasibility and validating MGV₀₀ and TEG for in-vivo use. A crucial step would be to scan each muscle at the exact same site across subjects to allow for comparability. The relevance of spatial gain parameters as characteristic and reliably measurable features could for instance be established in a study measuring young versus old and exercising versus inactive subjects. Other ideas include measuring sex differences for spatial gain parameters in specific muscles. These are often overshadowed by the dependence on SAT layer thickness and strength and it would therefore be of interest whether TEG could serve as an imaging parameter with a strong correlation with muscle quality independent of these confounders.¹⁰¹ A comparison of antigravity muscle to non-antigravity muscle could likewise offer a new perspective. Antigravity muscles, e.g., the soleus, quadriceps and paravertebral muscles, are responsible for

maintaining posture meaning they are activated almost consistently and over long periods. It explains why most of them consist mainly of aerobic slow type I fibers.¹¹³ This feature could help distinguish them in muscle ultrasound which has recently been proved possible but seems unreliable using solely EI.¹¹⁴ If significant differences were detected in antigravity muscles using spatial gain sonography, this could offer a new method to determine and track muscles that are most affected in bed-rest or microgravity.

It should be noted that implementing any of these ideas requires a set-up for reliable angulation of the probe. Internal beam steering of ultrasound waves offers a mechanism to change the insonation angle without physical manipulation of the probe. The impact of internal corrections associated with this feature such as automatic gain adaptation on EI remains to be determined. If this feature can be employed without any automatic internal corrections, spatial gain sonography could be used in any setting with little effort by the examiner and without much hardware other than a probe holder. Future tools would have to include measurement of pennation angle and echo intensity as well as calculation of MG_{V_00} and TEG within the ultrasound device for rapid applicability. With this in mind, spatial gain sonography has the potential to serve as an important tool in clinical diagnostics in the future.

6. References

- 1 Gillies AR, Lieber RL. Structure and function of the skeletal muscle extracellular matrix. *Muscle Nerve* 2011; **44**: 318–31. <https://doi.org/10.1002/mus.22094>.
- 2 Csapo R, Gumpenberger M, Wessner B. Skeletal Muscle Extracellular Matrix - What Do We Know About Its Composition, Regulation, and Physiological Roles? A Narrative Review. *Front Physiol* 2020; **11**: 253. <https://doi.org/10.3389/fphys.2020.00253>.
- 3 Sleboda DA, Stover KK, Roberts TJ. Diversity of extracellular matrix morphology in vertebrate skeletal muscle. *J Morphol* 2020; **281**: 160–69. <https://doi.org/10.1002/jmor.21088>.
- 4 Roberts TJ, Eng CM, Sleboda DA, et al. The Multi-Scale, Three-Dimensional Nature of Skeletal Muscle Contraction. *Physiology (Bethesda)* 2019; **34**: 402–08. <https://doi.org/10.1152/physiol.00023.2019>.
- 5 Järvinen TAH, Jozsa L, Kannus P, Jarvinen TLN, Jarvinen M. Organization and distribution of intramuscular connective tissue in normal and immobilized skeletal muscles. An immunohistochemical, polarization and scanning electron microscopic study. *J Muscle Res Cell Motil* 2002; **23**: 245–54.
- 6 Voorhees AP, Han H-C. A model to determine the effect of collagen fiber alignment on heart function post myocardial infarction. *Theor Biol Med Model* 2014; **11**: 6. <https://doi.org/10.1186/1742-4682-11-6>.
- 7 Csapo R, Gumpenberger M, Wessner B. Skeletal Muscle Extracellular Matrix - What Do We Know About Its Composition, Regulation, and Physiological Roles? A Narrative Review. *Front Physiol* 2020; **11**: 253. <https://doi.org/10.3389/fphys.2020.00253>.
- 8 Kovanen V. Intramuscular extracellular matrix: complex environment of muscle cells. *Exerc Sport Sci Rev* 2002; **30**: 20–25. <https://doi.org/10.1097/00003677-200201000-00005>.
- 9 Grounds MD, Sorokin L, White J. Strength at the extracellular matrix-muscle interface. *Scand J Med Sci Sports* 2005; **15**: 381–91. <https://doi.org/10.1111/j.1600-0838.2005.00467.x>.
- 10 Klein CS, Marsh GD, Petrella RJ, Rice CL. Muscle fiber number in the biceps brachii muscle of young and old men. *Muscle Nerve* 2003; **28**: 62–68. <https://doi.org/10.1002/mus.10386>.
- 11 Purslow PP. The structure and functional significance of variations in the connective tissue within muscle. *Comp Biochem Physiol A Mol Integr Physiol* 2002; **133**: 947–66.
- 12 Purslow PP. The Structure and Role of Intramuscular Connective Tissue in Muscle Function. *Front Physiol* 2020; **11**: 495. <https://doi.org/10.3389/fphys.2020.00495>.

- 13 Biltz NK, Collins KH, Shen KC, Schwartz K, Harris CA, Meyer GA. Infiltration of intramuscular adipose tissue impairs skeletal muscle contraction. *J Physiol (Lond)* 2020; **598**: 2669–83. <https://doi.org/10.1113/JP279595>.
- 14 Hijikata T, Wakisaka H, Niida S. Functional combination of tapering profiles and overlapping arrangements in nonspanning skeletal muscle fibers terminating intrafascicularly. *Anat Rec* 1993; **236**: 602–10. <https://doi.org/10.1002/ar.1092360403>.
- 15 Trotter JA, Salgado JD, Ozbaysal R, Gaunt AS. The composite structure of quail pectoralis muscle. *J Morphol* 1992; **212**: 27–35. <https://doi.org/10.1002/jmor.1052120104>.
- 16 Ramaswamy KS, Palmer ML, van der Meulen JH, et al. Lateral transmission of force is impaired in skeletal muscles of dystrophic mice and very old rats. *J Physiol (Lond)* 2011; **589**: 1195–208. <https://doi.org/10.1113/jphysiol.2010.201921>.
- 17 Zhang C, Gao Y. Effects of aging on the lateral transmission of force in rat skeletal muscle. *J Biomech* 2014; **47**: 944–48. <https://doi.org/10.1016/j.jbiomech.2014.01.026>.
- 18 Purslow PP. Muscle fascia and force transmission. *J Bodyw Mov Ther* 2010; **14**: 411–17. <https://doi.org/10.1016/j.jbmt.2010.01.005>.
- 19 HILL AV. The abrupt transition from rest to activity in muscle. *Proc R Soc Lond B Biol Sci* 1949; **136**: 399–420. <https://doi.org/10.1098/rspb.1949.0033>.
- 20 Marcucci L, Bondi M, Randazzo G, Reggiani C, Natali AN, Pavan PG. Fibre and extracellular matrix contributions to passive forces in human skeletal muscles: An experimental based constitutive law for numerical modelling of the passive element in the classical Hill-type three element model. *PLoS One* 2019; **14**: e0224232. <https://doi.org/10.1371/journal.pone.0224232>.
- 21 Blottner D, Moriggi M, Trautmann G, et al. Space Omics and Tissue Response in Astronaut Skeletal Muscle after Short and Long Duration Missions. *Int J Mol Sci* 2023; **24**. <https://doi.org/10.3390/ijms24044095>.
- 22 Yeung C-YC, Olesen AT, Wilson R, et al. Proteome profiles of intramuscular connective tissue: influence of aging and physical training. *J Appl Physiol (1985)* 2023; **134**: 1278–86. <https://doi.org/10.1152/jappphysiol.00675.2022>.
- 23 Cissell DD, Link JM, Hu JC, Athanasiou KA. A Modified Hydroxyproline Assay Based on Hydrochloric Acid in Ehrlich's Solution Accurately Measures Tissue Collagen Content. *Tissue Eng Part C Methods* 2017; **23**: 243–50. <https://doi.org/10.1089/ten.tec.2017.0018>.
- 24 Dubost A, Micol D, Meunier B, Lethias C, Listrat A. Relationships between structural characteristics of bovine intramuscular connective tissue assessed by image analysis and collagen and proteoglycan content. *Meat Sci* 2013; **93**: 378–86. <https://doi.org/10.1016/j.meatsci.2012.09.020>.
- 25 Fede C, Fan C, Pirri C, et al. The Effects of Aging on the Intramuscular Connective Tissue. *Int J Mol Sci* 2022; **23**. <https://doi.org/10.3390/ijms231911061>.

- 26 Thot GK, Berwanger C, Mulder E, et al. Effects of long-term immobilisation on endomysium of the soleus muscle in humans. *Exp Physiol* 2021; **106**: 2038–45. <https://doi.org/10.1113/EP089734>.
- 27 Arts IMP, Pillen S, Schelhaas HJ, Overeem S, Zwarts MJ. Normal values for quantitative muscle ultrasonography in adults. *Muscle Nerve* 2010; **41**: 32–41. <https://doi.org/10.1002/mus.21458>.
- 28 Nijboer-Oosterveld J, van Alfen N, Pillen S. New normal values for quantitative muscle ultrasound: obesity increases muscle echo intensity. *Muscle Nerve* 2011; **43**: 142–43. <https://doi.org/10.1002/mus.21866>.
- 29 Ota M, Ikezoe T, Kato T, Tateuchi H, Ichihashi N. Age-related changes in muscle thickness and echo intensity of trunk muscles in healthy women: comparison of 20-60s age groups. *European Journal of Applied Physiology* 2020; **120**: 1805–14. <https://doi.org/10.1007/s00421-020-04412-7>.
- 30 Pillen S, Tak RO, Zwarts MJ, et al. Skeletal muscle ultrasound: correlation between fibrous tissue and echo intensity. *Ultrasound Med Biol* 2009; **35**: 443–46. <https://doi.org/10.1016/j.ultrasmedbio.2008.09.016>.
- 31 Alfuraih AM, Tan AL, O'Connor P, Emery P, Wakefield RJ. The effect of ageing on shear wave elastography muscle stiffness in adults. *Aging Clin Exp Res* 2019; **31**: 1755–63. <https://doi.org/10.1007/s40520-019-01139-0>.
- 32 Eby SF, Cloud BA, Brandenburg JE, et al. Shear wave elastography of passive skeletal muscle stiffness: influences of sex and age throughout adulthood. *Clin Biomech (Bristol, Avon)* 2015; **30**: 22–27. <https://doi.org/10.1016/j.clinbiomech.2014.11.011>.
- 33 Edmunds KJ, Gíslason MK, Arnadottir ID, Marcante A, Piccione F, Gargiulo P. Quantitative Computed Tomography and Image Analysis for Advanced Muscle Assessment. *Eur J Transl Myol* 2016; **26**: 6015. <https://doi.org/10.4081/ejtm.2016.6015>.
- 34 Sinha U, Malis V, Chen J-S, et al. Role of the Extracellular Matrix in Loss of Muscle Force With Age and Unloading Using Magnetic Resonance Imaging, Biochemical Analysis, and Computational Models. *Front Physiol* 2020; **11**: 626. <https://doi.org/10.3389/fphys.2020.00626>.
- 35 Albayda J, van Alfen N. Diagnostic Value of Muscle Ultrasound for Myopathies and Myositis. *Curr Rheumatol Rep* 2020; **22**: 82. <https://doi.org/10.1007/s11926-020-00947-y>.
- 36 Dusang K. TRISH demonstrates performance of portable handheld ultrasound in space. <https://www.bcm.edu/news/trish-demonstrates-performance-of-portable-handheld-ultrasound-in-space> (accessed Feb 21, 2023).
- 37 Li J, Ming-Der Chow R, Vadivelu N, Kaye AD, eds. *Ultrasound Fundamentals*. Cham: Springer International Publishing, 2021.

- 38 Schlegel W, Karger CP, Jäkel O. Medizinische Physik. Berlin, Heidelberg: Springer Berlin Heidelberg, 2018.
- 39 Harput S, Zhou X, Tang M-X. Getting Started: Ultrasound Physics and Image Formation. <https://radiologykey.com/getting-started/#c1-fig-0001> (accessed May 07, 2024).
- 40 Wagner DR, Teramoto M, Judd T, Gordon J, McPherson C, Robison A. Comparison of A-mode and B-mode Ultrasound for Measurement of Subcutaneous Fat. *Ultrasound Med Biol* 2020; **46**: 944–51. <https://doi.org/10.1016/j.ultrasmedbio.2019.11.018>.
- 41 Hasgall, P. A., F. Di Gennaro, C. Baumgartner, E. Neufeld, B. Lloyd, M. C. Gosselin, D. Payne, A. Klingenböck, and N. Kuster. IT'IS Database for Thermal and Electromagnetic Parameters of Biological Tissues, Version 4.1. <https://itis.swiss/virtual-population/tissue-properties/database/dielectric-properties> (accessed May 07, 2024).
- 42 O'Neill JM. Musculoskeletal Ultrasound. New York, NY: Springer New York, 2008.
- 43 Quarato CMI, Lacedonia D, Salvemini M, et al. A Review on Biological Effects of Ultrasounds: Key Messages for Clinicians. *Diagnostics (Basel)* 2023; **13**. <https://doi.org/10.3390/diagnostics13050855>.
- 44 Costello JR, Arif H, Kalb B, Martin DR. Ultrasound. In: Maqbool M, ed. An Introduction to Medical Physics. Cham: Springer International Publishing, 2017: 329–70.
- 45 Torrescano G, ed. Determination of perimysium and endomysium thickness in bovine, ovine and caprine semimembranosus and semitendinosus muscles by video image analysis. M. Science (Ed.), 2001.
- 46 Ashir A, Jerban S, Barrère V, et al. Skeletal Muscle Assessment Using Quantitative Ultrasound: A Narrative Review. *Sensors (Basel)* 2023; **23**. <https://doi.org/10.3390/s23104763>.
- 47 Pinto RS, Pinto MD. Moving forward with the echo intensity mean analysis: Exploring echo intensity bands in different age groups. *Exp Gerontol* 2021; **145**: 111179. <https://doi.org/10.1016/j.exger.2020.111179>.
- 48 Carlson BM. The Muscular System. In: Bruce M. Carlson, ed. The Human Body. Chapter 5 - The Muscular System, Pages 111-136. Academic Press: Elsevier, 2019: 111–36.
- 49 Pillen S, van Keimpema M, Nievelstein RAJ, Verrips A, van Kruijsbergen-Raijmann W, Zwarts MJ. Skeletal muscle ultrasonography: Visual versus quantitative evaluation. *Ultrasound Med Biol* 2006; **32**: 1315–21. <https://doi.org/10.1016/j.ultrasmedbio.2006.05.028>.
- 50 Scholten RR, Pillen S, Verrips A, Zwarts MJ. Quantitative ultrasonography of skeletal muscles in children: normal values. *Muscle Nerve* 2003; **27**: 693–98. <https://doi.org/10.1002/mus.10384>.
- 51 Lexell J, Taylor CC, Sjöström M. What is the cause of the ageing atrophy? Total number, size and proportion of different fiber types studied in whole vastus lateralis muscle from

- 15- to 83-year-old men. *J Neurol Sci* 1988; **84**: 275–94. [https://doi.org/10.1016/0022-510x\(88\)90132-3](https://doi.org/10.1016/0022-510x(88)90132-3).
- 52 Hinks A, Jacob K, Mashouri P, et al. Influence of weighted downhill running training on serial sarcomere number and work loop performance in the rat soleus. *Biol Open* 2022; **11**. <https://doi.org/10.1242/bio.059491>.
- 53 Jacob I, Johnson MI, Jones G, Jones A, Francis P. Age-related differences of vastus lateralis muscle morphology, contractile properties, upper body grip strength and lower extremity functional capability in healthy adults aged 18 to 70 years. *BMC Geriatr* 2022; **22**: 538. <https://doi.org/10.1186/s12877-022-03183-4>.
- 54 Kobayashi K, Yagi M, Tateuchi H, et al. Effect of age on shear modulus, muscle thickness, echo intensity of the upper limb, lower limb, and trunk muscles in healthy women. *European Journal of Applied Physiology* 2022. <https://doi.org/10.1007/s00421-022-05099-8>.
- 55 Ryan ED, Rosenberg JG, Scharville MJ, Sobolewski EJ, Tweedell AJ, Kleinberg CR. Pennation angle does not influence the age-related differences in echo intensity of the medial gastrocnemius. *Ultrasound Med Biol* 2015; **41**: 618–21. <https://doi.org/10.1016/j.ultrasmedbio.2014.08.004>.
- 56 Bali AU, Harmon KK, Burton AM, et al. Muscle strength, not age, explains unique variance in echo intensity. *Exp Gerontol* 2020; **139**: 111047. <https://doi.org/10.1016/j.exger.2020.111047>.
- 57 Fukumoto Y, Yamada Y, Ikezoe T, et al. Association of physical activity with age-related changes in muscle echo intensity in older adults: a 4-year longitudinal study. *J Appl Physiol (1985)* 2018; **125**: 1468–74. <https://doi.org/10.1152/jappphysiol.00317.2018>.
- 58 MacLennan RJ, Sahebi M, Becker N, Davis E, Garcia JM, Stock MS. Declines in skeletal muscle quality vs. size following two weeks of knee joint immobilization. *PeerJ* 2020; **8**: e8224. <https://doi.org/10.7717/peerj.8224>.
- 59 Józsa L, Kannus P, Thöring J, Reffy A, Järvinen M, Kvist M. The effect of tenotomy and immobilisation on intramuscular connective tissue. A morphometric and microscopic study in rat calf muscles. *J Bone Joint Surg Br* 1990; **72**: 293–97. <https://doi.org/10.1302/0301-620X.72B2.2312572>.
- 60 Järvinen MJ, Einola SA, Virtanen EO. Effect of the position of immobilization upon the tensile properties of the rat gastrocnemius muscle. *Arch Phys Med Rehabil* 1992; **73**: 253–57.
- 61 Kannus P, Jozsa L, Kvist M, Järvinen T, Järvinen M. Effects of immobilization and subsequent low- and high-intensity exercise on morphology of rat calf muscles. *Scand J Med Sci Sports* 1998; **8**: 160–71. <https://doi.org/10.1111/j.1600-0838.1998.tb00187.x>.

- 62 Carlson BM. The Biology of Long-Term Denervated Skeletal Muscle. *Eur J Transl Myol* 2014; **24**: 3293. <https://doi.org/10.4081/ejtm.2014.3293>.
- 63 Scott JM, Downs M, Martin DS, et al. Teleguided self-ultrasound scanning for longitudinal monitoring of muscle mass during spaceflight. *iScience* 2021; **24**: 102344. <https://doi.org/10.1016/j.isci.2021.102344>.
- 64 Wong V, Spitz RW, Bell ZW, et al. Exercise induced changes in echo intensity within the muscle: a brief review. *J Ultrasound* 2020; **23**: 457–72. <https://doi.org/10.1007/s40477-019-00424-y>.
- 65 Rowe GS, Blazevich AJ, Haff GG. pQCT- and Ultrasound-based Muscle and Fat Estimate Errors after Resistance Exercise. *Med Sci Sports Exerc* 2019; **51**: 1022–31. <https://doi.org/10.1249/MSS.0000000000001873>.
- 66 Yoshiko A, Kaji T, Sugiyama H, Koike T, Oshida Y, Akima H. Twenty-Four Months' Resistance and Endurance Training Improves Muscle Size and Physical Functions but Not Muscle Quality in Older Adults Requiring Long-Term Care. *J Nutr Health Aging* 2019; **23**: 564–70. <https://doi.org/10.1007/s12603-019-1208-8>.
- 67 Ducomps C, Mauriège P, Darche B, Combes S, Lebas F, Doutreloux JP. Effects of jump training on passive mechanical stress and stiffness in rabbit skeletal muscle: role of collagen. *Acta Physiol Scand* 2003; **178**: 215–24. <https://doi.org/10.1046/j.1365-201X.2003.01109.x>.
- 68 Olesen AT, Malchow-Møller L, Bendixen RD, et al. Intramuscular connective tissue content and mechanical properties: Influence of aging and physical activity in mice. *Exp Gerontol* 2022; **166**: 111893. <https://doi.org/10.1016/j.exger.2022.111893>.
- 69 Miller BF, Olesen JL, Hansen M, et al. Coordinated collagen and muscle protein synthesis in human patella tendon and quadriceps muscle after exercise. *J Physiol (Lond)* 2005; **567**: 1021–33. <https://doi.org/10.1113/jphysiol.2005.093690>.
- 70 Wojtysiak D. Effect of Age on Structural Properties of Intramuscular Connective Tissue, Muscle Fibre, Collagen Content and Meat Tenderness in Pig longissimus lumborum muscle. *folia biol (krakow)* 2013; **61**: 221–26. https://doi.org/10.3409/fb61_3-4.221.
- 71 Girts RM, Harmon KK, Pagan JI, Alberto A, Hernandez MG, Stock MS. The influence of ultrasound image depth and gain on skeletal muscle echo intensity. *Appl Physiol Nutr Metab* 2022; **47**: 839–46. <https://doi.org/10.1139/apnm-2021-0810>.
- 72 Yoshiko A, Natsume Y, Makino T, et al. Higher and Lower Muscle Echo Intensity in Elderly Individuals Is Distinguished by Muscle Size, Physical Performance and Daily Physical Activity. *Ultrasound Med Biol* 2019; **45**: 2372–80. <https://doi.org/10.1016/j.ultrasmedbio.2019.05.029>.

- 73 Ticinesi A, Meschi T, Narici MV, Lauretani F, Maggio M. Muscle Ultrasound and Sarcopenia in Older Individuals: A Clinical Perspective. *J Am Med Dir Assoc* 2017; **18**: 290–300. <https://doi.org/10.1016/j.jamda.2016.11.013>.
- 74 Ishida H, Suehiro T, Suzuki K, Watanabe S. Muscle thickness and echo intensity measurements of the rectus femoris muscle of healthy subjects: Intra and interrater reliability of transducer tilt during ultrasound. *J Bodyw Mov Ther* 2018; **22**: 657–60. <https://doi.org/10.1016/j.jbmt.2017.12.005>.
- 75 Ishida H, Suehiro T, Suzuki K, Yoneda T, Watanabe S. Influence of the ultrasound transducer tilt on muscle thickness and echo intensity of the rectus femoris muscle of healthy subjects. *J Phys Ther Sci* 2017; **29**: 2190–93. <https://doi.org/10.1589/jpts.29.190>.
- 76 Pillen S, van Alfen N. Muscle ultrasound from diagnostic tool to outcome measure-- Quantification is the challenge. *Muscle Nerve* 2015; **52**: 319–20. <https://doi.org/10.1002/mus.24613>.
- 77 Rabello R, Pompeo KD, Almeida Paz I de, Lanferdini FJ, Pinto RS, Vaz MA. Echo Intensity Reliability From Two Ultrasound Systems. *Journal of Diagnostic Medical Sonography* 2020; **36**: 464–69. <https://doi.org/10.1177/8756479320929030>.
- 78 Dankel SJ, Abe T, Bell ZW, et al. The Impact of Ultrasound Probe Tilt on Muscle Thickness and Echo-Intensity: A Cross-Sectional Study. *J Clin Densitom* 2020; **23**: 630–38. <https://doi.org/10.1016/j.jocd.2018.10.003>.
- 79 Thijssen JM, Mischi M. Ultrasound Imaging Arrays. In: *Comprehensive Biomedical Physics*. Elsevier, 2014: 323–41.
- 80 Pigula-Tresansky AJ, Wu JS, Kapur K, Darras BT, Rutkove SB, Anthony BW. Muscle compression improves reliability of ultrasound echo intensity. *Muscle Nerve* 2018; **57**: 423–29. <https://doi.org/10.1002/mus.25779>.
- 81 Santos R, Armada-da-Silva PAS. Reproducibility of ultrasound-derived muscle thickness and echo-intensity for the entire quadriceps femoris muscle. *Radiography (Lond)* 2017; **23**: e51-e61. <https://doi.org/10.1016/j.radi.2017.03.011>.
- 82 Caresio C, Molinari F, Emanuel G, Minetto MA. Muscle echo intensity: reliability and conditioning factors. *Clin Physiol Funct Imaging* 2015; **35**: 393–403. <https://doi.org/10.1111/cpf.12175>.
- 83 Akima H, Yamamori K, Taniguchi K, et al. Effect of subcutaneous adipose tissue and muscle thicknesses on rectus femoris and vastus intermedius ultrasound echo intensities: a cadaver study. *J Ultrasound* 2023; **26**: 635–42. <https://doi.org/10.1007/s40477-022-00696-x>.
- 84 Paris MT, Letofsky N, Mourtzakis M. Site-specific skeletal muscle echo intensity and thickness differences in subcutaneous adipose tissue matched older and younger adults. *Clin Physiol Funct Imaging* 2021; **41**: 156–64. <https://doi.org/10.1111/cpf.12679>.

- 85 Alegre LM, Aguado X, Rojas-Martín D, Martín-García M, Ara I, Csapo R. Load-controlled moderate and high-intensity resistance training programs provoke similar strength gains in young women. *Muscle Nerve* 2015; **51**: 92–101. <https://doi.org/10.1002/mus.24271>.
- 86 Young H-J, Jenkins NT, Zhao Q, McCully KK. Measurement of intramuscular fat by muscle echo intensity. *Muscle Nerve* 2015; **52**: 963–71. <https://doi.org/10.1002/mus.24656>.
- 87 Fukumoto Y, Taniguchi M, Hirono T, et al. Influence of ultrasound focus depth on the association between echo intensity and intramuscular adipose tissue. *Muscle Nerve* 2022; **66**: 568–75. <https://doi.org/10.1002/mus.27677>.
- 88 Rabello R, Fröhlich M, Bueno AF, et al. Echo intensity reliability between two rectus femoris probe sites. *Ultrasound* 2019; **27**: 233–40. <https://doi.org/10.1177/1742271X19853859>.
- 89 Rauschendorfer P. Development of a method for the quantification of intramuscular connective tissue with ultrasound B-mode. Master Thesis. Regensburg, 2018.
- 90 Animal Biosciences, University of Guelph. Major Muscles of the Carcass. https://animalbiosciences.uoguelph.ca/~swatland/ch4_1.htm (accessed Oct 06, 2021).
- 91 Metzgerei Zieger. Metzgerei Zieger - Rindfleisch. <http://www.metzgerei-zieger.de/index-Dateien/Rindfleisch.htm> (accessed Oct 06, 2021).
- 92 Mitchell HH, Hamilton TS, Haines WT. Some Factors Affecting the Connective Tissue Content of Beef Muscle. *The Journal of Nutrition* 1928; **1**: 165–78. <https://doi.org/10.1093/jn/1.2.165>.
- 93 Purslow PP. Intramuscular connective tissue and its role in meat quality. *Meat Sci* 2005; **70**: 435–47. <https://doi.org/10.1016/j.meatsci.2004.06.028>.
- 94 Stirling Butchery. Key features of Beef Shank steak cut for steak lovers. https://stirlingbutchery.com/beef-shank/?__cf_chl_managed_tk__=pmd_ACoP9Q0HepzYW2lzYvoE2XX2hexGUuHH1gJPvOZK3sc-1633524458-0-gqNtZGzNArucnBszRNR (accessed Oct 06, 2021).
- 95 Albrecht E, Teuscher F, Ender K, Wegner J. Growth- and breed-related changes of muscle bundle structure in cattle. *J Anim Sci* 2006; **84**: 2959–64. <https://doi.org/10.2527/jas.2006-345>.
- 96 Albrecht E, Lembcke C, Wegner J, Maak S. Prenatal muscle fiber development and bundle structure in beef and dairy cattle. *J Anim Sci* 2013; **91**: 3666–73. <https://doi.org/10.2527/jas.2013-6258>.
- 97 Morse CI, Thom JM, Reeves ND, Birch KM, Narici MV. In vivo physiological cross-sectional area and specific force are reduced in the gastrocnemius of elderly men. *J Appl Physiol (1985)* 2005; **99**: 1050–55. <https://doi.org/10.1152/jappphysiol.01186.2004>.

- 98 Strasser EM, Draskovits T, Praschak M, Quittan M, Graf A. Association between ultrasound measurements of muscle thickness, pennation angle, echogenicity and skeletal muscle strength in the elderly. *Age (Dordr)* 2013; **35**: 2377–88. <https://doi.org/10.1007/s11357-013-9517-z>.
- 99 Arts IMP, Pillen S, Schelhaas HJ, Overeem S, Zwarts MJ. Normal values for quantitative muscle ultrasonography in adults. *Muscle Nerve* 2010; **41**: 32–41. <https://doi.org/10.1002/mus.21458>.
- 100 Nassiri DK, Nicholas D, Hill CR. Attenuation of ultrasound in skeletal muscle. *Ultrasonics* 1979; **17**: 230–32. [https://doi.org/10.1016/0041-624x\(79\)90054-4](https://doi.org/10.1016/0041-624x(79)90054-4).
- 101 Stock MS, Oranchuk DJ, Burton AM, Phan DC. Age-, sex-, and region-specific differences in skeletal muscle size and quality. *Appl Physiol Nutr Metab* 2020; **45**: 1253–60. <https://doi.org/10.1139/apnm-2020-0114>.
- 102 Oranchuk DJ, Stock MS, Nelson AR, Storey AG, Cronin JB. Variability of regional quadriceps echo intensity in active young men with and without subcutaneous fat correction. *Appl Physiol Nutr Metab* 2020; **45**: 745–52. <https://doi.org/10.1139/apnm-2019-0601>.
- 103 Pillen S, van Dijk JP, Weijers G, Raijmann W, Korte CL de, Zwarts MJ. Quantitative gray-scale analysis in skeletal muscle ultrasound: a comparison study of two ultrasound devices. *Muscle Nerve* 2009; **39**: 781–86. <https://doi.org/10.1002/mus.21285>.
- 104 O'brien TG, Cazares Gonzalez ML, Ghosh PS, Mandrekar J, Boon AJ. Reliability of a novel ultrasound system for gray-scale analysis of muscle. *Muscle Nerve* 2017; **56**: 408–12. <https://doi.org/10.1002/mus.25513>.
- 105 Rosahl SC, Rauschendorfer P, Arndt L, Voigtmann T, Mittag U, Rittweger J. Ex-vivo validation of spatial gain sonography for the quantification of echo intensity in fascicle-aligned ultrasound images in ten anatomical muscles in *Bos taurus*. *Sci Rep* 2024; **14**. <https://doi.org/10.1038/s41598-024-53852-0>.
- 106 Reimers K, Reimers CD, Wagner S, Paetzke I, Pongratz DE. Skeletal muscle sonography: a correlative study of echogenicity and morphology. *J Ultrasound Med* 1993; **12**: 73–77. <https://doi.org/10.7863/jum.1993.12.2.73>.
- 107 Akima H, Hioki M, Yoshiko A, et al. Intramuscular adipose tissue determined by T1-weighted MRI at 3T primarily reflects extramyocellular lipids. *Magn Reson Imaging* 2016; **34**: 397–403. <https://doi.org/10.1016/j.mri.2015.12.038>.
- 108 Stock MS, Thompson BJ. Echo intensity as an indicator of skeletal muscle quality: applications, methodology, and future directions. *European Journal of Applied Physiology* 2021; **121**: 369–80. <https://doi.org/10.1007/s00421-020-04556-6>.

- 109 Soji Z. Effect of the muscle nanostructure changes during post-mortem aging on tenderness of different beef breeds. *Anim Biosci* 2021; **34**: 1849–58. <https://doi.org/10.5713/ajas.20.0488>.
- 110 Watanabe Y, Yamada Y, Fukumoto Y, et al. Echo intensity obtained from ultrasonography images reflecting muscle strength in elderly men. *Clin Interv Aging* 2013; **8**: 993–98. <https://doi.org/10.2147/CIA.S47263>.
- 111 Zaidman CM, Malkus EC, Connolly AM. Muscle Ultrasound Quantifies Disease Progression Over Time in Infants and Young Boys with Duchenne Muscular Dystrophy. *Muscle Nerve* 2015; **52**: 334–38. <https://doi.org/10.1002/mus.24609>.
- 112 Gao J, Memmott B, Poulson J, Harmon B, Hammond C. Quantitative Ultrasound Imaging to Assess Skeletal Muscles in Adults with Multiple Sclerosis: A Feasibility Study. *J Ultrasound Med* 2019; **38**: 2915–23. <https://doi.org/10.1002/jum.14997>.
- 113 Lee PHU, Chung M, Ren Z, Mair DB, Kim D-H. Factors mediating spaceflight-induced skeletal muscle atrophy. *Am J Physiol Cell Physiol* 2022; **322**: C567-C580. <https://doi.org/10.1152/ajpcell.00203.2021>.
- 114 Terzis G, Vekaki E, Papadopoulos C, Papadimas G, Stasinaki A-N. Muscle Ultrasound Echo Intensity and Fiber Type Composition in Young Females. *J Funct Morphol Kinesiol* 2024; **9**. <https://doi.org/10.3390/jfmk9020064>.

7. Appendix

7.1. List of figures

Figure 1: Scanning electron microscopic images of a domestic turkey's lateral gastrocnemius muscle.	12
Figure 2: A Schematic drawing of the macroscopic organization of muscle fibers and IMCT	13
Figure 3: A Scanning electron micrograph of mouse EDL.....	14
Figure 4: Schematic diagram of a crimped collagen fiber.....	15
Figure 5: Trichrome stain of bovine muscle.....	18
Figure 6: Schematic model illustrating ultrasound wave propagation.....	20
Figure 7: Comparison of A-mode and B-mode ultrasound images.....	21
Figure 8: Ultrasound image of a bovine muscle	23
Figure 9: A Reflection and refraction of an ultrasound.....	23
Figure 10: A Bovine muscle scanned perpendicularly to the fascicle orientation.....	25
Figure 11: Ultrasound image of an infraspinatus muscle in fascicle-aligned orientation.....	26
Figure 12: Schematic demonstration of the function of the pennation angle.....	26
Figure 13: A Normal soleus muscle. B Immobilized soleus muscle.	28
Figure 14: A Normal gastrocnemius muscle B Immobilized gastrocnemius muscle.....	29
Figure 15: Changing the insonation angle via beam steering versus probe tilt with an angulated gel pad.....	33
Figure 16: Robotic axis controlled by an Arduino UNO unit.....	36
Figure 17: Schematic diagram of the reflection of an ultrasound ray.....	36

7.2. List of tables

Table 1: Speeds of sound in different tissues.....	22
Table 2: Overview of studies on effects of age, immobilization and exercise on IMCT structure vs. echo intensity.....	31

8. Pre-publication of results

Presentation

Fifth KNIMS Annual Conference (Kompetenznetzwerk Immobilisationsbedingte Muskelstörungen - Network of Expertise for Immobilization-induced Muscle Disorders), Cologne, March 3-4, 2023

Publication

Rosahl, S.C., Rauschendorfer, P., Arndt, L. et al. Ex-vivo validation of spatial gain sonography for the quantification of echo intensity in fascicle-aligned ultrasound images in ten anatomical muscles in *Bos taurus*. *Sci Rep* 14, 3808 (2024). <https://doi.org/10.1038/s41598-024-53852-0>